Aus der Klinik für Kardiologie und Pneumonologie
(Prof. Dr. med. G. Hasenfuß)
der Medizinischen Fakultät der Universität Göttingen

Characterization of the cardiogenesis in embryos of a Gse-1$^{tm-1a(EUCOMM)Wtsi}$ mouse line

INAUGURAL-DISSERTATION

zur Erlangung des Doktorgrades
der Medizinischen Fakultät der
Georg-August-Universität zu Göttingen

vorgelegt von

Eva Baier

aus

Bad Neustadt an der Saale

Göttingen 2020

Dekan:	Prof. Dr. med. W. Brück
Referentin	Prof. Dr. med. E. M. Zeisberg
Ko-Referent/in:	PD Dr. med. J. Männer
Drittreferent/in:	Prof. Dr. med. B. Wollnik

Datum der mündlichen Prüfung: 05.08.2021

Hiermit erkläre ich, die Dissertation mit dem Titel **"Characterization of the cardiogenesis in embryos of a Gse-1$^{tm-1a(EUCOMM)Wtsi}$ mouse line"** eigenständig angefertigt und keine anderen als die von mir angegebenen Quellen und Hilfsmittel verwendet zu haben.

Göttingen, den …… ……

(Unterschrift)

Table of contents

List of figures

List of tables

List of abbreviations

AGE	agarose gel electrophoresis
AV	aortic valve
APSS	aortico-pulmonary spiral septum
ASD	atrial septal defect
AVV	atrioventricular valves
BC	*bulbus cordis*
BMP-10	bone-morphogenic protein 10
bp	base pairs
BT shunt	Blalock-Taussig shunt
CHD	congenital heart disease
circRNA	circular RNA
COREST	RE1-silencing transcription-factor corepressor
Cre	cyclisation recombinase
CZ	compact zone
DA	*ductus arteriosus*
DNA	deoxyribonucleic acid
DORV	double outlet right ventricle
ECT	endocardial cushion tissue
EFE	endocardial fibroelastosis
EGA	estimated gestational age
EMT	epithelial-to-mesenchymal transition
En2 SA	engrailed 2 splicing acceptor
EndMT	endothelial-to-mesenchymal transition
EP	external phenotype
EPd	external phenotype detected
ES cells	embryonic stem cells
EUCOMM	European conditional mouse mutagenesis program
FAV	fetal aortic valvuloplasty
FCI	fetal cardiac intervention
FFPE	formalin-fixed, paraffin-embedded
floxed	flanked by LoxP (see there)
Flp	flippase
FRT	flippase-recognition target
Gse-1	genetic suppressor element 1
H.E.	hematoxylin and eosin
Hand1	heart and neural crest derivatives-expressed protein 1
HLHS	hypoplastic left heart syndrome
IKMC	international knockout mouse consortium
IMT	intermediate type
IRES	internal ribosomal entry side
Irx4/5	iroquois homeobox 4/5
lac-Z	β-galactosidase encoding gene

LOF	loss of function
LoxP	locus of cross over P
LV	left ventricle
lvCZ	left-ventricular compact zone
lvRR	left-ventricular reduction ratio
mBT shunt	modified Blalock-Taussig shunt
NA	neoaorta
nEPd	no external phenotype detected
PAA	proximal part of the ascending aorta
p.c.	*post conceptionem*
PCR	polymerase chain reaction
PDA	patent *ductus arteriosus*
PFA	paraformaldehyde
PLE	protein-losing enteropathy
poly-A	polyadenylation
PT	pulmonary trunc
PV	pulmonary valve
pVSD	physiological VSD
Qp	pulmonary perfusion
Qp/Qs	pulmonary-to-systemic-flow ratio
Qs	systemic perfusion
RS	red spots
rTEL	reticular telangiectasias
RV	right ventricle
rvCZ	right-ventricular compact zone
RVOT	right-ventricular outflow tract
rvRR	right-ventricular reduction ratio
SE	subcutaneous edema
TAE	tris base, acetic acid and ethylenediaminetetraacetic acid
Tm-1a	targeted mutation 1a
UMG	University medical center of Göttingen
VEGF	vascular endothelial growth factor
vCZ	ventricular compact zone
vRR	ventricular reduction ratio
VSD	ventricular septal defect
WT	wild type
Wt-1	Wilm's tumor gene 1

1 Introduction

1.1 The hypoplastic left heart syndrome

1.1.1 Definition, epidemiology and historical background

Tchervenkov used the hypoplastic left heart syndrome (HLHS) as a generic term to describe *"a spectrum of malformations characterised by severe underdevelopment of the left heart-aorta complex, consisting of mitral and/or aortic valve* [AV] *atresia, stenosis or hypoplasia with marked hypoplasia/absence of the left ventricle* [LV] *and hypoplasia of the ascending aorta and the aortic arch"* (Cox and Wilson 2007). HLHS is one of the most severe and complex congenital heart diseases (Bradley 1999). It encompasses a hypoplasia of the aortic and the mitral valve and varying degrees of left-ventricular hypoplasia. Because of a broad spectrum of possible anatomic variations, a differentiation between a severe form of HLHS, which encompasses an atresia of the AV and mitral valve combined with a non-existent LV, and a milder form, which is termed hypoplastic left heart complex, is commonly used (Tchervenkov et al. 2006).

HLHS is a lethal disease that necessicates therapeutical interference. Accounting for 25% of all CHD mortalities, HLHS is the leading cause of death in infants under the age of one year (Samánek et al. 1988; Gillum 1994; Bradley 1999). Roger and colleagues stated that HLHS amounts to 4-8% of all cardiovascular malformations (Roger et al. 2011), which is consistent with the findings of Bradley, who proclaimed it accounts for 3.8% of all CHD (Bradley 1999; Risebro and Riley 2006). Sokolowski and colleagues claimed HLHS to amount to 9.1% of prenatally diagnosed CHD (Sokolowski et al. 2019). According to the Baltimore-Washington infant study, the incidence is estimated to 0.16-0.27 per 1000 live births (Ferencz et al. 1985). Samánek and colleagues presented data about the apportionment of age at death of patients who suffer from HLHS without treatment. Most patients (89%) died within the first month of life and 100% had died by the age of ten months (Samánek et al. 1988). Compared to this, Noonan and Nadas published differing data years in advance, where the majority (82%) of infants died by the age of three months (Noonan and Nadas 1958).

The first case of aortic atresia, which was approved to be one morphological feature of HLHS several years later, was reported by Canton in the year 1849, who gave a brief narration about pathological findings (Gehrmann et al. 2001). In 1851, the pathologist Bardeleben published a report about an *"obliteration of the left ostium arteriosum in the heart of a*

half-year-old infant", which included a description about the pathophysiology, anatomical malformations, etiological notions and the clinical manifestations of this disease that found its final naming only 107 years later (Gehrmann et al. 2001). Then, in the year 1958, the pediatric cardiologists Noonan and Nadas were the first authors to use the term HLHS that decribes a variety of structural cardiac anomalies, which share the common feature of an underdevelopment of the left heart-aorta complex (Noonan and Nadas 1958). Even though the term HLHS did occur for the first time in 1958, it was Lev in the year 1952, who first described a series of hearts with an underdevelopment of the LV and an aortic tract hypoplasia, who referred to it as hypoplasia of the aortic tract complex (Lev 1952).

1.1.2 Diagnosis and clinical presentation

Systematic screening for cardiac aberrancies with means of fetal echocardiography enables the prenatal diagnosis of HLHS from as soon as the second trimester of pregnancy (Sokolowski et al. 2019). This positively affects postnatal survival rates (Beroukhim et al. 2015). The assessment of the cardiovascular status and hemodynamical parameters facilitates a severity stratification that directly implies peri- and postnatal treatment strategies, which differ in the degree of therapeutical urgency (Sanapo et al. 2017). Different authors proposed divergent classification systems, such as the emergency neonatal cardiac intervention (Pruetz et al. 2014), the level-of-care groups (Donofrio et al. 2015) or a three-group-based system proposed by Sokolowski (Sokolowski et al. 2019). They all tend to facilitate clinical decision making for treating HLHS patients. Sokolowski and colleagues collated prenatally diagnosed HLHS patients to three groups. The first group (severest HLHS) of highest urgency, with the severest clinical manifestations, necessitates immediate intervention. The second group (severe urgent HLHS) of severe urgency requires cardiac catheterization within 24 hours. In the third group (severe planned HLHS) neonates prove to be relatively stable (Sokolowski et al. 2019). For those HLHS patients that may be related to the third group, the clinical presentation can be asymptomatic at time of birth. Often, no signs of profound cyanosis, respiratory distress or an irregular APGAR score (acronym for appearance, pulse, grimace, activity and respiration) can be found (Noonan and Nadas 1958; Feinstein et al. 2012). Those HLHS patients that prenatally show echocardiographical signs of the severest cardiac impairments are assigned to the first group, where perinatal delivery is marked by rapid clinical deterioration within minutes to hours (Sokolowski et al. 2019).

Not every HLHS patient is prenatally diagnosed (Feinstein et al. 2012). Postnatal physical examination tightly correlates with the pathophysiology of HLHS. The right ventricle (RV) underlies a volume overload, which results in compensatory enlargement of

the heart because of dilation and hypertrophy. Roberts and colleagues described right-ventricular hypertrophy in 46% of patients (Roberts et al. 1976). At palpation of the chest, a prominent right ventricular impulse and decreased or absent peripheral pulses often become apparent (Watson and Rowe 1962). Roberts and colleagues found a soft nonspecific, systolic ejection murmur over the left sternal border to be auscultatorily audible, which occurs because of turbulent blood flowing through a constricting *ductus arteriosus* (DA; Yun 2011). Watson and colleagues explained the occurrence of a holosystolic murmur on the sternal border, which is consistent with tricuspid valve regurgitation, with proceeding dilation of the RV attended by an annular dilation (Watson and Rowe 1962). Furthermore, clinical signs of a pulmonary overcirculation may become apparent as tachypnea, hepatomegaly and gallop rhythm (Connor and Thiagarajan 2007). An aggravating tachypnea may also be a sign for compensation of the metabolic acidosis, which in turn represents a disturbance of the cardiac output (Moodie et al. 1972; Lloyd et al. 1986; Hebra et al. 1993; Kern et al. 1997; Tabbutt et al. 2001; Tworetzky et al. 2001; Stieh et al. 2006; Feinstein et al. 2012).

Transthoracic echocardiography represents the gold standard of diagnostic modalities, which offers a positive predictive value of 96-100% in some centers (Chang et al. 1991; Stümpflen et al. 1996; Bravo-Valenzuela et al. 2018). The parasternal long axis and the apical four-chamber view enable the evaluation of the mitral valve and AV. In case of aortic atresia, the flow pattern in the ascending aorta might be retrograde (Connor and Thiagarajan 2007; Yun 2011; Feinstein et al. 2012; Bravo-Valenzuela et al. 2018). The suprasternal and high parasternal view enable the assessment of the aortic morphology. Furthermore, the apical four-chamber view offers the possibility to assess the tricuspid valve and the possible occurrence of right-ventricular hypertrophy and dilation. The occurrence of endocardial fibroelastosis (EFE) can be diagnosed due to an echo-bright incidence of the left-ventricular endocardium (Shimada et al. 2015). Another diagnostical target is the evaluation of the *truncus arteriosus*. Its pattern of blood flow and indirect signs of pulmonary vascular resistance can be assessed. The evaluation of the patency and the blood-flow pattern of interatrial communication, which is enabled by the subcostal view, is of high therapeutical relevance (Yun 2011; Bravo-Valenzuela et al. 2018). The restriction degree of the atrial septal defect (ASD) represents a crucial point for clinical decision making. A mild restrictive degree of interatrial communication constitutes a beneficial state that attenuates pulmonary overcirculation. Immediate intervention prevents the life-threatening constellation of a highly restricted ASD (Atz et al. 1999; Rychik et al. 1999; Vlahos et al. 2004). Furthermore, low-speed perfusion across the atrial septum is a desirable condition for the postpartal period (Bravo-Valenzuela et al. 2018).

1.1.3 Treatment

1.1.3.1 Postnatal surgical palliation

The treatment of HLHS still is a surgical dominion. HLHS used to be a lethal illness before the period of operative palliation started to emerge in the 1980s (Sinha et al. 1968; Deely et al. 1971; Doty and Knott 1977; Knott and Doty 1977; Behrendt and Rocchini 1981; Norwood et al. 1983).

1.1.3.1.1 Preoperative management

Hemodynamical stabilization, sustainment of the patent *ductus arteriosus* (PDA) and retention of end-organ perfusion are the cornerstones of preoperative management (Tabbutt et al. 2001; Stieh et al. 2006; Feinstein et al. 2012). The rapid decrease in pulmonary vascular resistance endangers circulatory balance. Pulmonary perfusion (Qp) increases at the expense of cardiac output (Johnson et al. 2008). The pulmonary-to-systemic-flow ratio (Qp/Qs) augments, where Qs represents systemic perfusion. Barnea and colleagues accentuated that optimal availability of systemic oxygen can be achieved by a Qp/Qs of smaller than one (Barnea et al. 1994). Shortly after delivery and diagnosing HLHS, an intravenous infusion of prostaglandin E1 is required to maintain the DA patency (Connor and Thiagarajan 2007; Feinstein et al. 2012). As a sign of pulmonary overcirculation, an oxygen saturation around 90% is observed. In the pathophysiological setting of HLHS, too high parameters of oxygen saturation are counterproductive. It indicates that pulmonary hyperperfusion is predominant and the targeted aim of a circulatory balance is not established yet. Ideally, the measured oxygen saturation should decrease to around 80% (Tabbutt et al. 2001). Sedation, which leads to hypoventilation, and the inspiration of nitrogen and carbon dioxide are performed to increase the vascular resistance of the lungs (Shime et al. 2000; Johnson et al. 2008). Hypercarbia increases peripheral oxygen delivery (effect of Bohr). Ramaamoorthy and colleagues presented data that support the utilization of carbon dioxide over nitrogen due to a higher cerebral oxygenation, which results from intracerebral vasodilation because of hypercarbia (Ramamoorthy et al. 2002). Furthermore, Stieh and colleagues reported that the decrease of systemic afterload helps to prevent end-organ damage and in-hospital mortality by reduction of the decisive risk factor of preoperative artificial respiration (Stieh et al. 2006). Adjunct to prostaglandin, milrinone, sodium nitroprusside and phenoxybenzamine are often applied. Showing effects both inotropic and arterial vasodilating, diuretic therapy is of medicamentous concern, where furosemide is commonly used (Johnson et al. 2008).

1.1.3.1.2 Intraoperative management

Two different therapeutical possibilities delineate the operative management of neonates that suffer from HLHS. A continuous contention about the better practice exists (Bailey 2004; Elliott 2004; Chrisant et al. 2005). On the one hand, a three-staged operation presents one option, which shall find further explication below. On the other hand, orthotopic cardiac transplantation displays an alternative, which was first performed by Bailey in the year 1985, where a limited disposability of the donor hearts represents a huge point of restriction (Bailey et al. 1985).

The Norwood procedure represents the first stage of surgical palliation. The hypoplasticity of the LV impedes a proper ventricular function. Therefore, the RV is chosen to take over the support of systemic circulation in a mode of single-ventricle repair (Connor and Thiagarajan 2007). The hypoplastic ascending aorta represents a hemodynamical barrage. That is why, the construction of a neoaorta (NA) is required, which is compiled of the vessel walls of the proximal main-pulmonary artery and the ascending aorta in addition to a goretex mesh that is used for enlargement of the lumen of the NA (Silva et al. 2007). The performance of septectomy, in case no ASD exists, allows oxygenated blood to enter systemic circulation over the NA by an interatrial communication. A regulated Qp is aspired by the establishment of a so-called Blalock-Taussig shunt (BT shunt; Silva et al. 2007; Feinstein et al. 2012). For its construction the right-subclavian artery is connected to the right-pulmonary artery, where nowadays, the modified BT shunt (mBT shunt) is commonly applied. It uses a graft of polytetrafluoroethylene, which varies in its diameter and length, to connect those vessels (Silva et al. 2007; Feinstein et al. 2012). Operative alternatives are the so-called Sano modification and hybrid approaches. The Sano modification uses a RV-to-pulmonary-artery conduit (Frommelt et al. 2007; Silva et al. 2007). Hybrid approaches combine methodical areas of interventional cardiology with cardiothoracic surgery, such as stenting of the PDA or banding of the pulmonary arteries (Galantowicz and Cheatham 2005; Murphy et al. 2015). It bears certain benefits compared to operative approaches, which necessitate cardiopulmonary bypass and cardioplegic arrest (Li et al. 2007).

The second stage of operative treatment is the so-called bidirectional Glenn procedure, which was first drafted by Glenn in 1958. It is normally executed at the patient's age of two until 18 months (Glenn 1958; Ishii et al. 2014; Wilson et al. 2018). Its main purpose lies in the dissipation of the aortico-pulmonary shunt and connection of the superior vena cava with the pulmonary artery. The aim of this stage is to prevent pulmonary overcirculation.

Thereby, the development of pulmonary hypertension and remodeling of the RV shall be avoided (Ishii et al. 2014; Chen et al. 2015).

The so-called Fontan procedure is the third operative step, which was first applied in 1971 to treat tricuspid atresia (Fontan and Baudet 1971). It regularly is explicated at the patient's age of two until four years (Wilson et al. 2018). The ten-year survival of patients that undergo Fontan procedure accounts for 61%, based on a retrospective study by Pundi and colleagues (Pundi et al. 2015). The operative aim is to construct a cavopulmonary connection by linkage of the inferior vena cava to the pulmonary artery. The interposed conduit is fenestrated and connected to the right atrium to commute the venous flow (Hinton and Benson 2012). Survival rates have increased, nevertheless, cardiac arrhythmias, protein-losing enteropathy (PLE) and thrombembolic events are frequently observed complications (Pundi et al. 2015).

1.1.3.1.3 Postoperative management

The three-staged palliation of patients that suffer from HLHS is a mode of single-ventricle repair, which uses the RV to maintain systemic circulation. Management of volume and pressure overload of the RV marks postoperative treatment, which targets unloading of the right-ventricular workload (Hinton and Benson 2012). Frequent complications that occur in the immediate postoperative phase are hypoxemia and a dysbalance in acid-base status, which are crucial to be treated immediately with ventilatory assistance. Since, postoperative alimentation is decisive, the utilization of a nasogastric tube is indicated, if oral application is impossible (Hinton and Benson 2012).

1.1.3.2 Fetal cardiac interventions

Maxwell and colleagues first carried out fetal cardiac interventions (FCI) in the late 1980s (Maxwell et al. 1991; Feinstein et al. 2012). The pathomorphological sequence of an aortic stenosis leading to left-ventricular dilation, which secondarily promotes the occurrence of EFE and finally a hypoplastic LV, represents its therapeutical starting point (Danford and Cronican 1992; Mäkikallio et al. 2006; Selamet Tierney et al. 2007; McElhinney et al. 2009; Feinstein et al. 2012; Shimada et al. 2015). In this intervention, patients that were prenatally diagnosed with severe aortic stenosis during mid-gestation, but did not show EFE yet, undergo fetal aortic valvuloplasty (FAV) to reconstitute biventricular circulation. By doing so, the transition into HLHS is aspired to be prevented (Mäkikallio et al. 2006; McElhinney et al. 2009; Freud et al. 2014). FAV was aspired to become one alternative therapeutical

approach to postnatal surgical palliation (Freud et al. 2014). Despite growing technical expertise, the fetal loss from FCI accounts for 10-15% (Feinstein et al. 2012).

1.1.4 Long-term outcome

To point out the severity of HLHS, the long-term outcome of surgically palliated HLHS patients shall be presented. Freud and colleagues stressed that long-term morbidity still poses a crucial challenge (Freud et al. 2014), where Feinstein and colleagues estimated that 70% of HLHS patients, who underwent the three-staged surgical palliation, reach adulthood with a consecutive decline of survival, once having reached it (Feinstein et al. 2012). The five-year mortality of patients with a cyanotic heart disease that were treated with Fontan procedure accounts for 8.2%, where 30% of those adults with Fontan circulation that die, are assumed to die from sudden cardiac death (Feinstein et al. 2012). Adults with Fontan circulation expose a reduced exercise tolerance and an elevated risk for chronic heart failure, where 10% exhibit a progressive heart failure NYHA class III/ IV (New York heart association functional classification). Frequent complications of adult HLHS patients are PLE, cardiac arrhythmias, hepatopathies, thrombembolism or plastic bronchitis (Feinstein et al. 2012).

HLHS is a disease that offers no causal treatment. Despite of therapeutical advancements, which have been made so far, the limited long-term outcome reflects the necessity to invest more in better understanding of molecular mechanisms, which lead to HLHS, to develop new therapeutical strategies.

1.1.5 Pathophysiology and -morphology

HLHS is a cyanotic CHD, where systemic blood flow depends on the PDA (Cassidy et al. 2015). It belongs to the group of the so-called left-sided obstructive lesions (Yun 2011). Without patency of the DA, no oxygenated blood can enter systemic circulation, which leads to reduced blood flow, hypoxemia, metabolic acidosis, vascular shock and finally, if untreated, exitus (Connor and Thiagarajan 2007; Feinstein et al. 2012). Ductal contraction reduces the volume of blood, which would normally be conducted from the pulmonary trunk to the aorta. Ductal contraction coerces the blood flow to enter pulmonary circulation. As a result, oxygen saturation augments (Connor and Thiagarajan 2007; Vogel et al. 2010; Yun 2011; Tola et al. 2015). In addition, the pulmonary vasculary resistance decreases, which leads to an increase in pulmonary blood flow. As a result, systemic circulation is reduced and atrial pressure increases. Pulmonary congestion and volume overload of the RV are promoted, which potentially induces congestive heart failure (Connor and Thiagarajan 2007). In HLHS,

the LV is non-contributory to the maintenance of systemic circulation because of its hypoplasticity (Freedom et al. 1977; Thiene et al. 1979; Mahowald et al. 1982). The degree of left-ventricular hypoplasia is variable, which can range from ventricular absence to a LV of almost normal dimensions for the body-surface area of the patient (Kanjuh et al. 1965; Thiene et al. 1979; Mahowald et al. 1982; Hastreiter et al. 1983). In HLHS, the LV is frequently found to be associated with EFE (Lurie 2010; Shimada et al. 2015; Xu et al. 2015; Crucean et al. 2017; Graupner et al. 2018). Crucean and colleagues found an association between EFE and HLHS of 70% in 78 specimens (Crucean et al. 2017), where Graupner and colleagues pointed out the negative impairment of the surgical outcome of HLHS patients that expose EFE (Graupner et al. 2018). EFE, which is characterized by an endocardial broadening of elastin and collagen filaments with rarefied vascular and cellular components, prevents the LV from adequately responding to the growing demands of systemic circulation in a developing heart by left-ventricular growth retardation (Friehs et al. 2013; Shimada et al. 2015). Shimada and colleagues gave decided evidence that EFE secondarily occurs as a reaction to distention in the immature LV, which then leads to hypocontractility of a hypoplastic LV (Feinstein et al. 2012; Shimada et al. 2015). In the year 2015, Xu and colleagues published data, which showed that aberrant endothelial-to-mesenchymal transition (EndMT) causes EFE suggesting molecular mechanisms leading to HLHS (Xu et al. 2015). EndMT is a cellular process, where endothelial cells lose their cellular integrity and adopt mesenchymal identity (Zeisberg and Kalluri 2010). Its relevance for physiological and aberrant processes of cardiogenesis will be outlined below. Another pathomorphological hallmark of HLHS is the hypoplasia of the ascending aorta, which is associated with an atresia (or a stenosis) of the AV that allows very little (or no) egress of onward blood flow (Bharati and Lev 1984). A stenotic mitral valve exhibits a gauge of cusps, which is associated with brief and hypertrophic papillary muscles and chordae (Bharati and Lev 1984). In case atresia or stenosis of the mitral valve is featured, the pulmonary venous return is determined to pass a patent *foramen ovale* or a true ASD to connect with the cardiac main output. To refer to several authors, an intact atrial septum occurs up to 10% of patients with HLHS (Mahowald et al. 1982; Weinberg et al. 1986). It is associated with early exitus, in case it is not treated or rare anomalous morphological variations (such as a levoatrial cardinal vein) circumvent it (Daebritz et al. 2000; Hellmund et al. 2017). An association of coarctation with HLHS occured in 75% of all specimens (von Rueden et al. 1975). Several pathologists have affirmed the occurrence of ventricular septal defects (VSD) in around 0.9-14% (Kanjuh et al. 1965; Mahowald et al. 1982; Bharati and Lev 1984; Aiello et al. 1990).

1.1.6 Genetical background

Heritability plays a crucial, but not exclusive, role in the etiology of HLHS (Hinton et al. 2007; Feinstein et al. 2012). Its pathogenesis underlies a multifactorial genetical basis that encompasses aberrant molecular processes and its correlating expression of phenotypes (Mu et al. 2005; Hinton et al. 2007). A causative single-gene mutation was not identified, which is consistent with the generally supposed scheme of polygenetic causation in many types of CHD. Boughman and colleagues stated a recurrence risk for HLHS of 13.5% in siblings (Boughman et al. 1987). According to Hinton and colleagues, first-degree kinsmen exhibit a recurrence risk of 18% for any cardiovascular malformation (Hinton et al. 2007). The pathological finding of a bicuspid AV, which depicts a representative left-sided heart affection, has been most frequently reported in families of HLHS patients. This indicates a genetical relation between the occurrence of these two entities, which was further evidenced by subset-linkage analyses of Hinton and colleagues (Brenner et al. 1989; Loffredo et al. 2004; Hinton et al. 2007). They reported a recurrence risk for first-degree relatives of 3.5% for HLHS (Hinton et al. 2007). HLHS is considered as genetically heterogenous (Hinton et al. 2009). The occurrence of HLHS was found to be linked with several chromosomal disorders in about 10% of all affected patients (Natowicz et al. 1988; Grossfeld et al. 2004), which differs from an incidence of 4.2% reported by Pradat and colleagues, who reviewed three large registries of congenital malformations (Pradat et al. 2003). Most frequently, HLHS was found to be linked with trisomy 21, Turner syndrome, trisomy 18, Jacobsen syndrome and trisomy 13 (Natowicz and Kelley 1987; Jacobs et al. 1998; Tennstedt et al. 1999; Allen et al. 2005; Feinstein et al. 2012). Less prevalently, HLHS is associated with the Rubinstein-Taybi syndrome, Smith-Lemli-Opitz syndrome, Holt-Oram syndrome, Apert syndrome, Noonan syndrome and a diversity of chromosomal deletions and translocations (Natowicz et al. 1988; Morris et al. 1990; Consevage et al. 1996; Jacobs et al. 1998; Allen et al. 2005; Feinstein et al. 2012). A connection to the VACTERL association (acronym for vertebral anomalies, anorectal malformations, cardiovascular anomalies, tracheoesophageal fistula, esophageal atresia, renal and/or radial anomalies, limb defects) was further implied. Furthermore, HLHS was found to be associated with several mutations of genes, such as the cardiac homeobox gene Nkx-2.5, which is known to cause ASD and tetralogy of Fallot (Elliott 2004; McElhinney et al. 2009; Stallmeyer et al. 2010). The connexin-43-gap-junction gene and NOTCH-1, which plays a crucial role in physiological EndMT, are further important (Dasgupta et al. 2001; Risebro and Riley 2006; Iascone et al. 2012). To underline the notion of genetic heterogeneity, a linkage between HLHS to chromosomal loci, such as 6q23 and 10q22, was indicated (Hinton et al. 2009). Unpublished data from the Iascone laboratory

found the gene KIAA0182 to be *de novo* mutated in a child that suffered from HLHS, which caused a T-C-missense mutation in exon 9 of the isoform GSE-1-202. Also unpublished data from Hitz and colleagues showed the occurrence of a cardiac phenotype in zebrafish with a KIAA0182 knockout, which was marked by ventricular size reduction and atrial enlargement. This implies a crucial role of KIAA0182 in cardiogenesis[1]. Moreover, HLHS is frequently associated with EFE, which is caused by aberrantly occurring EndMT (Xu et al. 2015). Many signaling pathways have been shown to be involved in EndMT, such as NOTCH signaling, the vascular endothelial growth-factor (VEGF) and TIE-2 (Lin et al. 2012). Interestingly, KIAA0182 was detected to participate in the complex of the RE1-silencing transcription-factor corepressor (COREST), which was also found to be implied in epithelial-to-mesenchymal transition (EMT), while EndMT depicts one specific form of it (Yokoyama et al. 2008; Lin et al. 2010; Yang et al. 2011; Lin et al. 2012). Therefore, it appears reasonable that KIAA0182 is involved in aberrant molecular processes of the pathogenesis of HLHS.

KIAA0182 depicts a human gene, which features 23 exons, 217 orthologues and 16 transcripts (splicing variants). Among them, eight are protein-encoding with different isoforms of largely uncharted functions. The biggest isoform consists of 1217 amino acids (ncbi.nlm.nih.gov). In the year 1996, the Japanese research group of Nagase and colleagues published data that determined the coding sequences of 40 new genes, which were named KIAA0161 to 0200, among them was the gene KIAA0182 that offers alternating arginine and glutamate motifs (Nagase et al. 1996). To regard the orthologues of KIAA0182, the similarity to mouse accounts for 84.19% and to zebrafish for 60.63% (genecards.org). By offering 16 exons, the second transcript is the largest one with a size of 7495 base pairs (bp). The major difference between the frist and third transcript is missing of the second exon. A leucine-zipper motif was stated to be C-terminal, where the respective protein-encoding gene KIAA0182 was declared to have the cytogenetic location 16q24.1 (ensembl.org/Homo_sapiens; Chai et al. 2016). The gene Gse-1 (genetic suppressor element 1), the orthologue to KIAA0182 in mice, is located on the chromosome 8. It features seven transcripts and is associated with eight phenotypes, which are characterized by abnormal bone mineralization with a decreased bone-mineral density and a decrease of body weight and erythrocyte-cell number. Furthermore, increased circulating levels of alkaline phosphatase and total protein are phenotypically described (ensembl.org/Mus_musculus/Gene/Phenotype). Four out of seven splicing variants are protein-encoding (Gse-1-201, Gse-1-202, Gse-1-203 and Gse-1-206), where isoform Gse-1-201 depicts the largest one (ensembl.org/Mus_musculus/Gene

[1] The author of this doctoral thesis owes these notions (of the aforementioned unpublished data) to verbal remarks of Ms. Prof. Dr. med. E.M. Zeisberg, received in May, 2019

/TranscriptComparison). To consider integrated proteomics, Gse-1 is expressed in monocytes, CD-8 T-cells, natural-killer cells and adult tissue of retina, pancreas, placenta, cervix and testis. To regard fetal tissue, Gse-1 is known to be expressed in heart, liver, ovary and testis (genecards.org). In the year 2016, Chai and colleagues published data of immunohistochemical analyses, which implied Gse-1 to function as an oncogene in breast cancer. Suppressing Gse-1 resulted in a significant reduction of cancer-cell proliferation, migration and invasion. Furthermore, Gse-1 was recognized as a target of miR-489-5p, which was proven to be diminished in breast cancer cells (Chai et al. 2016). A case report, which included Gse-1, was published in the year 2013 that found a small *de novo* duplication (16p24.1) in one patient with a striking clinical phenotype with spastic paraplegia, severe epilepsy, mental retardation, arachnodactyly, malar hypoplasia and an arched palate (Quéméner-Redon et al. 2013). In the year 2012, data were published that emphazised the association between the risk of colorectal cancer and variant alleles of KIAA0182, which are part of a single-nucleotide polymorphisms within 3'-untranslated genetic areas (Landi et al. 2012). In the year 2008, Yokoyama and colleagues published data, which identified the histone-lysine-specific demethylase LSD1 as an interacting candidate of the orphan receptor NR2E1, also known as TLX. LSD1 mediates its transrepressive function in retinoblastoma cells. Among other interactants of TLX was the proline-rich protein KIAA0182 of uncharted function (Yokoyama et al. 2008). Hakimi and colleagues have shown five years in advance, that LSD1 interacts with KIAA0182 (Hakimi et al. 2003). Furthermore, LSD1 is part of many protein complexes, such as COREST (Yang et al. 2011). The tenary complex of LSD1, COREST and SNAIL1 is implied in EMT, where the process of EndMT depicts one form of it. In EMT, SNAIL1 was identified as a key-regulatory protein. COREST was shown to function as an enhancer of the stability of the tenary complex (Lin et al. 2010). Gse-1 is involved in the formation of circular RNA (circRNA), whose function is largely unknown (Memczak et al. 2013). Memczak and colleagues published data that allocate the function of post-transcriptional regulators to circRNA, which exhibits a *"mi*[cro]*RNA-binding capacity"* that is *"ten times higher than* [in] *any other known transcript"* (Memczak et al. 2013).

1.2 Cardiac development

1.2.1 Human cardiogenesis

Human cardiogenesis starts at the third week of development (estimated gestational age [EGA]) with a process known as gastrulation (Moorman et al. 2003), where the germ layers obtain their embryonic position. They consist of the ectoderm, the endoderm and the mesoderm. The last-mentioned contributes to the formation of the so-called cardiac crescent that simultaneously arises to the neural plate, which consists of ectoderm (Moorman et al. 2003). Different cell types populate the cardiac crescent, among others, promyocardial cells and endothelial strands. They contribute to the morphogenesis of the heart tube that is partially composed of an endocardial tube, which in turn enables the communication of the growing heart with a circulatory system (Moorman et al. 2003). Within the newly formed pericardial cavity, the endocardial tube is coated by myocardial cells. Looping of the heart tube represents the next procedural step, whose initiation is a requirement for chamber morphogenesis. It is the first asymmetric event during cardiogenesis, which occurs at around four weeks EGA (Moorman et al. 2003). The event of chamber formation is composed of simultaneously occurring ventricular and atrial morphogenesis, where the last-mentioned depends on the formation of the lungs. The pulmonary veins, which emanate form the pulmonary vascular plexus that surrounds the lung buds, connect with the heart tube's primary atrial component (Moorman et al. 2003). The formation of the ventricles advances by curvature ballooning of the heart loops apical part, where the atrio-ventricluar canal walls join the LV (Moorman et al. 2003). From day 48 until day 66 EGA, EndMT promotes valvular morphogenesis. The refinement of the semilunar and atrioventricular valves (AVV) occurs from day 56 EGA onwards (Krishnan et al. 2014; Gong et al. 2017). EndMT is known to contribute to crucial cardiogenetic events, such as the formation of the valves and the septum, but also pathogenetical processes like cardiac fibrosis (Person et al. 2005; Krenning et al. 2010). The process of septation, where the atrioventricular and ventricular septum is formed, occurs from eight until nine weeks EGA in human cardiogenesis (Krishnan et al. 2014).

1.2.2 Cardiogenesis in mice

The transferibility of cardiogenesis in mice to humans legitimates animal research in mice. Simplifyingly, mammalian cardiogenesis can be itemized into a multi-step process. Fate determinition of cardiomyocytes and their further specification, morphogenesis of the cardiac tube, formation of the heart loop, chamber maturation, morphogenesis of the vavular

structures from endocardial cushion tissue (ECT) by EndMT, the process of atrial and ventricular septation, myocardial compaction and valvular refinement will be explicated (Bartman and Hove 2005; Zhang et al. 2013; Krishnan et al. 2014). Among others, the descriptive attention will be drawn to a few selected cardiogenetic events, such as chamber maturation with the processes of trabeculation and compaction. **Figure 1** gives a simplified overview of the major cardiogenetic events, which are explicated in the continuous text.

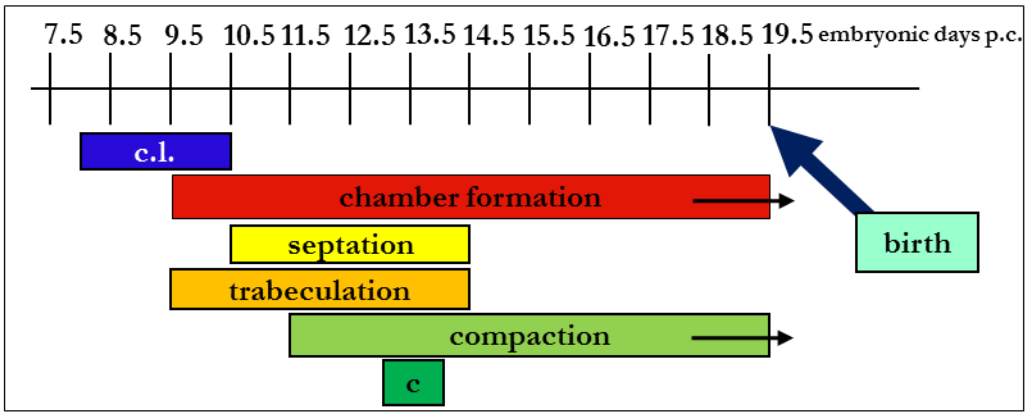

Figure 1: Timeline of important developmental events during cardiogenesis in mice; Legend: c: significant increase of compaction from E13 p.c. to E14 p.c., **p.c.:** *post conceptionem*; Events are highly simplified to four events, which allows a quick overview. Modified after Dhanantwari et al. (2009);

1.2.2.1 The primary and secondary heart field and the heart-tube formation

At an early developmental age in mice around E7 *post conceptionem* (p.c.), the heart begins to develop. An embryonic structure called primitive streak is populated by cardiac precursor cells of the primary heart field, which forms the cardiac crescent at E7.5 p.c. (Risebro and Riley 2006). Dorsally and medially to it, the second lineage is localized, which depicts a cardiogenic area from an additional population of pharyngeal mesoderm cells (Kelly and Buckingham 2002; Risebro and Riley 2006; Dyer and Kirby 2009). At around E8 p.c., the invading endoderm induces the tubular heart formation in the anterior lateral mesoderm by migration and fusion of progenitors of the primary heart field at the ventral midline of the embryo. Extracellular matrix (cardiac jelly) represents the formating basis for the juxtaposition of single-cell laminas of myocardium and endocardium (Bartman and Hove 2005; Risebro and Riley 2006; Zhang et al. 2013). The linear heart tube, which is connected to the thoracic wall by the dorsal mesocardium, is the originator of contractive waves (de Jong et al. 1992; Lamers and Moorman 2002; Risebro and Riley 2006). Retrospective clonal analysis is a biochemical method based on spontaneous mitotic recombination that utilizes an inactivated lac-Z-reporter gene. By means of it, it was revealed that the colonization of progenitor cells from both the primary and secondary heart field equally contribute to the

formation of the heart tube. In contrast to that, the outflow tract, which originates from the second lineage and the LV, obtains its cellular sources from the primary lineage (Meilhac et al. 2004; Risebro and Riley 2006). Conflictingly to these findings, genetic fate-mapping studies have implied that the cellular sources of the LV are not exclusively restricted to the primary lineage, but also originate from the secondary lineage (Verzi et al. 2005).

1.2.2.2 Cardiac looping

At embryonic age E8.25 p.c. until E10.5 p.c., rightward looping represents the next procedural step during cardiogenesis. Synchronically, the second cardiac lineage has a share in the formation of the venous and arterial pole of the heart by precursor migration of the second lineage (Risebro and Riley 2006). The fact that it occurs in every species of the vertebrates underlines the outstanding decisiveness of this event (Risebro and Riley 2006). Cardiac looping enables vascular positioning and ventricle formation. At the ending of this process, the atrioventricular canal forms the prospective LV. It is connected to the outflow area that will evolve into the great cardiac vessels and the inflow region, which is interlinked with the atria (Risebro and Riley 2006). CHD such as VSD or double outlet RV (DORV) can be attributed to aberrancies during cardiac looping with an ineligible outflow-tract formation or an incorrect connection of the vessel level and the ventricular septum (Risebro and Riley 2006). Several researchers have contributed to the revelation of molecular keyplayers in the event of cardiac looping with mouse models for loss of function (LOF). During the complex process of cardiac looping, several genes play decisive roles. Important representatives are the myocyte-specific enhancer factor 2C (Mef2c), the fibroblast growth factor (Fgf), the heart and neural crest derivatives-expressed protein 1 (Hand1), the gene Nkx-2.5 and the forkhead box protein H1 (FoxH1; Lyons et al. 1995; Lin et al. 1997; Linask et al. 2002; Dodou et al. 2004; von Both et al. 2004; Verzi et al. 2005).

1.2.2.3 Septation and valvulogenesis

The process of septation enables the formation of a definite two-sided heart. The processes of atrial, atrioventricular and ventricular septum formation can be distinguished by their own cellular characteristics (Anderson et al. 2003). Occuring between E10.5 p.c. and E14.5 p.c. in the mouse embryo, septation promotes the cardiac function of unidirectional blood circulation (Risebro and Riley 2006). Synchronically to cardiac looping and chamber morphogenesis, the formation of the interventricular septum (IVS) starts in the heart tube (Lamers and Moorman 2002). The abovementioned processes of EndMT and EMT are considered to play major roles by enabling cell transformation with the groundwork of ECT

to promote morphogenesis of membranous septa and valves (Kinsella and Fitzharris 1980; Eisenberg and Markwald 1995; Person et al. 2005; Risebro and Riley 2006; Zhang et al. 2008; Lin et al. 2012). Valve precursors colonize ECT, where the last-mentioned are progressed into valve formation by EndMT (Person et al. 2005). EndMT was further shown to play an important role in embryogenetic and neoplastic events, such as tumor progression and malignant transformation (Lin et al. 2012).

1.2.2.4 Chamber formation

The morphogenesis of chambers is promoted by formation of the *bulbus cordis* (BC). To cope with the increment in volume load, which enables oxygen and alimentary supply in the developing embryo, chamber maturation progresses by advancing ventricular septation, trabeculation and compaction (Risebro and Riley 2006). Extensive studies have been performed to examine the expression patterns of certain transcrpition factors, which proved to be chamber-specific. For instance, Hand1 is specifically expressed in the LV, where Hand2 prevailingly shows expression patterns in the RV (Srivastava et al. 1997). Christoffels and colleagues proposed a two-step model for chamber formation, which challenged and even rejected the predominant conception of a linear heart tube as an array of segments (Stalsberg 1969; Anderson et al. 1978; de la Cruz et al. 1989). Christoffels and colleagues performed in-situ hybridization with rat embryos to study gene expression in the developing heart, which led to the revision of the former conception and to common acceptance of the two-stepped ballooning model (Risebro and Riley 2006). The first step deals with the generation of a primary transcriptional signature, which is associated with the linear heart tube and the cardiac crescent. It is polarized along the anteroposterior and dorsoventral axes. The second step embraces the establishment of the secondary transcriptional program that is linked to the chambers of the heart (Christoffels et al. 2000). The primary transcriptional pattern is executed in the inflow and outflow tract, the atrioventricular canal and the inner curvature of the developing heart. The second transcriptional program is found to be active in the outer curvature of the looping heart that enables the chamber myocardium to balloon out. Expressed genes, such as the atrial natriuretic factor, Chisel, iroquois homeobox 5 (Irx5) and upregulated transcription factors like the sarcoplasmic reticulum-calcium ATPase 2a, Mlc2v and Irx4, were analyzed by in-situ hybridization that led to the assumption of side-specific morphogenesis of the chamber myocardium (Christoffels et al. 2000). This notion is further supported by regional differences in clonal growth found by other researchers. The LV finds its mophology by bulging out of the outer curvature, where the RV is shape-defined by tubular enlargement (Meilhac et al. 2004; Risebro and Riley 2006).

1.2.2.5 Ventricular trabeculation and compaction

At early midgestational age, the invagination of endocardial cells in addition to cardiomyocytes, which protrude into the lumen, facilitates accretive myocardial trabeculation. The exterior layers of cardiomyocytes give rise to progressive myocardial compaction (Zhang et al. 2013). The decisive role of endothelial induction of this process is widely accepted (Stainier et al. 1995; Liao et al. 1997). Extensive studies have been performed, which imply the importance of reciprocal interaction between the endo- and myocardium. To name representative signaling molecules, neuregulin, serotonin 2B and angiopoietin 1 proved to be important for the communication between the endo- and myocardium (Gassmann et al. 1995; Lee et al. 1995; Meyer and Birchmeier 1995; Sato et al. 1995; Suri et al. 1996; Miquerol et al. 1999; Puri et al. 1999; Nebigil et al. 2000). Trabecular expansion occurs via myocytical proliferating or recruiting, where trabeculation was suggested to be a means to cope with the increasing force demand of a growing heart. It enables oxygen and alimentary supply from E9.5 p.c. until around E14.5 p.c. (Sedmera et al. 2002; Risebro and Riley 2006; Zhang et al. 2013; Captur et al. 2016). By E14.5 p.c., myocardial compaction is completed (Sedmera et al. 2002; Risebro and Riley 2006; Zhang et al. 2013). Moreover, the occurrence of trabeculated myocardium is associated with a progressive replacement of cardiac jelly (Blausen et al. 1990). The regulation of cardiac jelly plays an important role in atrial chamber morphogenesis, which remains poorly understood compared to ventricular chamber formation (Kim et al. 2018).

Signaling of bone-morphogenic protein 10 (Bmp-10), which is important for atria formation after E13.5 p.c., was proven to be crucial for trabeculation between E9.0 p.c. and E13.5 p.c., where Bmp-10-deficient mice die around E10.5 p.c. because of insufficient trabecular growth (Chen et al. 2004). Mammalian hearts expose a morphological difference between right- and left-ventricular trabeculae (Risebro and Riley 2006). Among vertebrate species, differences in the trabecular morphology are statable with regard of human, rodents, avian and fish hearts, where humans expose right- and left-ventricular distinction concerning the myocardial width (Webb et al. 1996). Apical and basal disparities are observable in mammals and birds, in contrast to fish hearts that do not regionally differ in terms of an apical-to-basal axis (Hu et al. 2000). The process of trabeculation advances at a late midgestational age, where the major part of trabeculated myocardium becomes compacted by solidifying towards the ventricular wall. Thereby, it progressively takes over the function of contractile force supply (Sedmera and Thomas 1996; Hu et al. 2000; Zhang et al. 2013).

Induction of myocardial compaction is observable around E11.5 p.c., where a significant increase in ventricular compaction width with augmenting structural complexity is detectable at E13 p.c. to E14 p.c. (Wessels and Sedmera 2003; Risebro and Riley 2006). Several molecular keyplayers have been found to play a decisive role in the complex event of myocardial compaction. In the year 1993, two independent research groups from Japan and Canada demonstrated the importance of the transcription factor N-myc for the development of compacted myocardium (Moens et al. 1993; Sawai et al. 1993). N-myc is crucial for an advanced development of compacted ventricular layers in terms of expansion and interventricular septation, since N-myc-deficient mice expose severe defects in those categories and die around E10.5 p.c. (Moens et al. 1993; Sawai et al. 1993). Kokoszka and colleagues characterized ventricular non-compaction as "*the persistence of multiple prominent ventricular trabeculations and deep inter-trabecular recesses*" (Kokoszka et al. 2016). The complications that occur due to non-compaction in adult and in embryonic hearts are diverging. In adult humans, non-compaction exhibits a relatively broad pathological spectrum. It ranges from sudden cardiac death to a mild form of left-ventricular non-compaction that is typically marked by a triad of cardiac arrhythmias, the appearance of mural thrombi and heart failure. Often, it remains underdiagnosed (Waller et al. 1980; Wessels and Sedmera 2003; Jenni et al. 2007; Luxán et al. 2016; Choquet et al. 2018; Huang et al. 2018). In a review, Risebro and Riley stated that mice, which exhibit defects in myocardial compaction, usually die around E14 p.c. from congestive heart failure. This underlines the crucial function of effectual compaction during cardiogenesis (Risebro and Riley 2006). Sedmera and colleagues studied cellular changes, which occur because of left-atrial ligation in an embryonic HLHS-chick model (Sedmera et al. 2002). Embryonic cardiomyocytes are capable of proliferation-rate autoregulation, which adapts to mechanical requirements. It depicts the cellular basis for responsiveness to functional loading of the heart (Sedmera et al. 2002; Risebro and Riley 2006). Communicative signaling between compacted and trabeculated myocardium is another important process contributing to adequate chamber maturation in terms of trabeculation and compact-zone formation (Risebro and Riley 2006). In the HLHS-chick model, the interaction between mechanical loading and expanding of the LV is disturbed. This results in a hypoplastic LV with a striking reduction of ventricular volume (Sedmera et al. 2002; Risebro and Riley 2006). However, the transferability of the findings in chick embryos to human remains to be elucidated.

Synchronically to the process of compaction, the heart develops with respect to coronary vasculogenesis and interventricular septation, where the coronary development underlies a gradient from epi- to endocardium and from basis to apex (Pignatelli et al. 2003;

Risebro and Riley 2006). Regarding transmembrane type semaphorin 6D, which interacts with plexin A1, avian heart studies provided insights to the regulation of myocardial cell motility in analogy to its function in axonal guidance (Bashaw et al. 2000; Toyofuku et al. 2004). Many LOF-mouse models that presented the non-autonomous cell function of several genes have underlined the importance of the intricate interplay between myo- and epicardium. Mutant mice for Wilm's tumor gene 1 (Wt-1) are characterized by a thinned ventricular compact zone (vCZ) implying a non-autonomous cell function in contrast to the aforementioned N-myc, which participates in Notch signaling (Kreidberg et al. 1993; Moens et al. 1993; Sawai et al. 1993; Luxán et al. 2016). Among others, Wt-1 shows epicardial expression patterns (Kreidberg et al. 1993).

1.3 Mutagenesis strategies and Gse-1 mice

In the year 2003, the human genome project was declared completed after having unravelled the base sequence of the human genome, which enabled identifying about 20000 to 25000 genes in the human deoxyribonucleic acid (DNA; genome.gov). Deciphering the DNA sequence depicted a major step towards the elucidation of the biological functionality of the mammalian genome. But taken for itself, it is insufficient to explain cellular functionality of single genes. Facing a multidimensional complexity of intracellular molecule interactions has led to the development of diverse approaches to generate clear correlations between a gene and its biological function. Monogenetical diseases, such as sickle-cell anemia or cystic fibrosis, provided the principle of correlation between a single-gene mutation and its respective phenotype, where few diseases exhibit a monogenetical causation. It has been aspired by researchers to transfer this principle to animal models, which enable the inclusion of single-gene mutations in biological organisms. Biomolecular techniques, such as mutagenesis, allow a relatively targeted distraction of a cellular system on the level of genetic transcription. The possibility to produce mutations (by circumscribed controllable methods) represents a powerful implement of understanding the pathogenesis and evolution of many human diseases.

1.3.1 Gene trapping

The advent of gene trapping represents the transition between randomly and precisely defined mutations (Stanford et al. 2001). The introduction of a trapping vector can either be performed by retro-viral transfection or by electroporation, which is mostly leading to random genomic integration (Li and Zhang 2006). This method found its modification in

the species *drosophila melanogaster* and the mouse (Stanford et al. 2001). Three types of vectors presented the basis for gene trapping (gene-trap, enhancer and promoter vectors), where each one exhibits a profile of features, which originally was used for mutagenesis of embryonic stem (ES) cells (Stanford et al. 2001). Enhancer-trap vectors function to trap diverse loci by being juxtaposed to a cis-acting enhancer element, which favors expression of the lac-Z-reporting gene (Gossler et al. 1989). Seldomly, this method was found to be associated with LOF mutations in mice, which are highly requested. Promoter-trap vectors usually are constructed of a reporting gene, which is promoterless. It enables the function of selection in case of successful insertion (Stanford et al. 2001). Exonic insertions are commonly acquired with promoter-trap vectors because of their molecular construction. Therefore, promoter-trap vectors seldomly expose hypomorphic mutations, but show a lower frequency of vector insertion than enhancer traps (Stanford et al. 2001). Gene-trap vectors are characterized by fusion-transcript generation, which consists of the reporter gene and the upstream-coding sequence that enables the coincidental mutation of a gene. Since the occurrence of intron insertions lies at hand, one great detriment is the sporadic occurence of hypomorphic alleles (Stanford et al. 2001).

1.3.2 Knockout-first allele of Gse-1 mice and previous results

Depicting a modification of gene-trap vectors, the knockout-first allele, referred to as targeted mutation 1a (Tm-1a), was designed to provide a Gse-1 knockout on transcription level from the beginning on without further breedings (compare **figure 2**). Our research group acquired a mouse model based on the knockout-first Tm-1a allele with ES cells provided by the European conditional mouse mutagenesis program (EUCOMM). It systematically aims to provide ES cells of mutant mice on black-6N-genetic background for further research purposes to generate a library of protein-encoding genes and their correlating function. The EUCOMM is a member of the international knockout mouse consortium (IKMC), which consists of four great members and features the former mentioned core principles of the EUCOMM (mousephenotype.org). Being translated from the largest isoform Gse-1-002, the generated protein is supposed to be truncated, including the first 85 amino acids of the wild-type (WT) protein. The Tm-1a allele contains a triad of casettes with an engrailed 2 splicing acceptor (En2 SA), an internal ribosomal entry side (IRES) and a polyadenylation (poly-A) signal for termination of the transcription. It allows reporting of gene expression synchronically to terminating gene transcription of the targeted Gse-1 gene. The lac-Z casette encodes for the enzyme β-galactosidase, which enables a gene

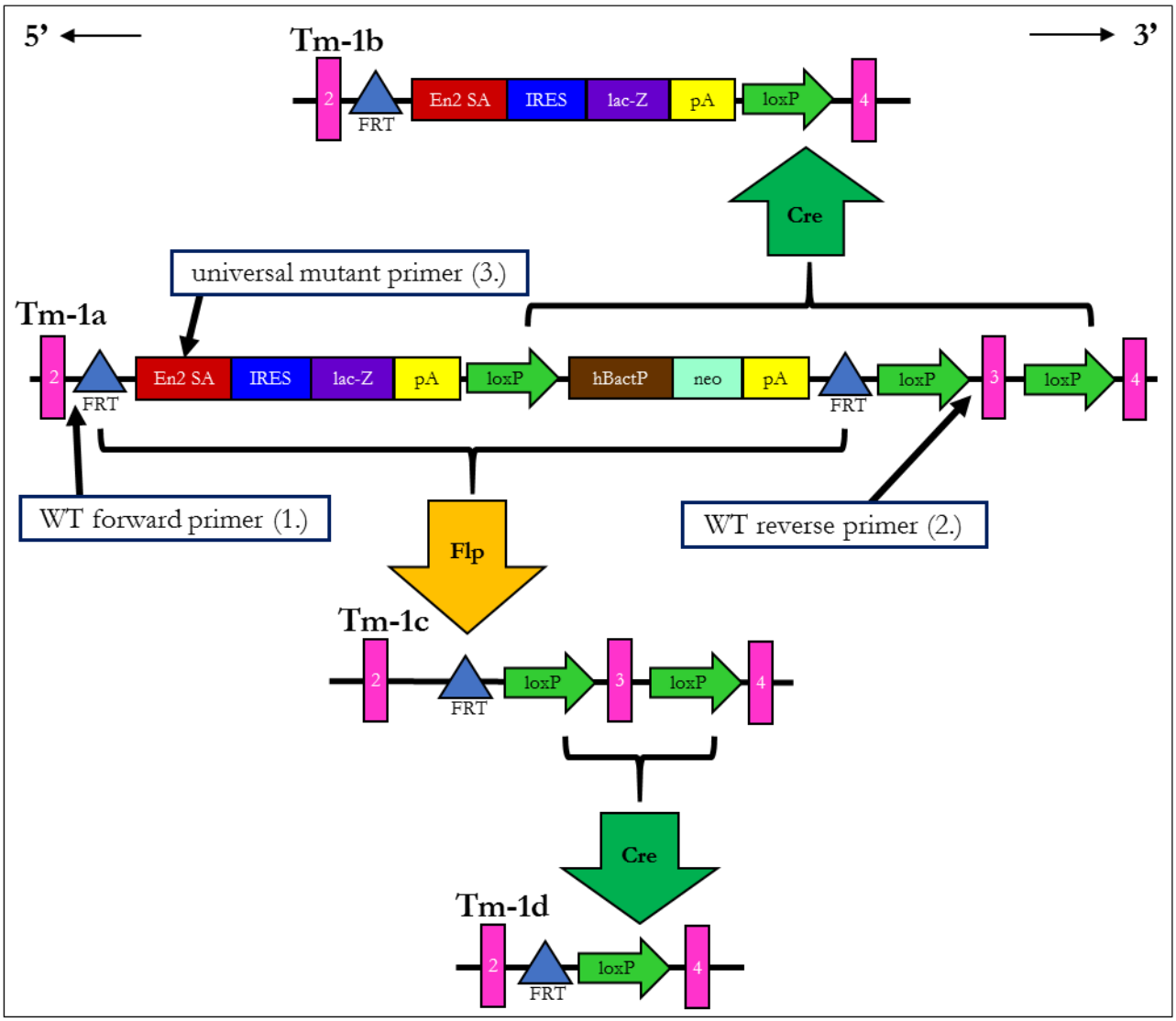

Figure 2: **Schematic of the knockout-first allele Tm-1a, its changeover in Tm-1b, Tm-1c and Tm-1d and the annealing positions of the three genotyping primers; Legend: Cre:** cyclisation recombinase, **En2 SA:** engrailed 2 splicing acceptor, **Flp:** flanked with loxP, **FRT**: Flp-recognition target, **hBactP:** human β-actin promoter, **IRES:** internal ribosomal entry side, **lac-Z:** β-galactosidase, **loxP:** locus of cross-over P, **neo:** neomycin, **pA:** polyadenylation-termination signal, **Tm-1a-1d**: targeted mutation 1a-1d; This schematic shows the design of the knockout-first allele Tm-1a, whose casettes offer different functions, which are explained in the continuous text. The Tm-1a allele corresponds to the isoform Gse-1-002. Three primers were used for genotyping Tm-1a mice: a WT forward primer (1.), a WT reverse primer (2.) and an universal mutant primer (3.). Modified after Skarnes et al. (2011) and knockoutmouse.org;

reporting function. The third exon of the isoform Gse-1-002 is flanked by two surrounding LoxP sites, which stands for locus of cross-over P. Therefore, the third exon is floxed (flanked by LoxP). After the En2SA/IRES/lac-Z casettes, a floxed triad of casettes follows, which consists of a promoter driven casette for the human β-actin autologous promoter (hBactP), a neomycin-resistance cassette, which is further followed by a poly-A-termination signal. The first and second triad of casettes is flanked by sites for the flippase-recognition

target (FRT) that enable rearrangement by the flippase (Flp) recombinase (Skarnes et al. 2011). When breeding Tm-1a mice to Flp-expressing mice, a conditional allele can be obtained, which is referred to as Tm-1c. It restores gene activity. This further can be converted into a null allele with an excision of the third exon that generates a frameshift mutation (Tm-1d) by breeding Tm-1c mice with mice that express a cyclisation recombinase (Cre). When breeding Tm-1a embryos directly to Cre-expressing mice, a lac-Z-tagged null allele can be achieved, which is called Tm-1b (compare **figure 2**; Skarnes et al. 2011; Ryder et al. 2014).

In a previously performed study by Alnour, heterozygous Gse-1 mice were mated and genotyping of their pubs was performed based on two protocols. Quality controls to affirm correct targeting of Gse-1 were performed by long-range and short-range polymerase chain reaction (PCR). Genotyping results of 134 newborn mice by three weeks of age from 23 litters showed that no homozygous mice were maintained, which strongly indicated embryonic lethality of Tm-1a homozygosity. With an expected Mendelian ratio of 1:2:1, the chi-square test offered a p-value of less than 0.0001 and a g-power of 99.999%. Genotyping of newborn mice from mating WT and heterozygous mice showed no significant deviation from the Mendelian ratio of 1:1 with a p-value of 0.125, which implied no lethal effect of Tm-1a heterozygosity (Alnour 2016).

1.4 Objective of this study

As described above, the overall aim of this study is to elucidate molecular mechanisms of HLHS. Based on a) the documented *de novo* mutation of KIAA00182 (analogue to Gse-1 in mice) in a child with HLHS and b) the documented lethality of homozygous Gse-1 mice by three weeks of age, the objectives were the following:

1. identify the timepoint of lethality in homozygous Gse-1 mice
2. analyze if a cardiac phenotype is present in homozygous Gse-1 mice

2 Experimental procedures and materials

2.1 Experimental procedures

2.1.1 Generation of Tm-1a mice

Mice were generated from ES cells provided by the EUCOMM, where the number of the project is 71610 and the number of the cell clone is EPD0557-2-C07 (knockoutmouse.org). All mice were maintained on black-6-N background. The allele (Gse-1$^{tm\text{-}1a(EUCOMM)Wtsi}$) has the previously described knockout-first design (compare **figure 2**). It was inserted in the gene region of Gse-1 by homologous recombination. This construct is designed to disrupt gene function on the transcriptional level. The provider has performed quality-control tests, including southern blotting, karyotyping, LoxP-sites confirmation, 3'- and 5'-end long-range PCR (knockoutmouse.org). The local animal-experimental committee of the University medical center of Göttingen (UMG) approved all animal experiments that were performed. The usage of all animals was conducted in accordance with the institutional guidelines. Furthermore, the mice received humane care (food and water supply *ad libitum*) and housing under standard conditions in the animal facility of the UMG.

2.1.2 Timed matings

To investigate potential developmental defects that lead to embryonic lethality, homozygous Tm1-a embryos were generated by mating heterozygous Tm1-a mice. Timed matings were arranged for the developmental days E11.5 p.c., E13.5 p.c. and E15.5 p.c. The appearance of a vaginal plug was designated as embryonic day E0.5 p.c. The pregnant mouse was fed with food and water based on the institutional guidelines for humane animal care. The weight of the mouse was gauged daily.

2.1.3 Dissection of embryos and labeling with identity number

Harvesting of embryos at the developmental timepoints E11.5 p.c., E13.5 p.c. and E15.5 p.c. was performed. Therefore, pregnant mice were anesthetized with isoflurane and laired on their abdomen. The mice were put to death by cervical dislocation in a dignified manner. After having turned them backwards, the abdominal cavity was disclosed by cutting open the abdominal wall. Both uterine horns were dissected in an attentive way. They were put into Dulbecco's phosphate-buffered saline. Embryos were separated from the layers of the

uterus, placenta, amnion and yolk sac. The number of the somites confirmed the embryonic age for early ages (E9.5 p.c. to E11.5 p.c.). Each embryo was labeled with an individual number of identity (in the following referred to as embryo ID) by the following scheme of y.x, where y depicts the three-figured number of identity of the maternal mouse and x is the ID number of the embryo. The y number indicates the fact that embryos are from the same litter. The succession of the labeling represents the order of embryonic dissection.

2.1.4 Morphological examination

Tissue samples, mostly the left-sided limbs, were extracted. Tm-1a embryos were photodocumented from both sides with a microscope (*Zeiss SteREO Lumar. V12*) and the respective program (*Axio Vision Rel 4.8*). The remnant embryo was fixated in 4%-paraformaldehyde (PFA). Tissue extractions were deep-frozen in liquid nitrogen. They were further utilized for the extraction of DNA.

2.1.5 Genotyping

2.1.5.1 Extraction of desoxyribonucleic acid

2.1.5.1.1 From freshly frozen tissue

Using the standard manufacturer's protocol, DNA extractions from freshly frozen tissue were performed with a commercial kit (*DNeasy Blood & Tissue*) by Qiagen. Tissue samples were incubated for 12 hours at 56 °C in a solution that contained lysis buffer and proteinase K (a serine protease from the fungus *engyodontium album)*, which led to cell lysis and DNA liberation. Subsequently, an ethanol precipitation was carried out. Several steps of centrifugation were performed to further purify the genomic DNA. To finish DNA extraction, a buffer was added to elute the DNA into a microcentrifuge tube. Subsequent measurements of the concentration were performed. The genomic DNA was stored at 4 °C.

2.1.5.1.2 From formalin-fixed, paraffin-embedded tissue

Using the standard manufacturer's protocol, DNA extractions from formalin-fixed, paraffin-embedded (FFPE) tissue were performed with a kit (*QIAamp DNA FFPE Tissue*) by Qiagen. Eight sections of an embryo-containing paraffin block were produced with the respective thickness of 5-8 µm. The first step is depicted by deparaffinization of the FFPE tissue with xylene. After having lysed the cells with a solution that contains lysis buffer and proteinase K, the samples were incubated at 90 °C to foster the cancellation of formalin crosslinks. To eradicate the contaminating components of the lysate, the DNA binded to a positively

charged membrane, where the contaminants seeped through the pores of the membrane. In several washing steps, the DNA was purified. To complete the extraction, the DNA was eluted with a buffer. After having subsequently measured the concentration, the DNA-containing solution was stored at 4 °C.

2.1.5.2 Polymerase chain reaction

To perform PCR, a solution was generated that had a reaction volume of 25 µl. It contained 0.3 µl taq-polymerase, 2.5 µl of a taq-polymerase-compatible buffer (ten-fold), 2.5 µl of a magnesium-chloride solution (25 mM), 1 µl of a desoxynucleotide-containing solution (2 mM), 50-100 ng of the genomic DNA, 20 µM of each primer, 0.5 µl of dimethyl sulfoxide and the differential volume of nuclease-free water. All PCRs were performed with 35 cycles. One cycle was arranged as follows: phase 1: 95ºC for ten min., phase 2: 95ºC for 15 sec., 60ºC for 30 sec., phase 3: 72ºC for 30 sec., 72ºC for eight min. Phase 2 was repeated 32 times, one cycle was finished with a holding temperature of 8ºC. The primer's sequence will be enlisted below (compare **table 3**). A triad of primers (Gse-1-5arm-WTF [1.], Gse-1-crit-WTR [2.] and Tm1a-5mut-R1 [3.]) was utilized for genotyping Tm-1a mice. Two PCR products were achieved. The first amplicon (WT band) with a size of 241 bp was obtained with the pair of primers WT forward (Gse-1-5arm-WTF [1.]) and WT reverse (Gse-1-crit-WTR [2.]). Gse-1-5arm-WTF (1.) anneals to the 5'-homology arm and Gse-1-crit-WTR (2.) anneals to the 3'-homology arm (compare **figure 2**). Because of the design of the Tm-1a allele, no PCR product is achieved in homozygous specimens, because the amplicon would be too big to be obtained under the former mentioned reaction conditions. Therefore, homozygous specimens show no WT band of 241 bp. The second amplicon offers a size of 127 bp, which is obtained with the primer pair of the universal mutant primer (Tm-1a-5mut-R1 [3.]) and the WT forward primer (Gse-1-5arm-WTF [1.]), where the third primer is set at the location before the first FRT site (compare **figure 2**). Because of the alellic set-up, WT embryos offers no annealing of the primer Tm-1a-5mut-R1, therefore, WT specimens do not expose a mutant band of 127 bp.

2.1.5.3 Agarose gel electrophoresis

The sizes of the maintained PCR products for the Tm-1a allele account for 241 bp and 127 bp. To visualize the amplified PCR product, a 3%-agarose gel was prepared. Therefore, 200 ml of a buffer, which contains tris base, ethylenediaminetetraacetic acid and acetic acid (TAE), was mixed with 6 g of agarose powder. It was boiled in a microwave for five min. A SYBR-containing gel stain was added in an attenuation of 1:10000 and equally distributed. Each gel pocket was filled with a volume of 15 µl of the PCR product and 5 µl of a six-fold

loading dye. Furthermore, to identify the size of the amplicon two DNA ladders were additionally added into separate gel pockets. Finally, the gel chamber (containing the loaded gel and TAE buffer) was left to run for 15 min. with 80 Volt and then approximately 45 min. with 120 Volt. The image of the gel was documented with the special equipment for image acquisition (*BioDocAnalyze*) to identify the genotype of the embryos. WT genotype offered one band of 241 bp, homozygous genotype produced one band of 127 bp and heterozygous genotype yielded both bands.

2.1.5.4 Statistical analysis

The acquired genotyping results were statistically analyzed with the chi-square test. The Mendelian ratio of 1:2:1 (WT: heterozygous: homozygous) of heterozygous Tm-1a breedings constitutes the expected quantities. P-values under 0.05 were considered to be statistically significant.

2.1.6 Histological methodology

2.1.6.1 Fixation of embryos

The entire embryos were fixated with 4%-PFA at 4°C for at least 24 hours. Alternatively, a fixation with a commercially acquired, acidfree, phosphate-buffered solution containing 4%-formaldehyde (*Roti Histofix 4%*) was applied.

2.1.6.2 Dehydration and ascending ethanol gradient

To prepare the embryos for paraffin embedding, the fixed embryos were put under slowly flowing tab water for 12 hours. They were dehydrated by using an ascending ethanol gradient (20%, 40%, 60%, 80%, 90%, 96% and 100%). After having gone through this ascending ethanol gradient, each for a duration of 30 min., the embryos were treated with xylene to proceed to paraffin embedding.

2.1.6.3 Embedding and orienting embryos in paraffin wax

Before cooling down the paraffinized embryos in a block of paraffin wax, one had to consider the proper orientation of the embryos. Depending on the mode of sectioning, i.e., whether the histology should be in line with transverse or sagittal sections, the embryos were oriented in the paraffin block. Each embryo of the identical litter was oriented in the same way to guarantee the same mode of sectioning for all embryos. Long-term storage of the paraffin blocks was carried out at room temperature.

2.1.6.4 Serial sectioning

Before producing serial sections, the paraffin blocks were cooled down at 4 °C for four hours to alleviate cutting. The correctly oriented paraffinized embryos were cut with a microtome. The thickness of each section depicted 5-8 µm. Each sequence of pelliciles was first put on the surface of cool water for at least 10 min. Then, it was proceeded to 37 °C-warm water for at least ten min. to guarantee an equal distribution of the paraffin layer. The paraffin pelliciles were collected on serially numbered object slides, which were labeled with the respective embryo ID.

2.1.6.5 Staining with hematoxylin and eosin

Table 1: The eight-stepped procedure of staining with hematoxylin and eosin;

step	procedure	duration	reagent
1	deparaffinization	20 min.	xylene
2	rehydration	5 min.	ethanol (100%)
		5 min.	ethanol (95%)
		5 min.	ethanol (70%)
3	stain	6 min.	hematoxylin
4	wash	10 min.	floating tap water
		1x	distilled water
5	counterstain	2 min.	eosin
6	wash	3x	distilled water
7	dehydration	1 min.	ethanol (96%)
		4 min.	ethanol (100%)
		10 min.	xylene
8	mount	variable	mounting medium

Table 1 shows the entire eight-stepped process of staining with hematoxylin and eosin (H.E.). For H.E. staining the object slides were deparaffinized with a descending alcohol gradient as follows. For 20 min. the slides were kept in xylene, then for five min. in 100%-ethanol, for five min. in 95%-ethanol and for five min. in 70%-ethanol. To continue, the slides were stained with hematoxylin for six min. to perform a nuclear staining. To complete the nuclear staining, the object slides were irrigated with floating tap water for ten min. Before eosin staining was conducted, the slides were shortly submerged in distilled water. To visualize the cellular cytoplasm, eosin staining was performed for two min. To this step another submerging in distillated water was affiliated. The stained sections first had to undergo an ascending alcohol sequence. They were kept in 96%-ethanol for one min., then in 100%-ethanol for four min. and finally in xylene for ten min. The staining procedure was finished as soon as the slides were covered with a mounting medium and glass covers.

2.1.6.6 Photographical acquisition

The examination and the photographical documentation of the H.E.-stained tissue sections were performed with a microscope (*Olympus-BX43*), a camera (*Olympus-SC30*) and the respective computer program (*cellSens Dimension 1.6*).

2.1.6.7 Measurement of the widths of the ventricular compact zone

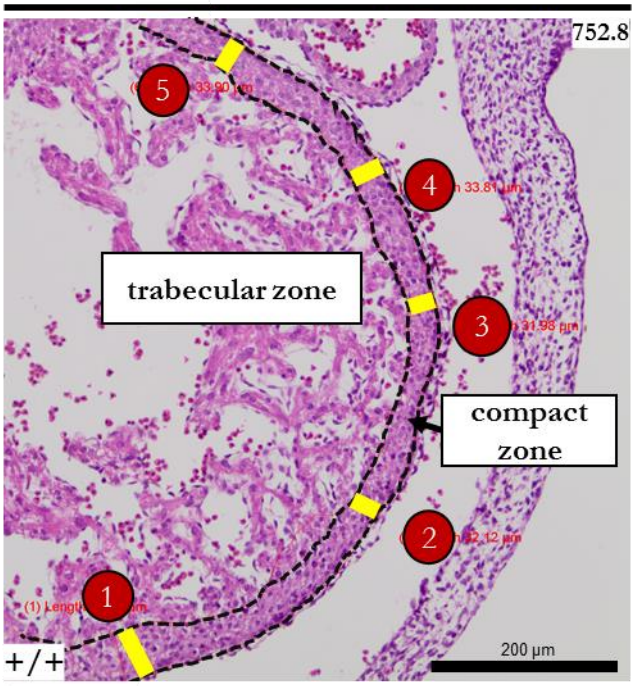

Figure 3: Schematic of the width measurement of the ventricular compact zone; <u>Legend:</u> red circled numbers: positions of width measurement (five in total), **yellow lines:** width of the ventricular compact zone; The positions of measurement were aspired to be equidistantly apart from each other.

Homozygous embryos with respective litter-internal WT controls from the genotyping cohort were included. The exact inclusion of candidates will be explicated in the results part. The width of the vCZ was separately gauged for the RV and LV five times in each section level. **Figure 3** shows a schematic of it. To enable a representative assessment of the entire ventricular myocardium, the assessed section levels were chosen to hold a minimum distance from each other. For E11.5 embryos, the four measured levels were chosen to be at least 10 µm apart, for E13.5 embryos, at least 30 µm apart and for E15.5 embryos, to be at least 50 µm apart from each other. In total, 20 measuring values were aquired per ventricle of the reviewed heart.

2.1.6.8 Statistical analysis

The average of 20 values was calculated for each measured heart, respectively for the RV and the LV. For each embryonic age of E13.5 p.c. or E15.5 p.c., two cohorts were formed. A cohort of homozygous specimens and a cohort of WT controls. Depending on the number of included specimens per embryonic age, the average values of the homozygous cohort were compared to the average values of the control cohort by means of an unpaired two-sided, homoscedastic Student's t-test. P-values smaller than 0.05 were regarded as statistically significant.

Table 2: List of buffers and chemical reagents;

name of chemical reagent	product no.	name of provider	usage
100 bp DNA ladder	G210A	Promega, Madison, USA	PCR
1 kbp DNA ladder	G571A	Promega, Madison, USA	PCR
Acetic acid solution	1370352500	Merck, Darmstadt, GER	AGE
Agarose gel grade ultrapure	840004	Biozym, Hessisch Oldendorf, GER	AGE
Aqua bidest.	3478.2	Roth, Karlsruhe, GER	HE
Blue/ Orange 6x loading dye	G190A	Promega, Madison, USA	AGE
dNTP Mix 10 Mm	18427-013	Invitrogen, Carlsbad, USA	PCR
DPBS	14190-094	life technologies, Carlsbad, USA	ED
EDTA 25 Mm	y02353	Invitrogen, Carlsbad, USA	AGE
Entellan new	107961	Merck, Darmstadt, GER	HE
Eosin staining solution	45260	Sigma-Aldrich, St. Louis, USA	HE
Ethanol	9065.2	Roth, Karlsruhe, GER	HE
Forane (Isoflurane)	B506	Abbvie, North Chicago, USA	ED
Magnesium Chloride	M8787-1.5ML	Sigma-Aldrich, St. Louis, USA	PCR
Nuclease-Free Water	129114	Qiagen, Hilden, GER	PCR
PCR buffer without MgCl2 10x	P2317-1VL	Sigma-Aldrich, St. Louis, USA	PCR
Roti Histofix 4% Formaldehyde	P087.3	Roth, Karlsruhe, GER	ED
Rotiophorese 10x TAE Buffer	T845.2	Roth, Karlsruhe, GER	AGE
SYBR safe DNA gel stain	P/ N S33102	Invitrogen, Carlsbad, USA	AGE
Taq-polymerase	D4545	Sigma-Aldrich, St. Louis, USA	PCR
Weigert's iron hematoxylin solution	HT107-500ML	Sigma-Aldrich, St. Louis, USA	HE
Xylene	9713.3	Roth, Karlsruhe, GER	HE

Legend: AGE: reagent was used for agarose gel electrophoresis, **bp:** base pairs, **ED:** reagent was used for embryonic dissection, **HE:** reagent was used for hematoxylin and eosin staining, **PCR:** reagent was used for polymerase chain reaction;

2.2 Materials

2.2.1 Buffers and chemical reagents

Table 2 presents a list of all buffers and chemical reagents, which found utilization.

2.2.2 Primers

The sequences of the primers, which were used for PCR, are shown in **table 3**.

Table 3: List of primers for genotyping Tm-1a mice;

primer	sequence
Gse-1-5arm-WTF (1.)	CCGCAGGTAGCATGATTGT
Gse-1-Crit-WTR (2.)	GTGGATCGGCCATATTGAGT
Tm-1a-5mut-R (3.)	GAACTTCGGAATAGGAACTTCG

Legend: numbers in brackets correspond to figure 2;

2.2.3 Commercial kits, instruments and equipment

Table 4: List of commercial kits;

name of commercial kit	product no.	name of provider
DNeasy Blood & Tissue Kit	69504	Qiagen, Hilden, GER
QIAamp DNA FFPE Tissue Kit	56404	Qiagen, Hilden, GER

Legend: FFPE: formalin-fixed, paraffin-embedded;

Table 4 shows all commercial kits, which were used for DNA extraction from freshly frozen tissue samples and FFPE tissue samples. **Table 5** shows an overview of the instruments and the equipment, which found utilisation in this project, where the respective function is outlined in the last column.

Table 5: List of instruments and equipment;

name of instrument	name of provider	function
Axio Vision Rel 4.8	Zeiss, Oberkochen, GER	photodocumentation
BioDocAnalyze	Biometra, Göttingen. GER	AGE
Centrifuge 5424R	Eppendorf, Hamburg, GER	centrifugation
Embedding casettes M4614	Roth, Karlsruhe, GER	embedding
Leica EG1140 C	Leica, Wetzlar, GER	embedding center
Leica EG1150H	Leica, Wetzlar, GER	embedding station
Forceps	UMG, Göttingen, GER	ED
liquid nitrogen	UMG, Göttingen, GER	ED
Marienfeld superior pencil	Marienfeld, Lauda-Königshofen, GER	labeling slides
BX43 OLYMPUS	Olympus, Shinjuku, JAP	microscope
Microscope slides	Superfrost Plus, Thermo scientific	sectioning
Feather N35 Type	Hartenstein, Würzburg, GER	microtome blades
Leica RM2165	Leica, Wetzlar, GER	microtome
NanoDrop 2000	Thermo Scientific, Waltham, USA	DNA-measuring
Olympus SC30 camera	Olympus, Shinjuku, JAP	photodocumentation
Owl Easycast B2	Thermo Scientific, Waltham, USA	AGE
GFL 1052	Fisher scientific, Hampton, USA	paraffin bath
Paraffin Warmer	Medax Nagel, Rendsburg, GER	sectioning
Pipette	Sarstedt, Nümbrecht, GER	pipetting
Pipette tips (20µl, 200µl, 1000µl)	Sarstedt, Nümbrecht, GER	pipetting
Safe-Lock tubes	Eppendorf, Hamburg, GER	pipetting
Scissor	UMG, Göttingen, GER	ED
Thermomixer comfort	Eppendorf, Hamburg, GER	DNA-extraction
Leica TP1020	Leica, Wetzlar, GER	tissue processor
Veriti 96 Well Thermo Cycler	Applied Biosystems, Foster City, USA	PCR
Vortex Genie 2	Bender & Hobein AG, München, GER	PCR
Zeiss SteREO Lumar V.12	Zeiss, Oberkochen, GER	microscope

Legend: AGE: reagent was used for agarose gel electrophoresis, **ED:** reagent was used for embryonic dissection, **PCR:** reagent was used for polymerase chain reaction;

3 Results

3.1 Genotyping results

Previous results showed that mating heterozygous Gse-1 mice delivered no homozygous Tm-1a pubs by the age of three weeks. Embryological lethality of Tm-1a homozygosity was hypothesized. Therefore, genotyping Tm-1a embryos was performed to identify the timepoint of embryonic lethality.

Three developmental ages have been chosen with the distance of two days in between them: E11.5 p.c., E13.5 p.c. and E15.5 p.c. For each defined timepoint, terminated matings were arranged to respectively collect at least 30 embryos. At the first timepoint (E11.5 p.c.), eight litters were collected. In total, 54 embryos resulted with an average litter size of 6.8 (SD +/- 1.5). The second timepoint of E13.5 p.c. yielded an amount of 47 embryos from five litters with an average of 9.4 (SD +/- 2.1) embryos per litter. The third delopmental age of E15.5 resulted in a collection of 37 embryos, which originated from six litters with an average litter size of 6.2 (SD +/- 2.6) embryos. The sum of all collected embryos was 138, including one autocatalyzed E15.5 embryo with an unknown genotype.

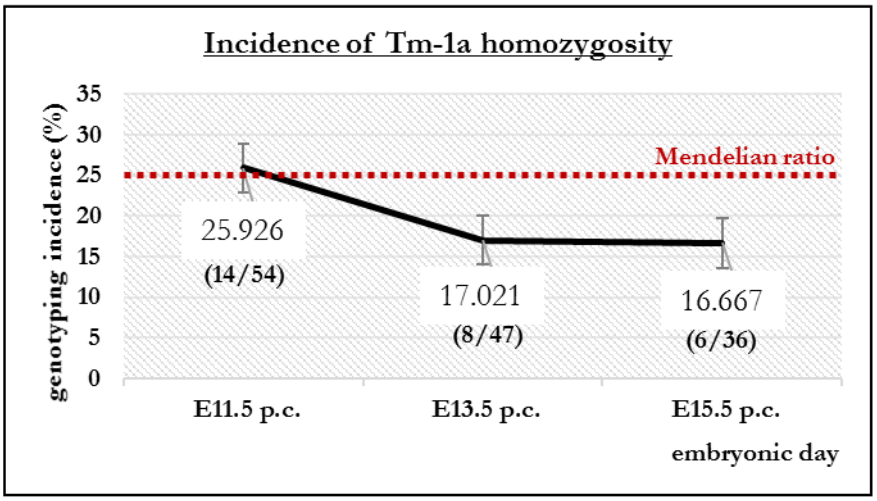

Figure 4: The incidence of homozygous Tm-1a embryos at three sequent timepoints decreases; Legend: red dotted line: expected Mendelian ratio of 25%, **numbers in brackets:** absolute figures correspond to table 6;

Figure 4 visualizes the genotyping results for Tm-1a homozygosity. The developmental age E11.5 p.c. offered an incidence of the homozygous embryos of 25.926%, because 14 out of 54 embryos were homozygous. The developmental stage of E13.5 p.c. provided a homozygous frequency of 17.021% with eight out of 47 embryos being genotyped

as homozygous. The embryonic age of E15.5 p.c. proved to have six homozygous from 36 embryos (one autocatalyzed embryo with an unknown genotype was excluded), which resulted in an incidence of 16.216%. It is noticable that the incidences of homozygous embryos for the developmental ages of E13.5 p.c. and E15.5 p.c. lie under the expected Mendelian ratio of 25%.

Table 6 visualizes the global genotyping results. At the embryonic day E11.5 p.c., 26 out of 54 embryos proved to be heterozygous. The incidence is 48.148%. At developmental day E13.5 p.c., the incidence of Tm-1a heterozygosity amounts to 46.809%, where 22 from 47 embryos were genotyped as heterozygous. The third timepoint E15.5 p.c. yielded a heterozygous incidence of 63.889% with 23 out of 36 embryos. At the developmental day E11.5 p.c., 14 from 54 embryos were WT, which accounted for 25.926%. The developmental stage of E13.5 p.c. provided a WT frequency of 36.17% (17 out of 47 embryos). The developmental age E15.5 p.c. yielded a WT incidence of 19.444% with seven out of 36 embryos, which proved to be WT. That autocatalyzed embryo with an unknown genotype was excluded.

Table 6: **Genotyping results at three developmental ages;** The expected Mendelian ratio of 25% for homozygous specimen is undercut by homozygous embryos at E13.5 p.c. and E15.5 p.c.

age	E11.5 p.c.		E13.5 p.c.		E15.5 p.c.	
genotype	**n**	**ratio (%)**	**n**	**ratio (%)**	**n**	**ratio (%)**
Tm-1a/Tm-1a	14	25.926	8	17.021	6	16.667
+/+	14	25.926	17	36.170	7	19.444
+/Tm1-a	26	48.148	22	46.809	23	63.889
autocat.	0	0.000	0	0.000	[1]	2.778
total	**54**		**47**		**36**	

Legend: angled brackets: excluded from calculation, **autocat.:** autocatalyzed, **n:** number of embryos;

To test whether the obtained genotyping incidences significantly differ from the expected Mendelian ratio of 1:2:1, a chi-square test was applied for two cohorts, which were divided into an E11.5 cohort and an after-E11.5 cohort. The E11.5 cohort offered the results of 14 homozygous, 26 heterozygous and 14 WT embryos. The calculated p-value amounted to 0.964, which is not significant. The after-E11.5 cohort offered the following figures: 14 homozygous, 45 heterozygous and 24 WT embryos. Based on it, the application of the chi-square test showed a p-value of 0.223, which also was regarded as not statistically significant. These data appear to allow different interpretations. Either the timepoint of lethality lies after

E11.5 p.c. or the sample size was too small to detect significant differences of genotyping incidences. These interpretations will critically be debated in the discussion part.

3.2 Whole-mount inspection of Tm-1a embryos

In addition to genotyping of embryos all collected embryos were inspected for their external morphology at each regarded developmental day. The objective of this approach was to detect a putative correlation of the genotype and the occurrence of external peculiarities.

All genotyped embryos were systematically screened for external aberrancies. Both sides of each embryo were evaluated and photodocumented. For each timepoint, a cohort of screened embryos resulted, which was identical to the genotyping cohorts for the developmental day E13.5 p.c. and E15.5 p.c. For the embryonic age E11.5 p.c., eleven embryos from two litters (270.x and 186.x) were photographically acquired. The remaining embryos could not be included because of phototechnical reasons.

3.2.1 Definition criteria of the external-phenotype score

Table 7: Definition of the external-phenotype score; Two major criteria with the respective point assignment are listed, where the second major criterion serves as an additional one.

criterion	definition the external-phenotype score	EPpoints
major	occurene of reticular telangiectasias per side	[2]
	plus: additional subcutaneous edema	[1]
minor	occurrence of more than four red spots	[1]
disqualification	occurrence of autocatalysis	[-1]

An external phenotype (EP) was observed. Definition criteria (EP criteria) were set up (compare **table 7**). Based on it, an EP score was constructed and applied, which facilitated the evaluation of the severity of the EP. The first major criterion is the occurrence of reticular telangiectasias (rTEL) in the torso region of the embryonic body, regarded per side. It accounts for two EP points per affected side. These rTEL appear as a three-dimensional network of sub- and intracutaneous vessels, which are bulged in sections of its transverse axis without disconnection to the up- and downstream region of the respective vessel. These telangiectatic networks occurred either unilateral or bilateral. That is why the EP score awards two points per side, which exposes rTEL. The fact that the three-dimensional structure of rTEL is better assessable with the simultaneous occurrence of subcutaneous edema (SE), is taken in account with the second major criterion (occurrence of SE), which was treated as an additional criterion. It awards one point, in case SE occur in addition to

rTEL. The occurrence of autocatalysis was handled as a criterion of disqualification, because autocatalysis is a multifactoral happening that sporadically occurs during embryogenesis. Its causative connection to Tm-1a homozygosity can neither be excluded, nor proven. Therefore, one minus EP point was assigned marking disqualification. Especially for E13.5 embryos, one minor criterion (the occurrence of more than four red spots [RS] in the torso region of the embryonic body) was additionally set up, because a putative correlation to the same etiology of the major criteria could not be excluded in advance. Therefore, it accounted for one point in the EP score. RS depict point- or oval-shaped hemorrhagic structures of a certain size, contour and colour being localized at the embryonic torso. The size of RS ranges from a fixed lower to an upper limit. The lower limit is oriented at the size of the developing hair follicles of the future whiskers of the respective embryo. The size of the respective eyeball constitutes the upper limit. The shade of red, which is characteristic for RS is defined to be a brighter red than the colour of the prominent temporal vessel in one representative of each litter. In case the litter was formalin-fixed with the result of oxydated hemoglobin, the evaluation of the red colour could not be applied, since methemoglobin is unitary brown, which allows no colour distinction. To concern the contour of RS, a more diffusely contoured shape depicts the reference compared to rTEL.

Table 8: Categories of the external-phenotype score;

points	category	degree
[5]	external phenotype detected	severe
[4]		
[3]		
[2]		light
[1]	intermediate type	
[0]	no external phenotype detected	
[-1]	disqualified	

Table 8 shows the categories of the EP score. The assignment of zero points was categorized as no EP detected (nEPd). The award of two until five points was defined as EP detected (EPd), where the principle of concordant correlation between the amount of points and the severity of EP lies at hand. The assignment of one point depicts an intermediate type (IMT), which lies between both prior mentioned groups. The award of one minus EP point was categorized as disqualified.

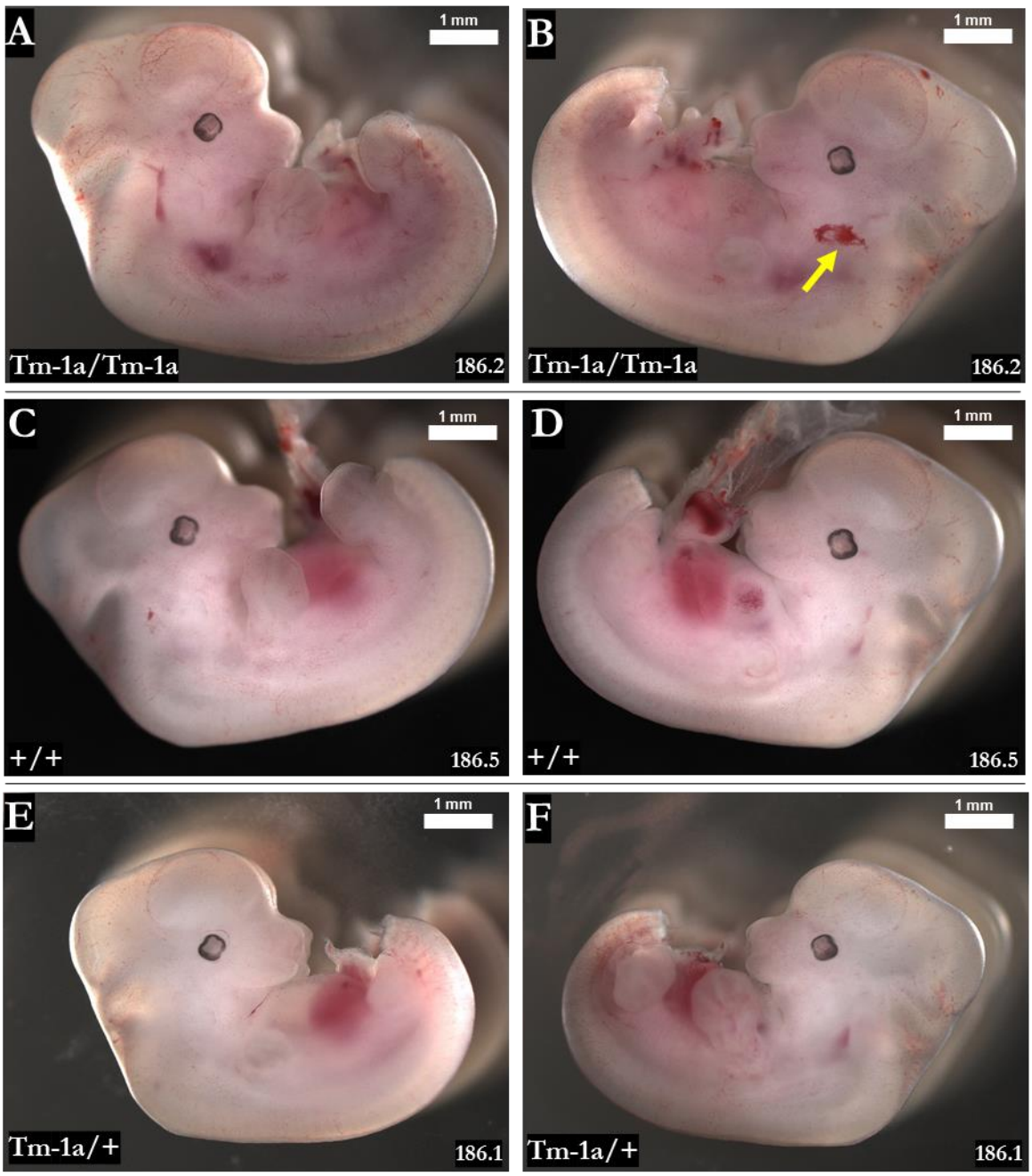

Figure 5: **External morphology of E11.5 embryos; Legend: A and B**: homozygous, **C and D**: WT, **E and F**: heterozygous, **arrow:** red spot; Three E11.5 embryos from the same litter (186.x) are shown. Both sides of the embryos are displayed that show the external morphology for each genotype, where pictures of one identical embryo are in horizontal juxtaposition.

3.2.2 E11.5 embryos

At the developmental age of E11.5 p.c., eleven embryos were inspected for external peculiarities in terms of the pre-defined major and minor criteria of the EP score. **Figure 5** gives a representative visual impression of the external morphology correlated to the determined genotype. From two homozygous, three WT and six heterozygous embryos,

none showed a pathology suiting the EP criteria. Two embryos were autocatalyzed with a known genotype (compare **table 9**). In this case, one autocatalzed embryo proved to be homozygous and the other embryo proved to be WT, where the underlying cause remains unclear. As aforementioned, autocatalysis served as a criterion of disqualification, because in utero death may routinely occur as a multifactorial happening.

Table 9: External-phenotype categorization of E11.5 embryos;

E11.5 p.c.		external-phenotype category			
genotype	total	**A**	**B**	**C**	**D**
Tm-1a/Tm-1a	2	1	0	0	1
+/+	3	2	0	0	1
Tm-1a/+	6	6	0	0	0
total	**11**	**9**	**0**	**0**	**2**

Legend: **A:** no external phenotype detected, **B:** intermediate type, **C:** external phenotype detected, **D:** disqualified;

3.2.3 E13.5 embryos

Figure 6 shows a visual impression of the external morphology of E13.5 embryos. At the embryonic day E 13.5 p.c., eight homozygous, 17 WT and 22 heterozygous embryos were externally inspected for the occurrence of an EP, where one autocatalyzed embryo proved to be homozygous (compare **table 10**). Among 17 WT embryos, none exposed criteria of the EP or the IMT.

Table 10: External-phenotype categorization of E13.5 embryos;

E13.5 p.c.		external-phenotype category			
genotype	total	**A**	**B**	**C**	**D**
Tm-1a/Tm-1a	8	2	1	4	1
+/+	17	17	0	0	0
Tm-1a/+	22	21	0	1	0
total	**47**	**40**	**1**	**5**	**1**

Legend: **A:** no external phenotype detected, **B:** intermediate type, **C:** external phenotype detected, **D:** disqualified;

Four out of eight inspected homozygous embryos showed an EP, where one embryo (257.7) exposed an IMT, which complied with the minor criterion. Two homozygous embryos did not expose an EP (nEPd) and one embryo (235.8) was disqualified because of external autocatalysis. From 22 regarded heterozygous embryos, 21 showed no detectable

external pathology, where one exposed an EP (218.6 [both sides: rTEL]). In other words, from five EPd, four proved to be homozygous, one was heterozygous and none manifested a WT genotype. One homozygous IMT was detected.

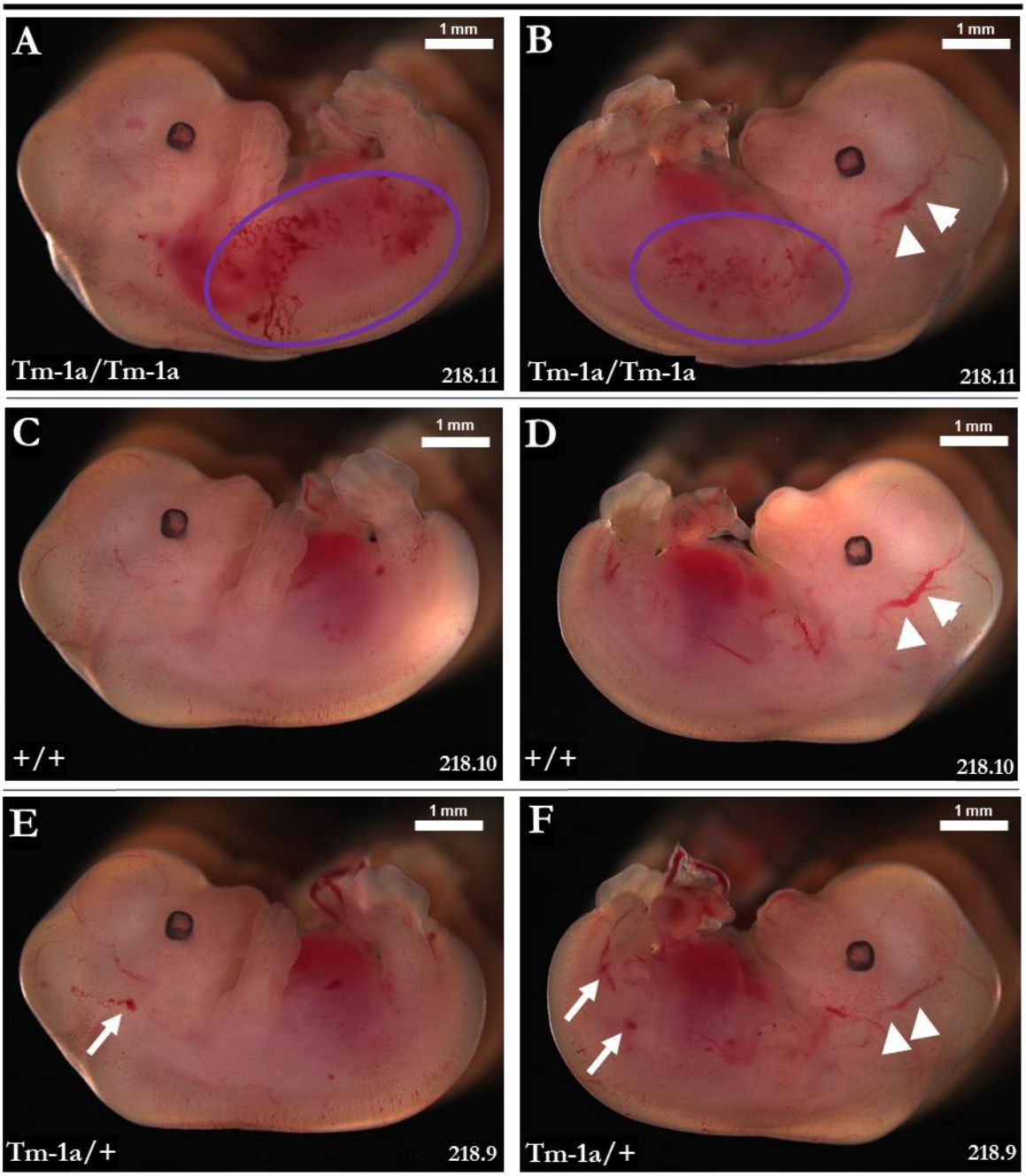

Figure 6: **External morphology of E13.5 embryos; Legend**: **A and B**: homozygous, **C and D**: WT, **E and F**: heterozygous, **arrow heads**: prominent temporal vessel, **arrows**: red spots, **purple circles:** reticular telangiectasias; Three E13.5 embryos from the same litter (218.x) are shown. Both sides of the embryos are displayed, which show the external morphology for each genotype, where two pictures horizontally next to each other belong to the same embryo.

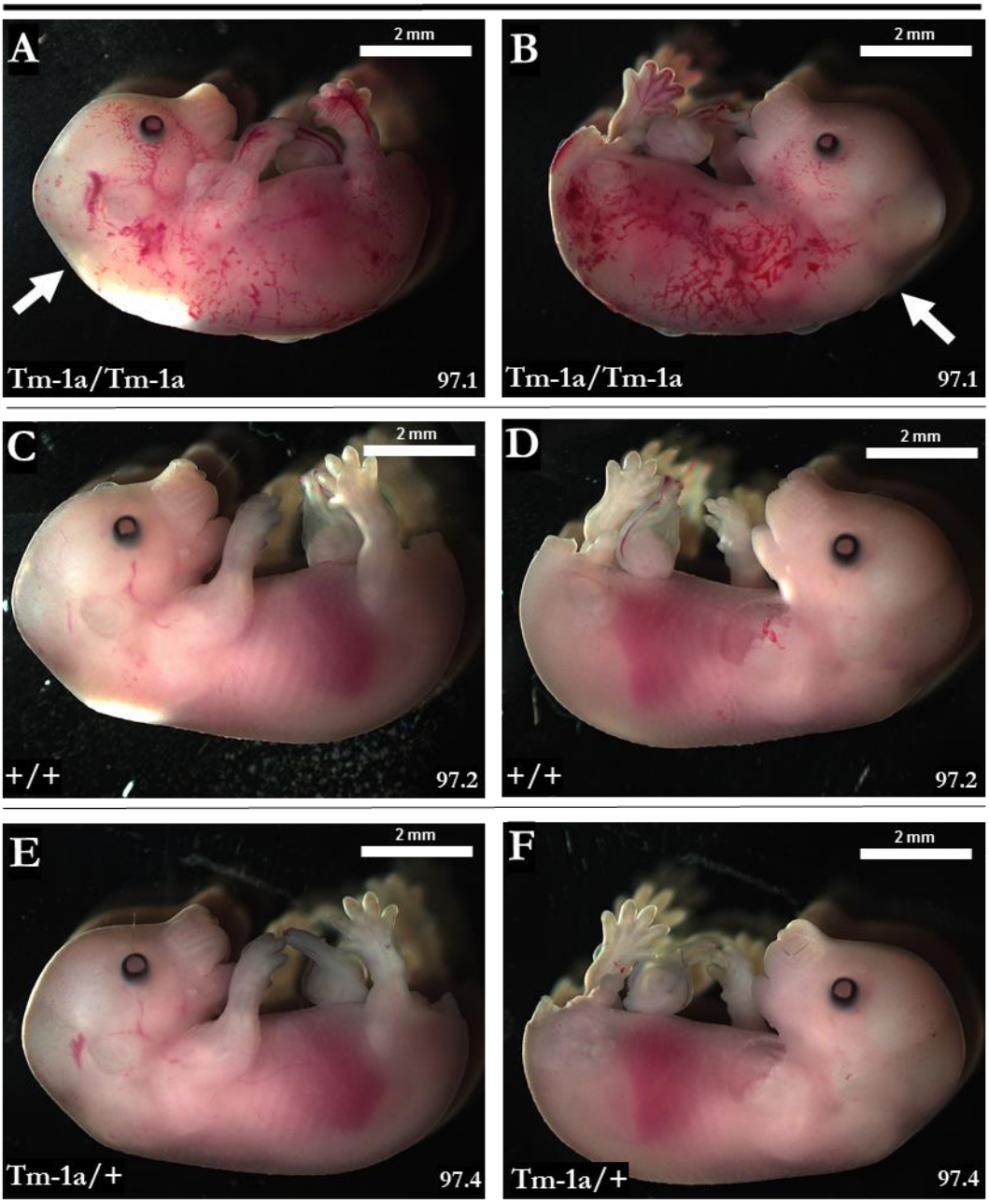

Figure 7: External morphology of E15.5 embryos; Legend: A and B: homozygous, **C and D**: WT, **E and F**: heterozygous, **arrows:** slight subcutaneous edema, which can be best assessed in the cervical groove; Three E15.5 embryos from the same litter (97.x) are shown. Both sides of the embryos are displayed, which show the external morphology for each respective genotype, where two pictures horizontally next to each other belong to the same embryo. The EP is characterized by rTEL, which can be observed on both sides of the homozygous embryo. The representative histology of the cutis of embryo 97.1 (homozygous) and 97.2 (WT) is shown in figure 12.

3.2.4 E15.5 embryos

Table 11: External-phenotype categorization of E15.5 embryos;

E15.5 p.c.		extemal-phenotype category			
genotype	total	**A**	**B**	**C**	**D**
Tm-1a/Tm-1a	6	1	0	4	1
+/+	7	7	0	0	0
Tm-1a/+	23	23	0	0	0
unknown	1	0	0	0	1
total	**37**	**31**	**0**	**4**	**2**

Legend: **A:** no external phenotype detected, **B:** intermediate type, **C:** external phenotype detected, **D:** disqualified;

Table 11 shows a brief overview of the observed external peculiarities of the E15.5 cohort. An augmentation of rTEL, which were detected in E13.5 embryos, is intensifyingly visible in homozygous E15.5 embryos. Four out of six homozygous embryos displayed at least one criterion of the pre-defined EP. One homozygous embryo (117.4) exposed no EP that followed the definition criteria. One homozygous embryo, which was autocatalyzed, was disqualified (106.4). Zero out of 23 heterozygous embryos showed an EP. Zero out of seven WT embryos exposed an EP. The genotypical apportionment of four E15.5 embryos, which showed an EP, is four homozygous, zero heterozygous and zero WT embryos. A visual outline of the external morphology of E 15.5 embryos is given by **figure 7**.

3.2.5 Synopsis: categorization of Tm-1a embryos

In the following the exact EP-point assignment shall be presented, where **table 12** shows an overview. Four evaluated embryos exposed a severe EP (218.11 [homozygous], 190.4 [homozygous] and 170.3 [homozygous], 218.6 [heterozygous]), which was scored with five EP points that indicate the occurrence of bilateral rTEL in addition to SE. The homozygous embryo 756.3 exposed rTEL at both sides, which resulted in four EP points. The homozygous embryo 170.5 exhibited rTEL at the left side and SE with three EP points. Three homozygous embryos showed a light form of EP that was awarded with two EP points, which reflects unilateral rTEL (752.6 [left side], 756.6 [left side] and 190.3 [left side]). One homozygous embryo (257.7) exposed more than four RS, therefore, was awarded with one EP point, which was classified as IMT. Because of the occurrence of autocatalysis five embryos were disqualified (186.3, 270.2, 235.8, 106.2 and 106.4).

Table 12: Synopsis of the external-phenotype categorization of Tm-1a embryos;

points	E11.5 p.c.	E13.5 p.c.	E15.5 p.c.	category
[5]	-	218.6, 218.11	190.4, 170.3	A
[4]	-	756.3	-	
[3]	-	-	170.5	
[2]	-	752.6, 756.6	190.3	
[1]	-	257.7	-	**B**
[0]	all others	all others	all others	**C**
[-1]	186.3, 270.2	235.8	106.2, 106.4	**D**

Legend: **A:** no external phenotype detected, **B:** intermediate type, **C:** external phenotype detected, **D:** disqualified;

The genotypical distribution of the occurrence of an EP lies on the part of Tm-1a homozygosity, since eight out of nine embryos, which exposed an EP have proven to be homozygous, where one embryo was heterozygous. Another striking notion is that among all 24 WT embryos, zero exposed an EP. For the timepoint E11.5 p.c., two out of eleven embryos showed autocatalysis, which officiated as a criterion of disqualification (compare **table 7**). In the homozygous 11.5 cohort, zero EPd and one nEPd were observed. Regarding the homozygous embryos of the E13.5 cohort, four EPd and two nEPd were detected. In the E15.5 cohort, four EPd and one nEPd were documented. Under the assumption that a correlation between a specific genotype and the EP randomly occurs, one would expect an equal distribution of one third per genotype. Applying the chi-square test with the expected absolute distribution and the factually aquired EP amount of eight homozygous, one heterozygous and zero WT counts, the p-value equals 0.018, which is by conventional criteria considered to be statistically significant. Therefore, the occurrence of the EP is significantly associated with Tm-1a homozygosity. These data give evidence that Tm-1a homozygosity is involved in the occurrence of an EP. Externally visible features, such as edema or alterations in the cutaneous surface, are predescribed by a variety of authors serving as the starting point of reasonable suspicion for cardiac impairment during embryogenesis (Lin et al. 2012; Abdelhamed et al. 2015).

3.3 Histological assessment of Tm-1a hearts

3.3.1 Part I: evaluation of non-ventricular structures

To investigate if an impairment of cardiogenesis in homozygous Tm-1a embryos is observable, histological analyses of the hearts were performed. H.E.-stained sections of

embryonic hearts at three developmental ages (E11.5 p.c., E13.5 p.c. and E15.5 p.c.) were systematically evaluated for predefined characteristics, which will be mentioned below. The explicit selection of these timepoints is decisive for the evaluation of cardiogenesis. Because at E11.5 p.c., myocardial development is completed neither in terms of compaction, nor in terms of trabeculation, it is reasonable to start its evaluation at E13.5 p.c. The histological evaluation of Tm-1a hearts was divided in part I (evaluation of non-ventricular structures) and part II (evaluation of ventricular structures) for E13.5 and E15.5 hearts.

For the histological examination at the developmental day E11.5 p.c., all six homozygous embryos from four representative litters (270.x, 186.x, 765.x and 763.x) were evaluated to be sagittally sectioned and analyzed. This resulted in four out of six potential homozygous candidates, where one homozygous embryo (270.2) was excluded, because it was autocatalyzed. Here, no litter-internal WT control was available. The other excluded embryo (763.7) was unevaluable due to histo-technical issues. The four homozygous embryos 186.2, 765.4, 763.2 and 763.9 were included and compared to seven litter-internal WT controls (186.7, 765.2, 765.7, 765.8, 763.3, 763.4 and 763.5). For the E13.5 cohort, four litters were included with a sum of twelve reviewed embryos, six homozygous ones and six WT controls. Litter I (752.x) contributed with two homozygous embryos (752.4 and 752.6) and two WT controls (752.8 and 752.9). Litter II (756.x) offered two homozygous embryos (756.3 and 756.6) and two WT controls (756.2 and 756.4). Litter III (235.x) yielded one homozygous embryo (235.8) and one respective WT control (235.6). Litter IV (257.x) offered one homozygous embryo (257.7) and one WT control (257.10). Two candidates had to be excluded because of histo-technical and paraffin-embedding issues. For the E15.5 cohort, three litters were included with an amount of ten embryos with five homozygous hearts, four WT controls and one heterozygous embryo, which served as the control in one litter (litter III: 190.x) under reservation.

Litter I contributed with two homozygous embryos (170.3 and 170.5) and three WT controls (170.7, 170.8 and 170.10). Litter II administered one homozygous embryo (117.4) and one WT control (117.1), where litter III offered two homozygous embryos (190.3 and 190.4) and one heterozygous control (190.1), whose EP exposed no pathologies. It was included under reservation, since among five embryos of this litter, no WT embryo was obtained. One homozygous candidate (106.4) was excluded because of advanced autocatalysis with no distinguishable tissue being left.

3.3.1.1 E11.5 hearts

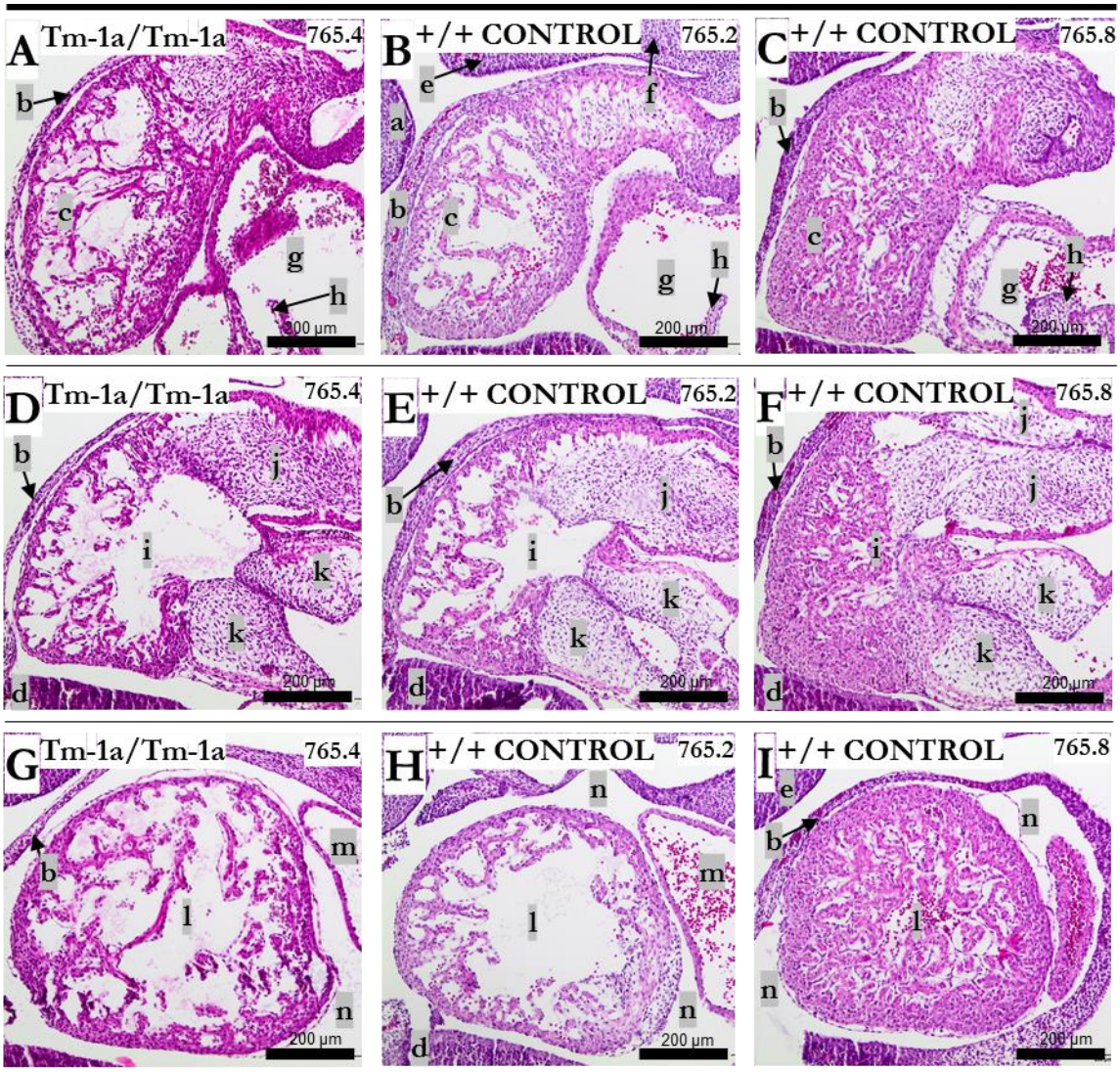

Figure 8: **H.E. staining of all three section levels in E11.5 hearts; Legend: A-C**: *bulbus cordis* (level I), **D-F:** endocardial cushion tissue (level II), **G-I:** common ventricular chamber (level III), **A/D/G**: homzygous, **B/C/E/F/H/I**: WT controls (litter-internal), which show a differing histomorphological, myocardial structure within the same genotype (compare B with C, E with F and H with I), **a:** medial nasal process, **b**: thoracic wall adjoining the pericardium, **c:** *bulbus cordis*, **d**: hepatic primordium, **e**: mandibular part of first branchial arch, **f:** second branchial arch, **g**: right-atrial chamber, **h**: venous valve, **i**: bulbo-ventricular canal, **j**: endocardial cushion tissue in outflow tract of the heart (future aortico-pulmonary spiral septum), **k**: endocardial cushion tissue lining the atrio-ventricular canal, **l**: common ventricular chamber (future left ventricle), **m**: cavity of the left atrium, **n**: pericardial cavity;

The BC hallmarks the section level I (compare **figure 8**, pic. A-C). This section enables the evaluation of the venous valves (1. rated criterion) with the right atrium (2. rated criterion), the morphology of the BC, its myocardial architecture in terms of the question whether a high degree of trabecular rarefication is detectable or not (3. rated criterion) and the evaluation of surrounding structures (compare **table 13**).

The section level II shows the ECT from both the outflow tract and the atrioventricular canal (compare **figure 8**, pic. D-F). This section level gives insights into the histomorphology of the myocardial construction in terms of the evaluation of the trabeculation (3. rated criterion), the formation of the ECT that lines the atrioventricular canal (1. rated criterion) and the outflow tract (2. rated criterion, compare **table 13**).

The common ventricular chamber is the evaluated section level III, which shows a marginal zone of the future left-ventricular myocardium in a relatively circular configuration. It allows the most undistracted evaluation of trabecular formation among all section levels of E11.5 hearts (2. rated criterion, compare **figure 8**, pic. G-I). Moreover, this level of sectioning gives insights into the cavitary morphology of the left atrium (1. rated criterion, compare **table 13**).

Table 13: **Histological analysis of E11.5 hearts;** Four homozygous embryos were compared with seven litter-internal WT controls.

E11.5 p.c.	genotype	**Tm-1a/Tm-1a**	**control**
	total	4	7
rated items			
bulbus cordis (level I)			
1. intact morphology of venous valve		3/3 [1]	3/3 [4]
2. intact morphology of right atrium		4/4 [0]	6/6 [1]
3. rarefied myocardial trabeculation		2/3 [1]	2/5 [2]
endocardial cushion tissue (level II)			
1. intact lining of atrioventricular canal		4/4 [0]	7/7 [0]
2. intact lining of the outflow tract		4/4 [0]	7/7 [0]
3. rarefied myocardial trabeculation		2/4 [0]	2/6 [1]
common ventricular chamber (level III)			
1. intact morphology of left atrium		3/3 [1]	7/7 [0]
2. rarefied myocardial trabeculation		1/3 [1]	2/7 [0]

Legend: figures in brackets: indicate how many of the respective embryos were excluded from the observation due to histo-technical reasons, **roman numerals:** section levels;

Table 13 and **figure 8** give overviews of the histological analysis of E11.5 hearts. For the section level I, three items were rated in four homozygous specimens and seven WT controls, where the rated items were evaluated in each specimen. In case one item was not evaluated because of histo-technical reasons, it was excluded from the total amount of reviewed embryos, as is indicated by angled brackets in **table 13**. For the first rated item, all homozygous and all WT controls exposed an intact morphology of the venous valves. Regarding the second rated item, all specimen showed an intact right-atrial formation. Two

out of three homozygous hearts (765.4 and 763.9) revealed rarefied ventricular trabeculation, where two out of five WT controls also exposed the former mentioned feature (765.2 and 763.5). Two WT controls were excluded because of unevaluable sections (186.7 and 765.7). The results of the section level II (ECT) show that all eleven embryonic hearts exposed an intact lining of the atrioventricular canal and the outflow tract by ECT, independent of their genotype. The myocardium in two out of four homozygous specimens (765.4 and 763.9) and two out of six WT controls exposed highly rarefied trabeculae (765.2 and 763.5). In section level III (common ventricular chamber), all evaluated specimens (three homozygous [182.2, 765.4 and 763.2] and seven WT hearts) showed an intact morphology of the left atrium. Three out of ten specimens (765.4, 765.2 and 763.5) exposed a rarefied trabeculated myocardium and five out of seven WT controls exposed a highly trabeculated myocardial architecture (186.7, 765.2, 765.7, 765.8, 763.3, 763.4 and 763.5).

Summarizingly, the reviewed hearts exhibit a fluctuating profile of myocardial trabeculation, whereas other cardiac structures expose intact formation. Rarefied trabeculation becomes apparent in homozygous and WT hearts, which implied that variations in the degree of trabeculation occur physiologically, without obligatory pathological significance.

3.3.1.2 E13.5 hearts

The aortico-pulmonary spiral septum (APSS) is the hallmark of the section level I (compare **table 14**). The APSS consists of embryonic connective tissue that structurally keeps the pulmonary trunk (PT) and the aorta in juxtaposition. This section level was chosen, because it reveals many crucial anatomical structures at one glance (compare **figure 9**, pic. A-D): the PT (2. rated criterion), the PDA, the proximal part of the ascending aorta (PAA; 3. rated criterion), the configuration of the right-ventricular outflow tract (RVOT; 4. rated criterion) and the atrial formation are assessable.

The AV depicts the section level II (compare **figure 9,** pic. E-H). This section level enables the evaluation of the morphology of the AV (1. rated criterion, compare **table 14**) and the interventricular septum (2. rated criterion).

The histological hallmark of the section level III is the physiological VSD (pVSD). It offers the evaluation of the morphology of the atrio-ventricular ECT and the morphology of the pVSD (1. rated criterion, compare **table 14** and **figure 9,** pic. I-L).

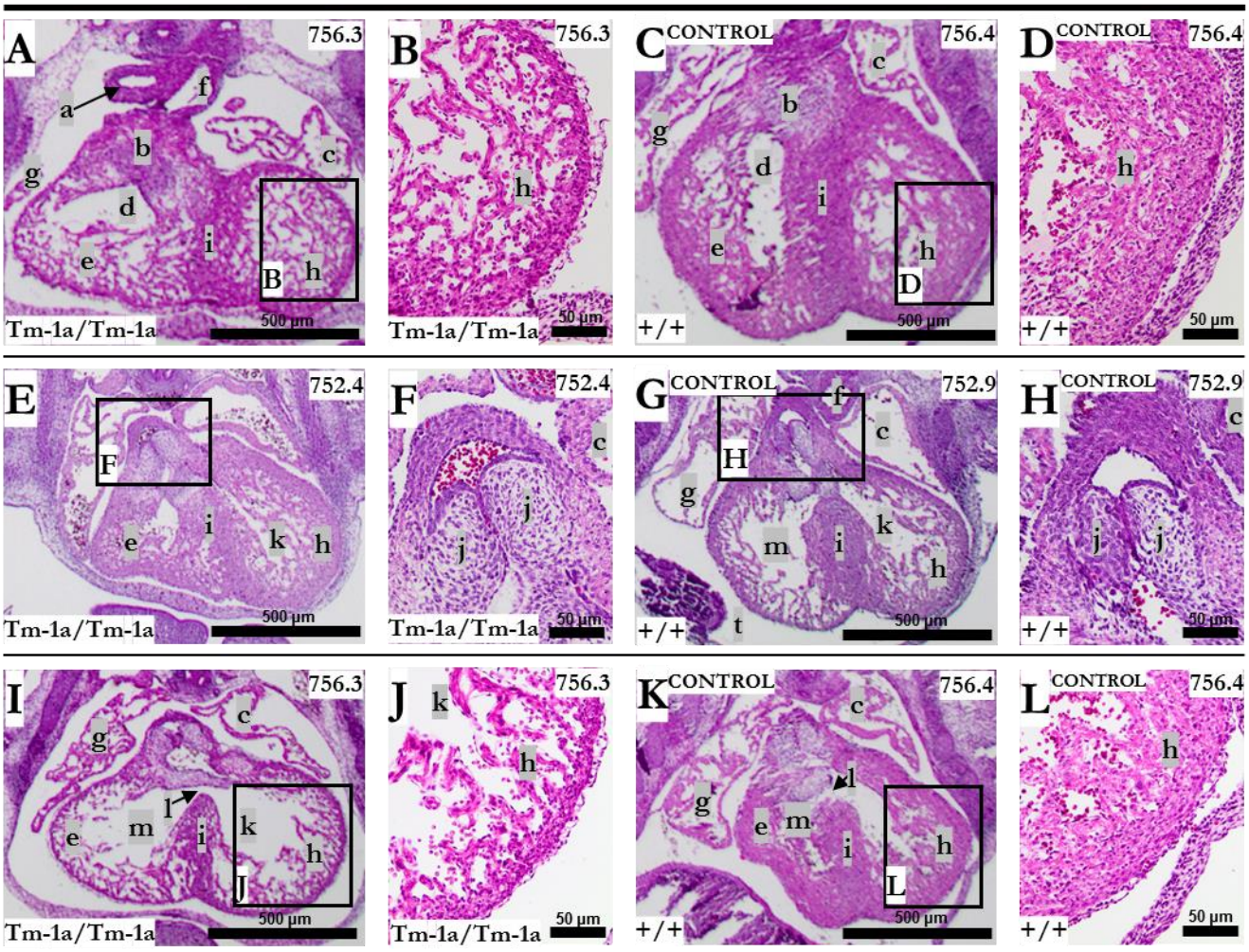

Figure 9: H.E. staining of all three section levels in E13.5 hearts; <u>Legend:</u> A-D: aortico-pulmonary spiral septum (level I), **E-H**: aortic valve (level II), **I-L:** physiological VSD (level III), **B:** detail of A, **D:** detail of C, **F:** detail of E, **H:** detail of G, **J:** detail of I, **L:** detail of K, **a**: proximal ascending part of the aorta, **b:** aortico-pulmonary spiral septum, **c**: right atrium, **d**: right-ventricular outflow tract, **e:** right-ventricular trabecular zone, **f**: proximal part of the pulmonary trunk, **g**: left atrium, **h**: left-ventricular myocardium, **i**: interventricular septum, **j:** leaflet of aortic valve, **k**: cavity of left ventricle, **l**: ventricular septal defect, **m:** right-ventricular cavity, **n**: pericardial cavity;

Table 14 presents the results of the histological analysis of the E13.5 embryos. To expound the findings of the section level I (compare **figure 9**), twelve embryos were rated with four items (compare **table 14**). All four items were targeted on the evaluation of the intact morphology of blood-conductive (RVOT, PT and PAA) or tissue-connective (APSS) structures. All six homozygous E13.5 embryos exposed a physiological configuration, except for two homozygous embryos (752.6 and 756.6) that did not allow the evaluation of the PT, because serial sections did not expose it. All WT control hearts exposed an intact morphology of the prior mentioned structures. The serial sections of 756.2 did not allow the evaluation of the APSS, PT, PAA and RVOT. Serial sections of 752.9 did not enable the review of the PT and PAA. Therefore, they were excluded from the assessment.

Table 14: Histological analysis of E13.5 hearts; Five homozygous embryos were compared with five litter-internal WT controls.

E13.5 p.c.	genotype	**Tm-1a/Tm-1a**	**control**
	total	6	6
rated items			
aortico-pulmonary spiral septum (level I)			
1. intact morphology of aortico-pulmonary spiral septum		6/6 [0]	5/5 [1]
2. intact morphology of pulmonary trunc		4/6 [0]	4/4 [2]
3. intact morphology of proximal part of ascending aorta		6/6 [0]	4/4 [2]
4. intact morphology of right-ventricular outflow tract		6/6 [0]	5/5 [1]
aortic valve (level II)			
1. intact valvular morphology		6/6 [0]	6/6 [0]
3. intact formation of the interventricular septum		6/6 [0]	6/6 [0]
physiological ventricular, septal defect (level III)			
1. ventricular septal defect detected		4/6 [0]	3/6 [0]

Legend: **figures in brackets:** indicate how many of the respective embryos were excluded from the observation due to histo-technical reasons, **roman numerals:** section levels;

For the section level I, all twelve E13.5 embryos were included for validation. They exposed an intact formation of the AV and the interventricular septum (IVS). To present the results of the section level III, in four out of six homozygous hearts and in three out of six WT controls a VSD was detected (compare **figure 9**).

Table 15: **Histological analysis of E15.5 hearts;** Five homozygous embryos were compared to the respective controls from the identical litter, mostly WT. One litter (190.x) recovered no WT embryo, only two homozygous embryos and three heterozygous embryos. Both homozygous embryos were analyzed and compared to heterozygous embryos.

E15.5 p.c.	genotype	**Tm-1a/Tm-1a**	**control**
	total	5	5
rated items			
pulmonary valve (level I)			
1. intact valvular morphology		4/4 [1]	5/5 [0]
2. intact formation of right-ventricular outflow tract		4/4 [1]	5/5 [0]
3. patency of *ductus arteriosus*		4/4 [1]	5/5 [0]
4. sufficient formation of the proximal part of ascending aorta		4/4 [1]	5/5 [0]
aortic valve (level II)			
1. intact valvular morphology		4/4 [1]	5/5 [0]
2. intact formation of atria		4/4 [1]	5/5 [0]
atrioventricular valves (level III)			
1. intact morphology of the atrioventricular valves		5/5 [0]	5/5 [0]
2. ventricular septal defect detected		3/5 [0]	0/5 [0]

Legend: **figures in brackets:** indicate how many of the respective embryos were excluded from the observation due to histo-technical reasons, **roman numerals:** section levels;

Deductively, in E13.5 embryos histocardial structures such as vasculature and the APSS showed no signs of impairment. Since septation is expected to be completed around E14.5 p.c., the detection of VSD in both homozygous and WT control hearts was regarded as physiological.

3.3.1.3 E15.5 hearts

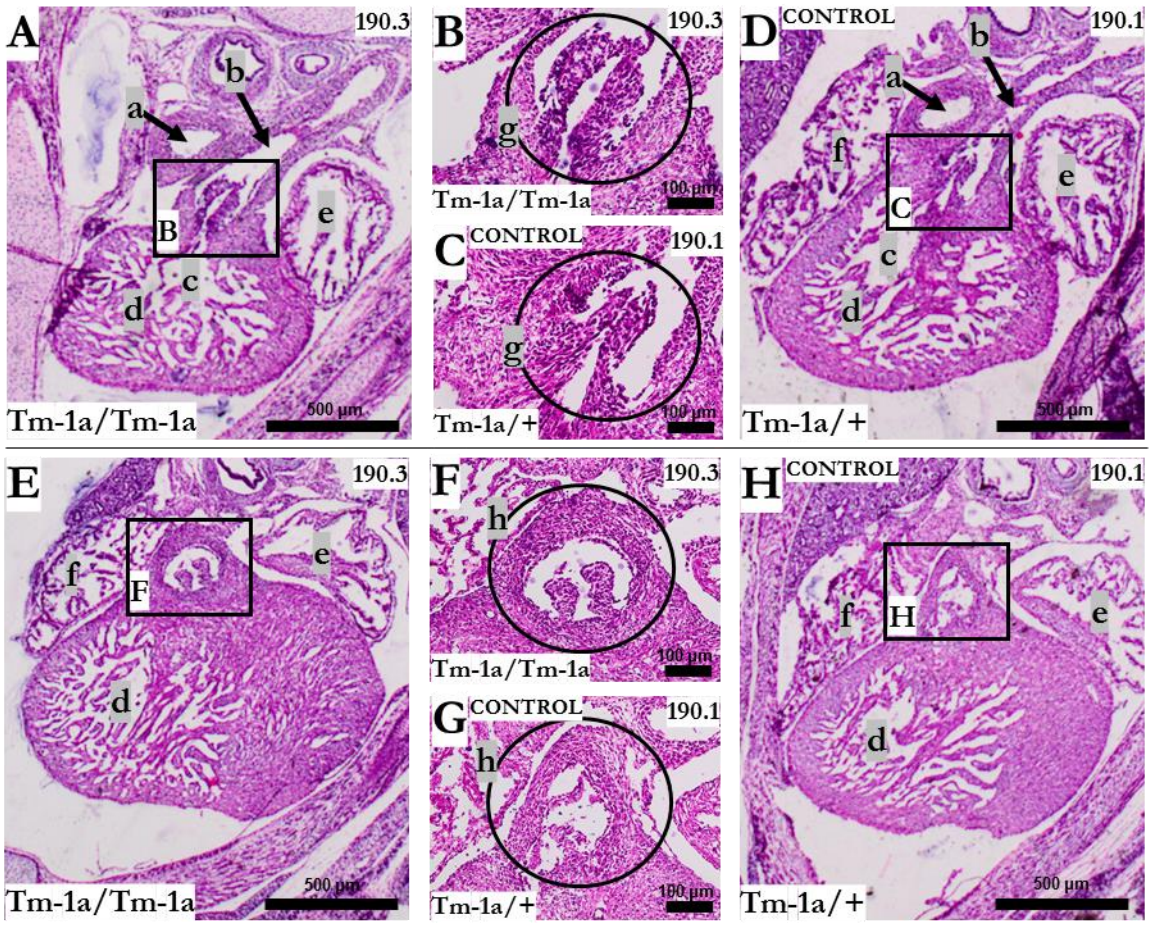

Figure 10: H.E. staining of the section levels I and II in E15.5 hearts; <u>Legend</u>: **A-D**: pulmonary valve (level I), **E-H:** aortic valve (level II), **A**: overview, **B**: detail of A, **C**: detail of D, **D**: control overview, **E**: overview, **F:** detail of E, **G**: detail of H, **H**: control overview, **a:** proximal part of the ascending aorta, **b:** patent *ductus arteriosus*, **c:** right-ventricular outflow tract, **d:** cavity of the right ventricle, **e:** left atrium, **f:** right atrium, **g:** pulmonal valve, **h:** aortic valve;

The hallmark of the section level I is the pulmonary valve (PV) that consists of three cuspids (anterior, left and right cuspid) and connects the RVOT with the PT. Furthermore, the aortic arch and the PDA, which connects the PT with the distal part of the aortic arch (dAA), were assessed. The evaluation of the area of the former APSS was also aspired (compare **figure 10,** pic. A-D).

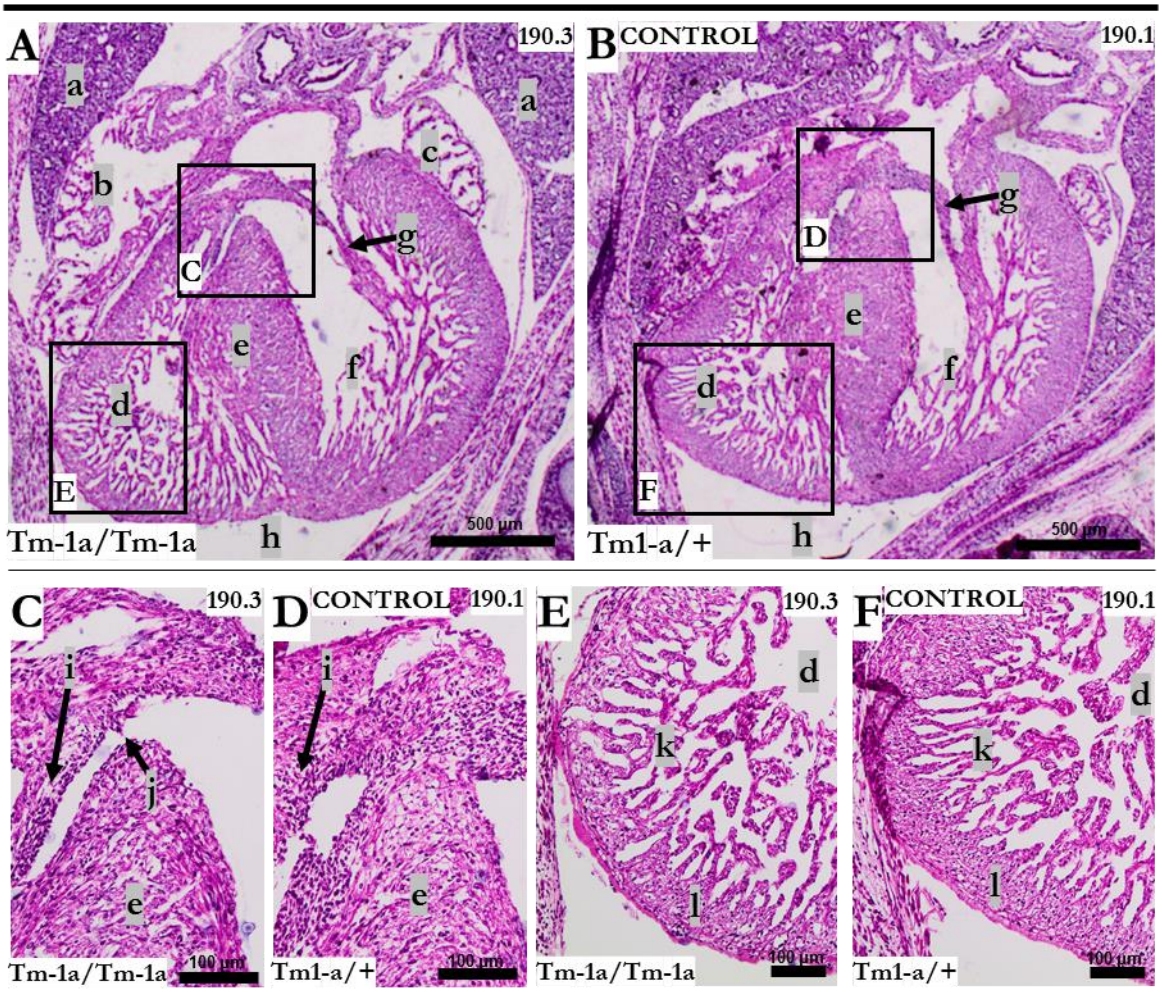

Figure 11: H.E. staining of the section level III in E15.5 hearts; Legend: A and B: atrioventricular valves (level III), **C**: VSD in a homozygous heart (detail of A), **D**: respective control heart shows no VSD (detail of B), **E**: right-ventricular myocardium of a homozygous heart (detail of A), **F**: right-ventricular myocardium of a control heart (detail of B), : **a:** lung bud, **b:** right atrium; **c:** left atrium; **d:** cavity of the right ventricle, **e:** interventricular septum, **f:** cavity of the left ventricle, **g:** leaflet of mitral valve, **h:** pericardial cavity, **i:** leaflet of the tricuspid valve, **j:** ventricular septal defect, **k:** right-ventricular trabeculated part of the myocardium, **l:** right-ventricular compacted part of the myocardium;

The section level II is represented by the AV. The formation of the aortic leaflets and the fibrous anulus were evaluated (compare **figure 10,** pic. E-H).

The AVV hallmark the section level III (compare **figure 11**). All four chambers of the heart are assessable. The AVV were examined regarding connection to chordae tendinae and formation of the atrioventricular cuspids. Potential intercavitary communications are assessable in terms of a potential VSD, since septation is physiologically completed around E14.5 p.c.

Table 15 gives an overview of the histological analysis of the transverse sections of ten E15.5 hearts. To regard the first two section levels, all included E15.5 embryos exposed an intact AV and PV formation, an adequately formed PDA, an intact morphology of the RVOT, an adequate formation of the PAA and a physiological formation of both atria. One homozygous embryo (117.4) was excluded, because of histo-technically unevaluable sections. In section level III, ten out of ten embryonic hearts exhibited an intact formation of the AVV, independent of the genotype. To concern the rated VSD-detecting item, three out of five homozygous embryos showed a VSD (190.3, 190.4 and 170.3). Two specimens exposed no VSD (170.5 and 117.4). All controls showed no VSD (compare **table 15**).

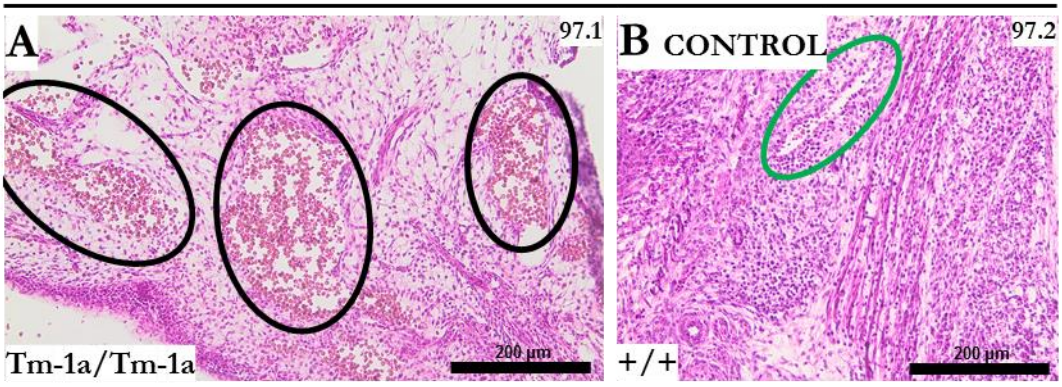

Figure 12: H.E. staining of the skin of E15.5 embryos reveals congested subcutaneous vessels in homozygous specimens compared to WT controls; **Legend:** **A**: H.E. staining of the cutis of a homozygous embryo (97.1) that has been shown whole mount in figure 7 with representative littermates. **B:** Cutis of the litter-internal WT-control embryo (97.2), **black circles:** ectatic vessels that reveal an intact endovascular border, which supports the suspected etiology to be of congestive nature, **green circle:** intact wall of a non-congested vessel;

As an excursus, the cutis was histologically assessed in E13.5 and E15.5 embryos (compare **figure 12**). In contrast to cutaneous hemorrhages (such as RS), telangiectasias expose an intact endothelial border, which is microscopically demonstrated in **figure 12** (pic. A) and macroscopically leads to the sharp contour of rTEL. This notion of intact vessel walls further supports the hypothesis that circulatory congestion induces EP occurrence. The representative litter-internal WT controls showed no histological or macroscopical signs of congestive vessels (compare **figure 12**, pic. B).

3.3.2 Part II: evaluation of ventricular structures

The histological assessment of E13.5 and E15.5 hearts offered the impression of a differing myocardial structure in terms of a varying width of the vCZ. In part I, all cardiac structures, except for the ventricular myocardium, were examined in homozygous and control hearts.

Part II of the histological assessment will evaluate ventricular structures by width quantification of the vCZ in homozygous hearts compared to WT controls in E13.5 and E15.5 embryos. Thereby, the question will be addressed, whether Tm-1a homozygosity can be nominated as an influencing factor that affects the formation of the myocardium during cardiogenesis in Tm-1a embryos.

To generate a representative cohort of analyzed hearts, all homozygous and WT embryos of part I were evaluated for the width measurement of the vCZ in the RV and the LV, respectively. For the E13.5 cohort, the litters 752.x, 756.x, 235.x and 257.x were included with a total number of six homozygous and six WT embryos. For the E15.5 cohort, the litters 170.x and 117.x were included with three homozygous embryos and four WT controls. The E15.5 litter 190.x was excluded from part II, because it offered no WT embryo. Tm-1a heterozygosity was not enough to serve as control in part II, because the non-affection of the myocardial structure could not be assured in advance. Shortly summarized, four sequential section levels were analyzed per embryo, where one section slide showed both ventricles, whose perpendicular width of the vCZ was measured in five fixed positions (apical to basal). In total, an amount of 20 measuring values resulted per ventricle of each specimen. The respective average was calculated. An unpaired, two-sided, homoscedastic Student's t-test was performed, which compared the calculated means of the homozygous samples to the WT-control means for each cohort.

3.3.2.1 E13.5 hearts

Table 16 visualizes the descriptive statistics of the width measurement of the vCZ in E13.5 hearts. Litter I (752.x) offered two homozygous specimens (752.4 and 752.6), whose right-ventricular widths averaged out at 37,199 µm (752.4) with a SD of 8.463 µm and 18.961 µm (752.6) with a SD of 4.013 µm. The LV means of CZ width of 752.4 and 752.6 depicted 51.516 µm (with a SD of 8.317 µm) and 29.521 µm (with a SD of 6.998 µm). Two WT embryos were included and measured (752.8 and 752.9). The right-ventricular compact-zone (rvCZ) means amounted to 34.028 µm and 44.512 µm with a SD of 7.978 µm (752.8) and 18.856 µm (752.9). The LV mean of 752.8 (WT) averaged out at 40.611 µm with a SD of 8.796 µm. The WT specimen 752.9 showed a LV mean of 50,201 µm with a SD of 19.111 µm. Litter II exhibited the inclusion of two homozygous embryos (756.3 and 756.6) with a respective mean of the rvCZ width of 17.058 µm (and a SD of 6,647 µm) and 19.525 µm (with a SD of 6,740 µm). The homozygous embryo 756.3 offered the mean of left-ventricular compact zone (lvCZ) of 28.186 µm with a SD of 9.864 µm, where embryo 756.6 shows a LV mean of 20.268 µm with a SD of 8.240 µm. For the WT control 756.2, the mean of the rvCZ

Table 16: Quantitative assessment of the ventricular compact zone in E13.5 hearts; The means (µm) and the SD (µm) of the ventricular width of the compact zone are shown, separately regarded in the right and left ventricle. Per side of ventricle (right or left) five positions within one ventricle (apical to basal) were measured in four different section levels. In total, 20 values per specimen resulted. The unpaired two-sided, homoscedastic student's t-test compares each respective mean of the compact-zone width of six homozygous embryos with the means of six WT embryos, separately regarded for the right and the left ventricle. The p-value for the figures of the right ventricle equals 0,054 and for the left ventricle 0,127. Therefore, both p-values were not regarded as statistically significant.

compact zone width:			right ventricle				left ventricle			
genotype	**litter**	**ID**	**mean (µm)**	**p**	**SD (µm)**	**n**	**mean (µm)**	**p**	**SD (µm)**	**n**
Tm-1a/Tm-1a	I	752.4	37.199	0.054	8.463	20	51.516	0.127	8.317	20
(E13.5 p.c.)	I	752.6	18.961		4.013	20	29.521		6.998	20
	II	756.3	17.058		6.647	20	28.186		9.865	20
	II	756.6	19.525		6.740	20	20.268		8.240	20
	III	235.8	39.978		18.118	20	41.051		9.184	20
	IV	257.7	44.714		15.559	20	62.674		22.711	20
+/+	I	752.8	34.028		7.978	20	40.611		8.796	20
(E13.5 p.c.)	I	752.9	44.512		18.856	20	50.201		19.111	20
	II	756.2	25.403		15.769	20	33.138		12.043	20
	II	756.4	55.916		21.348	20	53.011		8.789	20
	III	235.6	72.503		33.572	20	77.339		13.569	20
	IV	257.10	59.319		19.646	20	84.723		13.819	20

Legend: **p:** p-value (<0.05: significant), **n:** measured values per specimen;

width was 25.403 µm with a SD of 15.769 µm. The averaged width of the second WT control 756.4 was 55.916 µm with a SD of 21.348 µm. The mean of the lvCZ width of 756.2 (WT) depicted 33.138 µm with a SD of 12.043 µm. The LV mean for 756.4 accounted for 53.011 µm with a SD of 8.789 µm. In litter III, the mean of the rvCZ width of homozygous embryo 235.8 averaged out at 39.978 µm with a SD of 18.118 µm, where the RV mean of the WT embryo 235.6 amounted to 72.503 µm with a SD of 33.572 µm. The lvCZ mean of 41.051 µm (SD 9.184 µm) was calculated for the homozygous embryo 235.8 with a WT control LV mean (235.6) of 77.339 µm (SD 13.569 µm). In litter IV, the homozygous embryo 257.7 exhibited an average of rvCZ width of 44.714 µm with a SD of 15.559 µm. The WT embryo 257.10 showed a RV width mean of 59.319 µm (SD 19.646 µm). The lvCZ mean of the homozygous embryo 257.7 was 62.674 µm (SD of 22.711 µm). The WT control (257.10) showed a LV mean of 84.723 µm with a SD of 13.819 µm.

Table 16 shows the results of an unpaired two-sided, homoscedastic Student's t-test, separately performed for the RV and LV. The p-value equals 0.054 for the RV and 0.127 for the LV, which are both regarded as not statistically significant. This implies that the influencing factor Tm-1a homozygosity has no significant effect on the width of vCZ in

E13.5 hearts, which is one leading parameter for the evaluation of ventricular compaction. In other words, these data give evidence that ventricular compaction is not significantly affected by Tm-1a homozygosity in E13.5 hearts. Furthermore, **figure 13** visualizes the relationship of the genotype and the width of the vCZ in the E13.5 cohort.

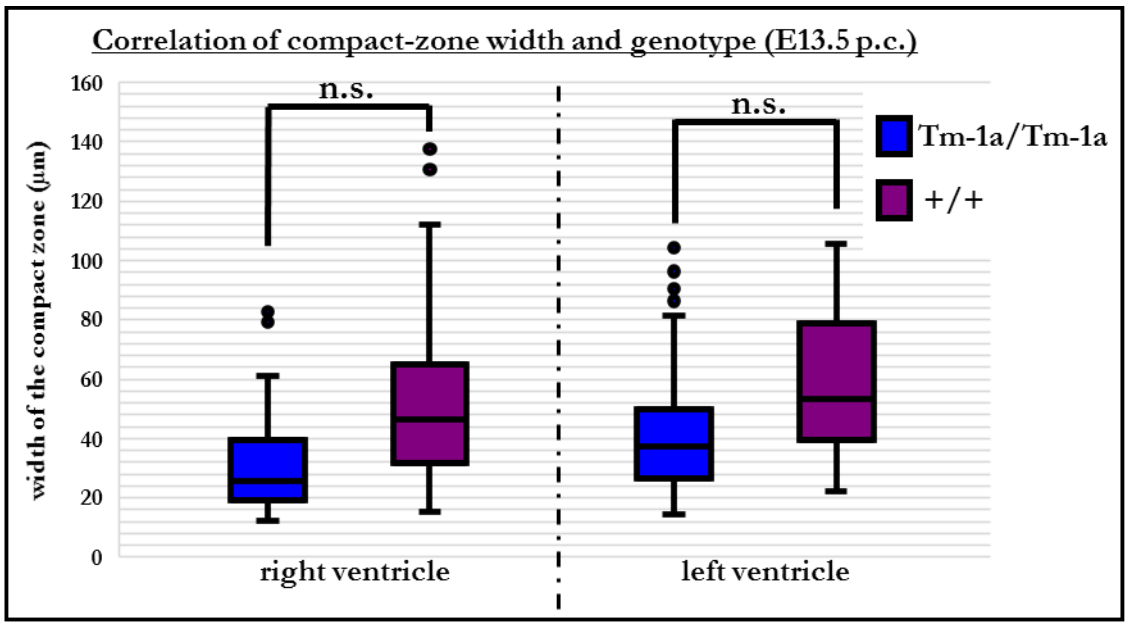

Figure 13: Correlation of compact-zone width and genotype (E13.5 p.c.); Legend: n.s.: not significant, **dots above or below the whiskers:** outliners defined by the Tukey's correction, **blue color:** values of homozygous specimens, **purple color:** values of WT specimen; Box plots of the E13.5 cohort are shown, which visualize the width of the compact zone depending on the genotype, regarded in the right and left ventricle.

3.3.2.2 E15.5 hearts

Table 17 shows an overview of the descriptive statistics for the E15.5 cohort. Two litters (170.x and 117.x) were recruited with a total amount of three homozygous embryos and four WT embryos. In litter I, two homozygous embryos (170.3 and 170.5) were measured with a RV mean of 54.021 µm (SD 32.609 µm) and 78.498 µm (SD 47.098 µm). The RV mean of WT specimen 170.7 averaged out at 148.715 µm with a SD of 40.270 µm. The WT specimen 170.8 showed a RV mean of 168.105 µm with a SD of 18.998 µm. The RV mean of the WT embryo 170.10 amounted to 171.192 µm (SD of 35.300 µm). For the LV in litter I, the mean for 170.3 averaged out at 120.121 µm with a SD 26.873 µm. For the homozygous specimen 170.5, the LV mean amounted to 130.854 µm with a SD of 24.026 µm. The WT specimen 170.7 showed a LV mean of 192.978 µm with a SD of 29.781 µm. The embryo 170.8 exposed a LV mean of 165.390 µm with a SD of 14.478 µm. WT embryo 170.10 showed a LV mean of 202.077 µm with a SD of 35.495 µm. In litter II, the RV mean of the homozygous embryo 117.4 depicted 107.563 µm with a SD of 17.932 µm, where the RV mean of 117.4 (WT

control) averaged out at 175.171 µm with a SD of 26.457 µm. In litter II, the lvCZ mean of the homozygous embryo 117.4 depicted 135.620 µm with a SD of 38.535 µm. The LV mean of the WT control 117.1 amounted to 185.516 µm with a SD of 25.745 µm.

Table 17: Quantitative assessment of the ventricular compact zone in E15.5 hearts; The means (µm) and the SD (µm) of the ventricular width of the compact zone are shown, separately regarded in the right and left ventricle. Three homozygous embryos and four WT embryos from the E15.5 cohort were included. Per side of ventricle (right or left) five positions within one ventricle (apical to basal) were measured in four different section levels. In total, 20 values per specimen resulted. The unpaired two-sided, homoscedastic student's t-test compares each mean of the compact-zone width of three homozygous embryos with the means of four WT embryos, separately regarded for the right and the left ventricle. The p-value for the the right ventricle equals 0,002 and for the left ventricle also 0,002. Therefore, both p-values were regarded as statistically significant.

compact zone width:			right ventricle				left ventricle			
genotype	**litter**	**ID**	**mean (µm)**	**p**	**SD (µm)**	**n**	**mean (µm)**	**p**	**SD (µm)**	**n**
Tm-1a/Tm-1a	I	170.3	54.021	0.002	32.609	20	120.121	0.002	26.873	20
(E15.5 p.c.)	I	170.5	78.498		47.098	20	130.854		24.026	20
	II	117.4	107.564		17.932	20	135.620		38.535	20
+/+	I	170.7	148.715		40.270	20	192.978		29.781	20
(E15.5 p.c.)	I	170.8	168.105		18.998	20	165.390		14.478	20
	I	170.10	171.192		35.300	20	202.077		35.495	20
	II	117.1	175.171		26.457	20	185.516		25.745	20

Legend: **p:** p-value (<0.05: significant), **n:** measured values per specimen;

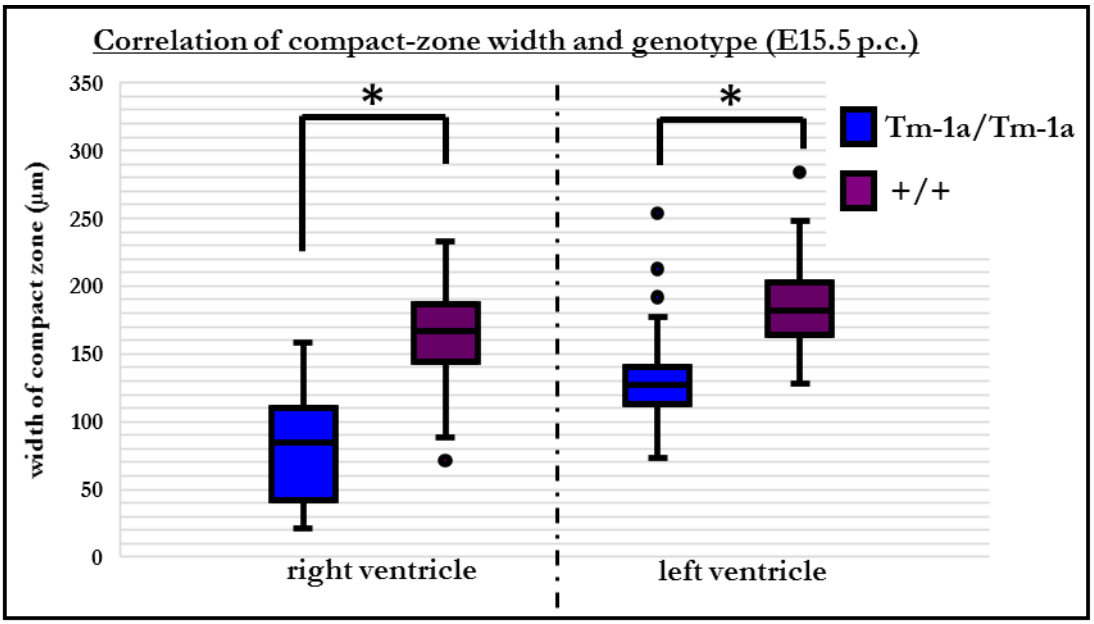

Figure 14: Correlation of compact-zone width and genotype (E15.5 p.c.); Legend: *: significant, **dots above or below the whiskers:** outliners defined by the Tukey's correction, **blue color:** values of homozygous specimens, **purple color:** values of WT specimens; Box plots of the E15.5 cohort show the width of the compact zone depending on the genotype, regarded in the right and left ventricle.

Also, for the E15.5 cohort an unpaired two-sided, homoscedastic Student's t-test was performed to address the question whether the width of vCZ in homozygous specimens significantly differs from those in WT controls. **Table 17** shows the calculated p-values. Both rounded p-values equal 0.002. Therefore, p-values were regarded as statistically significant. These data imply that the width of the vCZ is significantly reduced compared to WT controls in the E15.5 cohort. Thus, biventricular non-compaction can be demonstrated. Therefore, it seems conceivable that Tm-1a homozygosity impedes the developmental process of myocardial compaction. **Figure 14** shows the correlation of the compact-zone width and the genotype in the E15.5 cohort.

3.3.3 Synopsis: histological assessment of Tm-1a hearts

The results of the histological analysis of embryonic hearts at three developmental timepoints showed no differences in the following items: morphology of valves (venous valves in E11.5 embryos and atrioventricular and semilunar valves in E13.5 and E15.5 embryos), the outflow tracts, the ECT lining of the atrioventricular canal and the formation of blood-conductive vasculature (PT, PAA and PDA). The VSD occurrence was documented in three out of five homozygous E15.5 embryos, where five out of five WT controls showed no VSD. In part II, biventricular non-compaction was proven to occur in homozygous E15.5 hearts. In E13.5 hearts, the vCZ in homozygous hearts was not significantly reduced compared to WT controls.

3.4 Correlation of the external-phenotype score and the ventricular reduction ratio

$$\mathrm{vRR} = 1 - \frac{\bar{x}\ (\text{widths of compact zone of homozygous embryo of litter y})}{\bar{x}\ (\text{widths of comopact zone of all WT embryos of litter y})}$$

Figure 15: Formula of the ventricular reduction ratio; The ratio of the widths mean of the compact zone of one homozygous specimen and the widths mean of the compact zone of all WT controls of the same litter is substracted from one. It depicts a dimensionless figure that reflects the degree of ventricular non-compaction.

After having presented the results of measuring the vCZ width in twelve E13.5 and seven E15.5 hearts, the connection of chapter 3.2 and 3.3 will be promoted to address the question whether the occurrence of an EP can be traced back to differences in the respective CZ width.

Table 18: Assignment of the external-phenotype points and ventricular reduction ratio in all homozygous embryos of the E13.5 and E15.5 cohort; The homozygous embryos 218.6 and 218.11 could not be histologically assessed because of technical reasons. The homozygous embryos 106.2 and 106.4 were autocatalyzed and not histologically assessable. Therefore, they were disqualified from scoring. The presented values are further visualized in figure 16.

age (p.c.)	ID	points	A	B
E13.5	218.6	5	-	-
E13.5	218.11	5	-	-
E15.5	170.3	5	0.668	0.357
E13.5	756.3	4	0.580	0.346
E15.5	170.5	3	0.517	0.300
E13.5	756.6	2	0.520	0.529
E13.5	752.6	2	0.517	0.350
E13.5	257.7	1	0.246	0.260
E13.5	752.4	0	0.053	-0.135
E15.5	117.4	0	0.386	0.269
E13.5	235.8	-1	0.449	0.469
E15.5	106.2	-1	-	-
E15.5	106.4	-1	-	-

Legend: **A:** right-ventricular reduction ratio, **B:** left-ventricular reduction ratio, **external-phenotype points: [-1]:** disqualified, **[0]:** no external phenotype detected, **[1]:** intermediate type, external phenotype detected: **[2]:** light, **[3]:** moderate, **[4]:** severe, **[5]:** severest;

The ventricular reduction ratio (vRR) was calculated to assess the degree of width reduction in homozygous embryos that were EP scored and whose hearts were measured (compare **figure 15**). The vRR is a dimensionless figure that reflects the degree of ventricular non-compaction. The vRR is calculated by subtraction of the following ratio from one: the ratio is calculated by dividing the mean of the CZ width of one homozygous specimen by the total mean of the WT control(s) of the same litter (compare **figure 15**). The bigger vRR, the higher the degree of non-compaction can be stated.

Table 18 shows an overview of the EP-point assignment and the calculated vRR for the RV and the LV in the E13.5 and E15.5 cohort, which is further visualized in **figure 16**. In the following, the vRR of the E13.5 cohort will be presented. Because of histo-technical reasons, the litter of the embryos that were EP scored with five points (218.6 and 218.11) could not be included in the histological assessment. Still, both embryos are listed. Being assigned with four EP points, because of bilateral rTEL, the homozygous embryo 756.3

featured a right-ventricular reduction ratio (rvRR) of 0.580 and a left-ventricular reduction ratio (lvRR) of 0.346. The homozygous embryo 752.6 featured unilateral rTEL, therefore, was asssigned with two EP points. It exhibited a rvRR of 0,517 and a lvRR of 0.350. The homozygous embryo 756.6 was assigned with two EP points, because of unilateral rTEL.

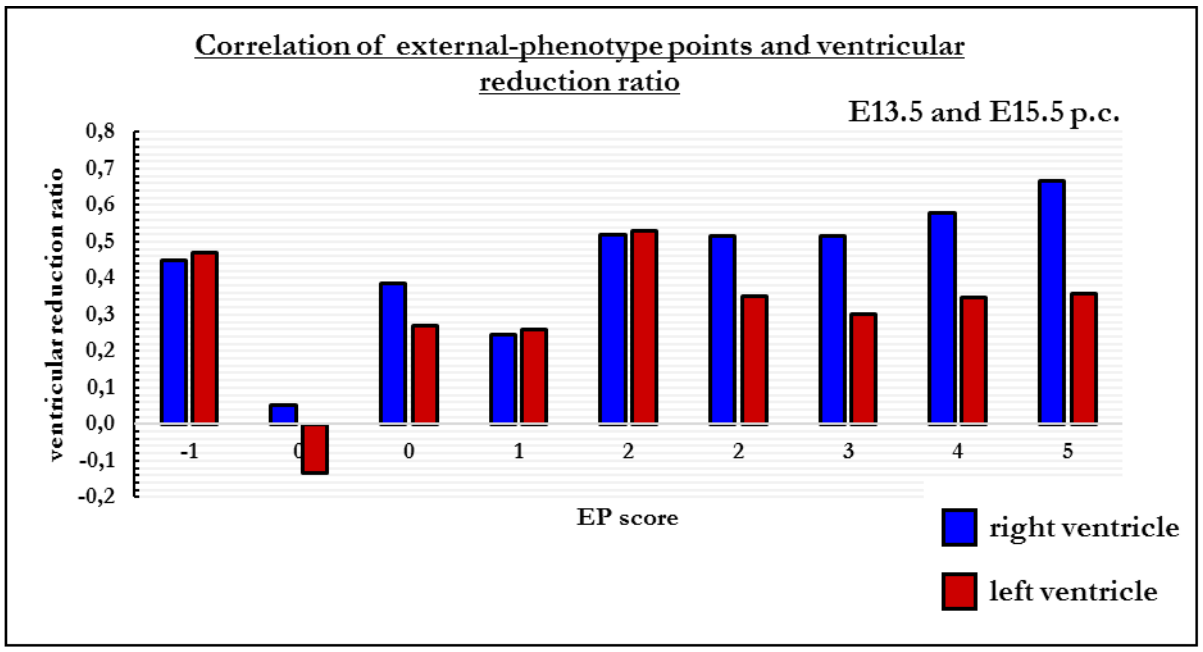

Figure 16: Correlation of the external-phenotype points and the ventricular reduction ratio; Legend: external-phenotype score: [-1]: disqualified, **[0]:** no external phenotype detected, **[1]:** intermediate type, external phenotype detected: **[2]:** light, **[3]:** moderate, **[4]:** severe, **[5]:** severest, **blue color:** right ventricle, **red color:** left ventricle; Precise figures can be taken from table 18.

It offered a rvRR of 0.520 and a lvRR of 0.529. Exhibiting an IMT with one EP point, the homozygous embryo 257.7 featured a rvRR of 0.246 and a lvRR of 0.260. The homozygous embryo 752.4 that exposed no EP (zero EP points) offered a rvRR of 0.053 and a lvRR of 0.135. Because of external autocatalysis, the homozygous embryo 235.8 was disqualified. Still, it offered inner organs that were histologically assessable despite of progressive external autocatalysis. Its rvRR depicted 0.449 and the lvRR accounted for 0.469. To regard the E15.5 cohort, two homozygous embryos were assigned with five EP points, which mophologically reflects bilateral rTEL with additional SE (190.4 and 170.3). The homozygous embryo 190.4 was excluded from width measurement as previously mentioned, because no WT control was available within the litter 190.x. The vRR of the second homozygous E15.5 embryo that was EP scored with five EP points (170.3) amounted to 0.668 (rvRR) and 0.357 (lvRR). The homozygous embryo 170.5 was EP scored with three EP points and featured a rvRR of 0,517 and a lvRR of 0.3. The homozygous embryo that exposed no EP (117.4) offered a rvRR of 0.386 and a lvRR of 0.269. Progressed autocatalysis

frustrated histological assessment of the heart in two homozygous embryos (106.2 and 106.4). **Figure 16** shows the correlation of the respectively assigned EP score and the respective vRR in the E13.5 and the E15.5 cohort. To consider the rvRR from two EP points upwards, a tendency of positive correlation can be assumed: The higher the rvRR, the severer the EP. For the LV no positive regression could be concluded, neither in the E13.5, nor in the E15.5 cohort.

4 Discussion

The objective of this study was to elucidate potential molecular machanisms that lead to HLHS. The candidate gene KIAA00182 (analogue to Gse-1 in mice), which was found to be *de novo* mutated in a child that suffered from HLHS, was hypothesized to be involved in the pathogenesis of HLHS. In addition to this, embryological lethality of homozygous Tm-1a mice of the Gse-1 mouse model was proven to occur in a previously performed study with a g-power of 99.999% (Alnour 2016). The aim of this study was to determine the timepoint of embryonic lethality and to identify a putative cardiac phenotype of homozygous Tm-1a embryos of the knockout-first mouse line. An established method to detect the timepoint of embryonic lethality is to determine the genotypical incidence at consecutive embryonic ages. In this study, embryonic cohorts at three developmental timepoints were genotyped. The selection of the embryonic ages of E11.5 p.c., E13.5 p.c. and E15.5 p.c. was carried out, because the exact timepoint of in utero death of homozygous Tm-1a embryos was hard to anticipate without vanguard knockledge on this field. Therefore, a certain timeslot was chosen, where cardiogenesis in its early but also later events was covered. Based on the genotyping results, homozygous Tm-1a embryos start to die after E11.5 p.c. A decline of genotypical incidence was observed, which started to emerge at E13.5 p.c and augmented at E15.5 p.c. This fact appears to reflect the onset of developmental impairment of homozygous embryos. The genotypical incidences of E13.5 p.c. until E15.5 p.c. offered no significant p-values, which may have occurred because of different reasons. Either the incidence of Tm-1a homozygosity significantly decreases after E15.5 p.c., which indicates that homozygous embryos die after E15.5 p.c., or the p-value of the after-E11.5 cohort was not significant, because the sample size was too small to detect a difference of the acquired and expected incidences. The calculated g-power of each cohort must be considered, when the evaluation of its significance is aspired. The E13.5 and E15.5 cohorts offered a g-power of only around 33%, which indicated that a type-II error might be commited in 67% of the cases (type-II error: eventhough a real difference lies at hand, the nullhypothesis is mistakenly affirmed), which results from too small sample sizes.

The small genotyping sample size that led to small g-power values represents one limitation of this study. The smaller the differences that are aspired to be detected, the bigger the sample size must be to achieve a satisfactory g-power, such as 80%. As an important future outline, larger cohorts should be pursued to achieve higher g-power values. In addition to that, later developmental timepoints (such as E18.5 p.c.) must be investigated, since the

homozygous incidence at birth (E19.5 p.c.) is 0%. Therefore, a dramatical decline of incidence should be detectable between E15.5 p.c. and the time of birth.

Looking at the genotyping results for the WT and heterozygous embryos, certain discrepancies became apparent. While the expected Mendelian ratio of 50% was approximately observed for Tm-1a heterozygosity for the embryonic ages E11.5 p.c., a clear deviation from the expected genotypical apportionment was found for E15.5 p.c. One would expect that the portion of genotypical gain for heterozygous and WT specimens augments in the ratio of 2:1. In this case, the homozygous incidence was reduced by around 9%. Therefore, it would have been expected that the heterozygous incidence rises around 6% and WT gains 3%. So, a total incidence of 56% for heterozygous and 28% for WT should have been traceable. Instead of this, the incidences were around 64% for heterozygous and about 20% for WT. Since the WT genotype is characterized by the absence of the second amplicon of 127 bp, which is present in heterozygous specimens, sporadic cases of contamination of specimens must be assumed.

To conclude the onset of the embryonic phenotype, the results of genotyping, whole-mount evaluation and histological analysis were synoptically regarded. The results of the external morphology assessment of Tm-1a embryos gave definite evidence that Tm-1a homozygosity is highly implied in the occurrence of a so-called EP. At E13.5 p.c., homozygous Tm-1a embryos expose external aberrancies, which were aspired to be systematically assessed by an EP score. It was intended to enable a genotype-independent detection of abnormalities of the external morphology. Therefore, the application of the EP score was a primary blinded assessment of external features. The major criteria of the EP score were characterized by the occurrence of rTEL and SE. These external aberrancies deteriorated in their severity in the E15.5 cohort compared to the E13.5 cohort. With an increasing age, the fraction of those homozygous embryos that expose an EP increased. In the E15.5 cohort, 80% of homozygous embryos showed an EP. The fact that one homozygous E15.5 embryo (20%) was scored as nEPd reflects the diagnostical imprecision of the EP score. Continuative studies of the Gse-1 project have shown that Gse-1 knockout embryos expose an impaired hematopoesis, which majorly takes place in the hepatic primordium during embryogenesis. Because of this, homozygous embryos exposed anemia and as a result of impaired hematopoesis a paler hepatic region, which is even retrospectively visible in homozygous Tm-1a embryos. Taking this important finding into account, the major criteria of the EP turn out to be incomplete. The minor criterion of RS even appears of marginal importance, since its relevance could not be asserted. The fact that groundbreaking findings often cannot be anticipated in advance is reflected by a myriad of

clinical scores and classifications that found posterior modification. This principle can also be applied here, to the first draft of the EP score. As a future outline, a modified version of the EP score (modified EP score) should be considered that handles the paleness of the hepatic region, which gleams through the embryonic cutis below the right costal arch, as one further major criterion. By application of the modified EP score, that one homozygous E15.5 embryo (117.4), which seemingly exposed no EP, would also have been detected as pathological, since it exposed a paler hepatic region compared to non-homozygous litter mates.

A significant biventricular non-compaction and the increased occurrence of VSD of Tm-1a homozygous hearts were proven to occur at E15.5 p.c., where no significant difference in the degree of ventricular compaction in homozygous embryos compared to WT controls was shown at E13.5 p.c. This finding constitutes the first description of a cardiac phenotype in the Tm-1a knockout-first mouse line. Therefore, it depicts one major discovery in the quest of deciphering, why Tm-1a homozygous embryos die. Taken for itself, the cardiac phenotype is insufficient to explain embryonic lethality of Tm-1a homozygosity. Future studies will tie up to these findings.

Furthermore, the tendency of a positive correlation of the EP score and the rvRR was assumed. The vRR is a dimensionless value that is reflecting the degree of ventricular non-compaction. By regression of the scored EP and the vRR of the respective embryo, a rvRR-threshold of around 50% can be hypothesized, at which embryos start to expose an EP (two EP points or more). Regarding the lvRR, no obvious correlation was asserted, which appears contradictory to the results of biventricular non-compaction in E15.5 embryos. As a future outline, further improvement into the design of the vRR should be undertaken to stratify its diagnostical virtue. Eventhough, biventricular non-compaction only was proven to significantly occur in the E15.5 cohort, the vRR calculation involved also the homozygous embryos of the E13.5 cohort. Here, the developmental tendency of an emerging non-compaction in earlier timepoints than E15.5 p.c., such as E13.5 p.c., appears to be hinted, which even became qualitatively visible in the histological assessment of homozygous E13.5 hearts. Eventhough, quantitative analysis did not prove biventricular non-compaction in homozygous E13.5 specimens, the onset of myocardial impairment of the CZ can be hypothesized to occur earlier than E15.5 p.c., such as E14 p.c.

The notion that Tm-1a embryos expose external signs of congestion because of cardiogenetic impairment seems pathophysiologically reasonable. In this case, cardiac impairment is constituted by biventricular non-compaction and the incidence of VSD at the

age E15.5 p.c. These aberrancies cause circulatory congestion that becomes externally visible in the manifestation of SE and rTEL. These teleangiectatic lesions were histologically verified. They exposed intact vessel walls.

By means of statistical analysis, it was proven that the width of the vCZ is significantly reduced in homozygous E15.5 embryos in both ventricles. For the statistical analysis by means of an unpaired two-sided, homoscedastic Student's t-test the comparison of the calculated width means of homozygous and WT controls was ensured, since a non-affection of heterozygous vCZ could not be excluded in advance. Therefore, the E15.5 litter 190.x, which offered three homozygous and two heterozygous embryos, was excluded from the quantitative assessment of the width of the vCZ in part II of chapter 3.3. In contrast to that, this litter was used for the qualitative visualization of the histological results in part I of chapter 3.3, since the technical quality of this litter in the process of methodological reprocessing was – compared to other pairs of homozygous specimens and controls – the best. Therefore, the histological pictures of chapter 3.3, which utilized mostly 190.x for E15.5 p.c., may be considered as representative under reservation, since the quantitative evaluation of the myocardium was restricted to part II.

After having pointed out the weakness of the EP score above, primary considerations that led to the first draft of the EP score shall be mentioned. The morphologies of E11.5, E13.5 and E15.5 embryos were inspected, where the EP was defined by morphological criteria. The EP score consisted of two major criteria, which defined the EP. They were differingly emphasized with points due to the following factors. The occurrence of rTEL per side was awarded with two EP points. This contributed to the fact that an embryo, which exposed bilateral rTEL, automatically was scored higher than an embryo that exposed unilateral rTEL. By this, the importance of the phenomenon of rTEL for the EP was pointed out. The following notions support the presumption of the congestive nature of rTEL. The histological inspection of rTEL in homozygous E13.5 and E15.5 embryos compared to litter-internal WT controls revealed the intact vessel border with no egression of erythrocytes in the surrounding connective tissue. The intactness of the vessel walls defines telangiectatic lesions. The macroscopically sharp contour of rTEL, the progredient generalization of rTEL regarded from E13.5 p.c. to E15.5 p.c. and the impression of a three-dimensional vessel network supported the etiology of rTEL to be congestive. In other words, if an embryo was classified as EPd, it had to expose rTEL at least at one side of the embryonic body. The sole occurrence of SE was counted as unsufficient to be considered as an EP defining event because of the following notions. The evaluation of SE is more error-prone than the assessment of rTEL. Therefore, it was handled as one additional major criterion. Especially

in E11.5 and E13.5 embryos, whose cutis exposes no proper *stratum corneum* yet, the impact of accidental storage in fluids that potentially change the extent of the SE (such as 4%-PFA) cannot absolutely be excluded. Another factor, which potentially causes bias in the evaluation of SE is of technical nature and depicted by the fact that the recognition of SE highly depends on the right exposure to light during the photographical aquisition of each embryo. The photodocumentation of SE was less error-prone in E15.5 embryos, which is caused by an advanced development of the *stratum corneum* of the cutis that detains liquid impairment. Because of all these factors, the occurrence of SE was handled as a major criterion, since its correlation to cardiac congestion is highly implied in literature. If one embryo would have exposed SE without rTEL, it would not have been awarded with one point, because of the above-mentioned biasing factors, which would have led to wrong-positive counts. Interestingly, this theoretical case did not occur once, which adds to the primary importance of rTEL. With the award of EP points, the degree of severity of the EP was classified, where the assignment of five EP points indicated the most severe form of EP, which implied bilateral rTEL and the additional occurrence of SE. This case occurred four times among 95 evaluated embryos (eleven E11.5, 47 E13.5 and 37 E15.5 embryos). The lightest form of EP with the award of two EP points occurred three times. The cases of the award of three and four EP points occurred once, respectively. While evaluating E13.5 embryos, another phenomenon became apparent, whose appearance was included in the definition criteria of the EP (the occurrence of more than four RS). Because of the lacking final formation of the *stratum corneum* with a high extent of cutaneous transparency, the external morphology (of E13.5 embryos) was highly characterized by a variety of red structures (cutaneous vessels), blood-egressive formations (diffuse hemorrhages), point-shaped configurations (RS) and further phenomenons (erythrocytes-contaminated cutaneous surfaces). Among all these phenomenons with likely different etiologies, the lowest common denominator between the EP and the variety of red structures had to be determined, because a potential etiological connection could not be excluded in advance. The fact that in chapter 3.2 many RS items had to be defined reflects the high degree of uncertainty that surrounds this minor criterion, which aspires to distinct betweeen a relevant item and mere diffuse hemorrhagic structures, which resemble background noise. The possibility of the occurrence of traumatic hemorrhages is higher in acral regions of the embryonic body, because during emryonic dissection, the head or the limbs were accidentally used to be pulled with the forceps to separate the embryo from the amniotic sac and the rest of the maternal uterus. Therefore, only the torso localization was regarded for counting RS. The threshold of four is an empiric figure that helps in the distinction of embryos that expose a higher amount of RS. It underlies

an artificial construction of the threshold, where the two major criteria featured less insecure characteristics that resemble the principle of a visual diagnosis. These discrepant factors were regarded, while designing the minor criterion of the EP score. It resulted in the award of one EP point to those embryos that exposed more than four RS on one side of the embryonic body. It accounted for the IMT that neither belongs to the group of EPd, nor nEPd. In other words, the mere occurrence of more than four RS was not enough to detect an EP. This aspect finds further support in the fact that the coincidence of the major and minor criteria did not occur in one single case, which putatively indicates an independent etiology. As aforementioned, in ongoing studies the minor criterion of RS has found no noteworthy relevance. One criterion of disqualification was introduced, which was awarded with one minus point: autocatalysis that represented in utero death. To regard the degree of autocatalysis, great differences became apparent. Where some autocatalyzed embryos exposed such an advanced extent of autocatalysis that genotyping proved unsuccessful because of DNA decay (106.2), other autocatalyzed embryos were genotypable and even histologically assessable with quantifiable cardiac structures, such as the histologically included E13.5 embryo 235.8. All in all, autocatalysis is an erratic event during embryogenesis. To concern all five cases of autocatalysis in the E11.5, E13.5 and E15.5 cohorts, three embryos were homozygous, one proved to be WT and one remained with an unknown genotype. Whether autocatalysis is part of the homozygous phenotype can neither be proven nor completely be excluded, because of the superimposing fact of routine in utero death and the small sample size. Therefore, it was designated as disqualifying criterion. Thus, the EP score turned out to be a coding system that simultaneously expressed a certain combination of phenomena and enabled a genotype-independent classification of the external morphology of Tm-1a embryos.

The onset of the EP was observable at E13.5. Therefore, the E13.5 and E15.5 cohort will be regarded in the following. Eight out of nine embryos that exposed an EP were homozygous and one was heterozygous. To regard the WT embryos, zero out of 24 embryos showed an EP. To consider all 14 homozygous embryos, eight of them exposed an EP (four from the 13.5. and four from the E15.5. cohort), three showed no EP (two of the E13.5 and one of the E15.5 cohort), one embryo was accounted as IMT and two embryos were disqualified because of autocatalysis. As mentioned above, the modified EP score would have detected that one homozygous E15.5 embryo that seemingly showed no EP, since it exposed a paler hepatic region. In analogy to this revision, also those two homozygous E13.5 embryos (752.1 and 752.4), which were nEPd classified, exposed a paler hepatic region,

which serves as a sign of impaired hematopoesis in the hepatic primordium that results in anemia.

Certain aspects point at the notion that the cardiac phenotype occurs as a secondary event. Hemodynacis are commonly considered to play an important role in cardiogenesis. The process of compaction is highly dependent on hemodynamics during development. Interestingly, responsiveness to shear stress was shown for many transcription factors, such as the superfamily of transforming growth factors β (TGF-β) and the BMP endothelial regulator, which are implied in EndMT (Poelmann and Gittenberger-de Groot 2018). The hypothesized implication of Gse-1 in EndMT constituted the reasonable suspicion for homozygous Tm-1a embryos to expose a cardiac phenotype. In contrast to adult hearts, both ventricles play an utmost important role during embryogenesis in the support of systemic circulation and the maintenance of growing hemodynamical requirements. The fact that biventricular non-compaction occurs in homozygous Tm-1a embryos at E15.5 p.c. appears to reflect that non-compaction results from a still unknown triggering factor, which accordingly affects the more required part of the myocardium. The heterogenous picture of the EP and the paucity of one definite timepoint of embryonic lethality at early ages of cardiogenesis further support this notion that cardiac non-compaction appears not to be the primary result of a gene knockout. A primary triggering factor is putatively necessary for the developing heart of homozygous Tm-1a mice to correspond to it in such dramatical way. To a certain degree, the results of this thesis reflect the decisiveness of the complex pathogenetical interplay, which is commonly assumed to occur in CHD. In several previous studies, hypoxia was described to be one major-triggering factor for myocardial non-compaction in addition to further severe congenital heart defects (Kenchegowda et al. 2014). The experimental production of hypoxic conditions in the developing embryos of a certain mouse model at early stages of cardiac development, such as E9.5 p.c., induced severe cardiac malformations like DORV or conotruncal defects. The induction of hypoxia at later timepoints, such as E13,5 p.c., showed no effects on cardiogenesis (Kenchegowda et al. 2014). Physiologically, embryonic hearts expose mechanisms to cope with hypoxia. The occurrence of the cardiac phenotype might secondarily occur, as a response to anemia-conditioned hypoxia during a hypoxia-sensitive phase of myocardial cardiogenesis.

The results of this thesis remain on a relatively descriptive level. It cannot exactly be answered how the Tm-1a allele is involved in the pathogenesis of biventricular non-compaction at E15.5 p.c. Still, these results enable further investigations as a groundwork to understand the specific mechanisms that lead to embryonic lethality of homozygous Tm-1a embryos. As an important future outline further mechanistic insights of Gse-1 will be

aspired, such as identifying the expression pattern of Gse-1 in Tm-1a hearts by means of lac-Z staining and continuative investigation of the mouse lines Tm-1b, -1c and -1d.

The pathogenetical model that congenital heart disease occur as a result from a multifactorial happening is commonly accepted. Environmental factors face genetical predispositions that, furthermore, meet still unknown events, which finally may result in such dramatical and life-threatening diseases such as HLHS. Gittenberger-de Groot and colleagues pointed out that transgenic animal models allow insights, which - in combination with human pathology - lead to a better understanding of congenital heart diseases (Gittenberger-de Groot et al. 2005). 'From bench to bedside' is a bon mot that expresses the translational quest as an ideal giuding theme of medical basic research. With this thesis, the groundwork for further mechanistic insights of the molecular function of Gse-1 during embryo- and especially cardiogenesis was set that enables the identification of translational approaches to treat HLHS patients.

5 Summary

Introduction and objective of this study: HLHS is classified as a cyanotic heart disease, which accounts for 25% of all CHD mortalities. It is the leading cause of death in infants under the age of one year (Gillum 1994; Bradley 1999). HLHS is multifactorially caused. One human candidate gene called KIAA00182 (Gse-1 in mice) was hypothesized to be implied in the pathogenesis of HLHS because of a) a *de novo* mutation of it, which was found in a child suffering from HLHS, and b) the documented lethality of homozygous Gse-1 mice by the age of three weeks. The objective of this study was to determine the timepoint of embryonic lethality of homozygous Tm-1a embryos and to identify a putative cardiac phenotype.

Experimental methods: The genotype of embryos at three embryonic ages (E11.5 p.c., E13.5 p.c. and E15.5 p.c.) was determined by PCR. The external morphology was inspected and assessed with a scoring system (external-phenotype score), which allowed a severity classification of external aberrancies. In two parts, the hearts of Tm-1a embryos were histologically analyzed, where part I focussed on the evaluation of non-ventricular structures. In part II, the quantitative assessment of the ventricular compact zone was performed. The quantification was further substantiated by the calculation of a ventricular reduction ratio, which reflects the degree of myocardial non-compaction. Regarded for E13.5 and E15.5 embryos, the correlation of the external-phenotype score and the ventricular reduction ratio was promoted.

Results: Genotyping Tm-1a embryos of three developmental ages showed a decline of Tm-1a homozygosity from 25.92% to 16.67% with an increasing age. By whole-mount inspection of Tm-1a embryos, the occurrence of an external phenotype was documented, whose major characteristics were reticular telangiectasias and subcutaneous edema. It was shown that its occurrence is highly associated with Tm-1a homozygosity. Histological assessment of embryonic hearts showed a significant biventricular non-compaction in homozygous E15.5 hearts, whereas in homozygous E13.5 embryos no significant non-compaction occurred.

Conclusion: Homozygous Tm-1a embryos start to die after E11.5 p.c., where the onset of developmental impairment appears to start between E12.5 p.c. and E13.5 p.c. In homozygous Tm-1a embryos, a time slot of embryonic lethality, which putatively starts to emerge between E13.5 p.c. and E16.5 p.c., seems pathogenetically conceivable. The discovery of biventricular non-compaction in homozygous E15.5 hearts constitutes the first description of a cardiac phenotype of the Gse-1 mouse line, which was identified as one element of aberrant pathogenesis that further appears to contribute to embryonic lethality of Tm-1a homozygosity. The paucity of one definite timepoint of embryonic lethality and the heterogenous picture of the external phenotype support a suspected secondary etiology of the cardiac phenotype. In future studies, still unknown primary causative factors must be identified.

6 List of references

Abdelhamed ZA, Natarajan S, Wheway G, Inglehearn CF, Toomes C, Johnson CA, Jagger DJ (2015): The Meckel-Gruber syndrome protein TMEM67 controls basal body positioning and epithelial branching morphogenesis in mice via the non-canonical Wnt pathway. Dis Model Mech 8, 527–541

Aiello VD, Ho SY, Anderson RH, Thiene G (1990): Morphologic features of the hypoplastic left heart syndrome--a reappraisal. Pediatr Pathol 10, 931–943

Allen RH, Benson CB, Haug LW (2005): Pregnancy outcome of fetuses with a diagnosis of hypoplastic left ventricle on prenatal sonography. J Ultrasound Med 24, 1199–1203

Alnour F: 'Knockout-first' mouse model as a biological tool to study the role of KIAA0182 gene in hypoplastic left heart syndrome. Med. diss. Göttingen 2016

Anderson RH, Wilkinson JL, Becker AE (1978): The bulbus cordis--a misunderstood region of the developing human heart: its significance to the classification of congenital cardiac malformations. Birth Defects Orig Artic Ser 14, 1–28

Anderson RH, Webb S, Brown NA, Lamers W, Moorman A (2003): Development of the heart: (2) Septation of the atriums and ventricles. Heart 89, 949–958

Atz AM, Feinstein JA, Jonas RA, Perry SB, Wessel DL (1999): Preoperative management of pulmonary venous hypertension in hypoplastic left heart syndrome with restrictive atrial septal defect. Am J Cardiol 83, 1224–1228

Bailey LL (2004): Transplantation is the best treatment for hypoplastic left heart syndrome. Cardiol Young 14 Suppl 1, 109–111; discussion 112-114

Bailey LL, Nehlsen-Cannarella SL, Concepcion W, Jolley WB (1985): Baboon-to-human cardiac xenotransplantation in a neonate. JAMA 254, 3321–3329

Barnea O, Austin EH, Richman B, Santamore WP (1994): Balancing the circulation: theoretic optimization of pulmonary/systemic flow ratio in hypoplastic left heart syndrome. J Am Coll Cardiol 24, 1376–1381

Bartman T, Hove J (2005): Mechanics and function in heart morphogenesis. Dev Dyn 233, 373–381

Bashaw GJ, Kidd T, Murray D, Pawson T, Goodman CS (2000): Repulsive axon guidance: Abelson and Enabled play opposing roles downstream of the roundabout receptor. Cell 101, 703–715

Behrendt DM, Rocchini A (1981): An operation for the hypoplastic left heart syndrome: preliminary report. Ann Thorac Surg 32, 284–288

Beroukhim RS, Gauvreau K, Benavidez OJ, Baird CW, LaFranchi T, Tworetzky W (2015): Perinatal outcome after prenatal diagnosis of single-ventricle cardiac defects. Ultrasound Obstet Gynecol 45, 657–663

Bharati S, Lev M (1984): The surgical anatomy of hypoplasia of aortic tract complex. J Thorac Cardiovasc Surg 88, 97–101

Blausen BE, Johannes RS, Hutchins GM (1990): Computer-based reconstructions of the cardiac ventricles of human embryos. Am J Cardiovasc Pathol 3, 37–43

Boughman JA, Berg KA, Astemborski JA, Clark EB, McCarter RJ, Rubin JD, Ferencz C (1987): Familial risks of congenital heart defect assessed in a population-based epidemiologic study. Am J Med Genet 26, 839–849

Bradley SM (1999): Neonatal repair and dealing with a single ventricle. J S C Med Assoc 95, 335–338

Bravo-Valenzuela NJ, Peixoto AB, Araujo Júnior E (2018): Prenatal diagnosis of congenital heart disease: A review of current knowledge. Indian Heart J 70, 150–164

Brenner JI, Berg KA, Schneider DS, Clark EB, Boughman JA (1989): Cardiac malformations in relatives of infants with hypoplastic left-heart syndrome. Am J Dis Child 143, 1492–1494

Captur G, Wilson R, Bennett MF, Luxán G, Nasis A, de la Pompa JL, Moon JC, Mohun TJ (2016): Morphogenesis of myocardial trabeculae in the mouse embryo. J Anat 229, 314–325

Cassidy AR, White MT, DeMaso DR, Newburger JW, Bellinger DC (2015): Executive Function in Children and Adolescents with Critical Cyanotic Congenital Heart Disease. J Int Neuropsychol Soc 21, 34–49

Chai P, Tian J, Zhao D, Zhang H, Cui J, Ding K, Liu B (2016): GSE1 negative regulation by miR-489-5p promotes breast cancer cell proliferation and invasion. Biochem Biophys Res Commun 471, 123–128

Chang AC, Huhta JC, Yoon GY, Wood DC, Tulzer G, Cohen A, Mennuti M, Norwood WI (1991): Diagnosis, transport, and outcome in fetuses with left ventricular outflow tract obstruction. J Thorac Cardiovasc Surg 102, 841–848

Chen H, Shi S, Acosta L, Li W, Lu J, Bao S, Chen Z, Yang Z, Schneider MD, Chien KR, et al. (2004): BMP10 is essential for maintaining cardiac growth during murine cardiogenesis. Development 131, 2219–2231

Chen Q, Tulloh R, Caputo M, Stoica S, Kia M, Parry AJ (2015): Does the persistence of pulsatile antegrade pulmonary blood flow following bidirectional Glenn procedure affect long term outcome? Eur J Cardiothorac Surg 47, 154–158; discussion 158

Choquet C, Nguyen THM, Sicard P, Buttigieg E, Tran TT, Kober F, Varlet I, Sturny R, Costa MW, Harvey RP, et al. (2018): Deletion of Nkx2-5 in trabecular myocardium reveals the developmental origins of pathological heterogeneity associated with ventricular non-compaction cardiomyopathy. PLoS Genet 14, e1007502

Chrisant MRK, Naftel DC, Drummond-Webb J, Chinnock R, Canter CE, Boucek MM, Boucek RJ, Hallowell SC, Kirklin JK, Morrow WR, Pediatric Heart Transplant Study Group (2005): Fate of infants with hypoplastic left heart syndrome listed for cardiac transplantation: a multicenter study. J Heart Lung Transplant 24, 576–582

Christoffels VM, Habets PE, Franco D, Campione M, de Jong F, Lamers WH, Bao ZZ, Palmer S, Biben C, Harvey RP, Moorman AF (2000): Chamber formation and morphogenesis in the developing mammalian heart. Dev Biol 223, 266–278

Connor JA, Thiagarajan R (2007): Hypoplastic left heart syndrome. Orphanet J Rare Dis 2, 23

Consevage MW, Seip JR, Belchis DA, Davis AT, Baylen BG, Rogan PK (1996): Association of a mosaic chromosomal 22q11 deletion with hypoplastic left heart syndrome. Am J Cardiol 77, 1023–1025

Cox H, Wilson DI (2007): Genetics of hypoplastic left heart syndrome. Fetal Matern Med Rev 18, 103–119

Crucean A, Alqahtani A, Barron DJ, Brawn WJ, Richardson RV, O'Sullivan J, Anderson RH, Henderson DJ, Chaudhry B (2017): Re-evaluation of hypoplastic left heart syndrome from a developmental and morphological perspective. Orphanet J Rare Dis 12, 138

Daebritz SH, Nollert GD, Zurakowski D, Khalil PN, Lang P, del Nido PJ, Mayer JE, Jonas RA (2000): Results of Norwood stage I operation: comparison of hypoplastic left heart syndrome with other malformations. J Thorac Cardiovasc Surg 119, 358–367

Danford DA, Cronican P (1992): Hypoplastic left heart syndrome: progression of left ventricular dilation and dysfunction to left ventricular hypoplasia in utero. Am Heart J 123, 1712–1713

Dasgupta C, Martinez AM, Zuppan CW, Shah MM, Bailey LL, Fletcher WH (2001): Identification of connexin43 (alpha1) gap junction gene mutations in patients with hypoplastic left heart syndrome by denaturing gradient gel electrophoresis (DGGE). Mutat Res 479, 173–186

de Jong F, Opthof T, Wilde AA, Janse MJ, Charles R, Lamers WH, Moorman AF (1992): Persisting zones of slow impulse conduction in developing chicken hearts. Circ Res 71, 240–250

de la Cruz MV, Sánchez-Gómez C, Palomino MA (1989): The primitive cardiac regions in the straight tube heart (Stage 9) and their anatomical expression in the mature heart: An experimental study in the chick embryo. J Anat 165, 121–131

Deely WJ, Ehlers KH, Levin AR, Engle MA (1971): Hypoplastic left heart syndrome. Anatomic, physiologic, and therapeutic consideraons. Am J Dis Child 121, 168–175

Dhanantwari P, Lee E, Krishnan A, Samtani R, Yamada S, Anderson S, Lockett E, Donofrio M, Shiota K, Leatherbury L, Lo CW (2009): Human cardiac development in the first trimester: a high-resolution magnetic resonance imaging and episcopic fluorescence image capture atlas. Circulation 120, 343–351, figure 6, p.343

Dodou E, Verzi MP, Anderson JP, Xu S-M, Black BL (2004): Mef2c is a direct transcriptional target of ISL1 and GATA factors in the anterior heart field during mouse embryonic development. Development 131, 3931–3942

Donofrio MT, Skurow-Todd K, Berger JT, McCarter R, Fulgium A, Krishnan A, Sable CA (2015): Risk-stratified postnatal care of newborns with congenital heart disease determined by fetal echocardiography. J Am Soc Echocardiogr 28, 1339–1349

Doty DB, Knott HW (1977): Hypoplastic left heart syndrome. Experience with an operation to establish functionally normal circulation. J Thorac Cardiovasc Surg 74, 624–630

Dyer LA, Kirby ML (2009): The role of secondary heart field in cardiac development. Dev Biol 336, 137–144

Eisenberg LM, Markwald RR (1995): Molecular regulation of atrioventricular valvuloseptal morphogenesis. Circ Res 77, 1–6

Elliott MJ (2004): A European perspective on the management of hypoplastic left heart syndrome. Cardiol Young 14 Suppl 1, 41–46

Feinstein JA, Benson DW, Dubin AM, Cohen MS, Maxey DM, Mahle WT, Pahl E, Villafañe J, Bhatt AB, Peng LF, et al. (2012): Hypoplastic left heart syndrome: current considerations and expectations. J Am Coll Cardiol 59, S1-42

Ferencz C, Rubin JD, McCarter RJ, Brenner JI, Neill CA, Perry LW, Hepner SI, Downing JW (1985): Congenital heart disease: prevalence at livebirth. The Baltimore-Washington Infant Study. Am J Epidemiol 121, 31–36

Fontan F, Baudet E (1971): Surgical repair of tricuspid atresia. Thorax 26, 240–248

Freedom RM, Dische MR, Rowe RD (1977): Conal anatomy in aortic atresia, ventricular septal defect, and normally developed left ventricle. Am Heart J 94, 689–698

Freud LR, McElhinney DB, Marshall AC, Marx GR, Friedman KG, del Nido PJ, Emani SM, Lafranchi T, Silva V, Wilkins-Haug LE, et al. (2014): Fetal aortic valvuloplasty for evolving hypoplastic left heart syndrome: postnatal outcomes of the first 100 patients. Circulation 130, 638–645

Friehs I, Illigens B, Melnychenko I, Zhong-Hu T, Zeisberg E, Del Nido PJ (2013): An animal model of endocardial fibroelastosis. J Surg Res 182, 94–100

Frommelt PC, Sheridan DC, Mussatto KA, Hoffman GM, Ghanayem NS, Frommelt MA, Tweddell JS (2007): Effect of shunt type on echocardiographic indices after initial palliations for hypoplastic left heart syndrome: Blalock-Taussig shunt versus right ventricle-pulmonary artery conduit. J Am Soc Echocardiogr 20, 1364–1373

Galantowicz M, Cheatham JP (2005): Lessons learned from the development of a new hybrid strategy for the management of hypoplastic left heart syndrome. Pediatr Cardiol 26, 190–199

Gassmann M, Casagranda F, Orioli D, Simon H, Lai C, Klein R, Lemke G (1995): Aberrant neural and cardiac development in mice lacking the ErbB4 neuregulin receptor. Nature 378, 390–394

Gehrmann J, Krasemann T, Kehl HG, Vogt J (2001): Hypoplastic left-heart syndrome: the first description of the pathophysiology in 1851; translation of a publication by Dr. Bardeleben from Giessen, Germany. Chest 120, 1368–1371

Gillum RF (1994): Epidemiology of congenital heart disease in the United States. Am Heart J 127, 919–927

Gittenberger-de Groot AC, Bartelings MM, Deruiter MC, Poelmann RE (2005): Basics of cardiac development for the understanding of congenital heart malformations. Pediatr Res 57, 169–176

Glenn WW (1958): Circulatory bypass of the right side of the heart. IV. Shunt between superior vena cava and distal right pulmonary artery; report of clinical application. N Engl J Med 259, 117–120

Gong H, Lyu X, Wang Q, Hu M, Zhang X (2017): Endothelial to mesenchymal transition in the cardiovascular system. Life Sci 184, 95–102

Gossler A, Joyner AL, Rossant J, Skarnes WC (1989): Mouse embryonic stem cells and reporter constructs to detect developmentally regulated genes. Science 244, 463–465

Graupner O, Enzensberger C, Wieg L, Degenhardt J, Wolter A, Khalil M, Schranz D, Yerebakan C, Doelle A, Herrmann J, Axt-Fliedner R (2018): Endocardial Fibroelastosis of the Left Ventricle Affects Right Ventricular Performance in Fetuses with Hypoplastic Left Heart Syndrome: A Prospective Study Using M-Mode, PW- and Tissue Doppler Techniques. Ultraschall Med 39, 413–421

Grossfeld PD, Mattina T, Lai Z, Favier R, Jones KL, Cotter F, Jones C (2004): The 11q terminal deletion disorder: a prospective study of 110 cases. Am J Med Genet A 129A, 51–61

Hakimi M-A, Dong Y, Lane WS, Speicher DW, Shiekhattar R (2003): A candidate X-linked mental retardation gene is a component of a new family of histone deacetylase-containing complexes. J Biol Chem 278, 7234–7239

Hastreiter AR, Van der Horst RL, Dubrow IW, Eckner FO (1983): Quantitative angiographic and morphologic aspects of aortic valve atresia. Am J Cardiol 51, 1705–1708

Hebra A, Brown MF, Hirschl RB, McGeehin K, O'Neill JA, Norwood WI, Ross AJ (1993): Mesenteric ischemia in hypoplastic left heart syndrome. J Pediatr Surg 28, 606–611

Hellmund A, Berg C, Herberg U, Geipel A, Kempe A, Gembruch U (2017): Levoatrial Cardinal Vein in a Series of Five Prenatal Cases with Hypoplastic Left Heart Syndrome and Intact Atrial Septum. Ultraschall Med 38, 206–211

Hinton RB, Benson DW: Hypoplastic Left Heart Syndrome; In: Moller JH, Hoffman JIE (Eds.): Pediatric Cardiovascular Medicine, 2nd Edition; John Wiley & Sons, Chichester 2012, 523–533

Hinton RB, Martin LJ, Tabangin ME, Mazwi ML, Cripe LH, Benson DW (2007): Hypoplastic left heart syndrome is heritable. J Am Coll Cardiol 50, 1590–1595

Hinton RB, Martin LJ, Rame-Gowda S, Tabangin ME, Cripe LH, Benson DW (2009): Hypoplastic left heart syndrome links to chromosomes 10q and 6q and is genetically related to bicuspid aortic valve. J Am Coll Cardiol 53, 1065–1071

Hu N, Sedmera D, Yost HJ, Clark EB (2000): Structure and function of the developing zebrafish heart. Anat Rec 260, 148–157

Huang W-H, Sung K-T, Tsai J-P, Lo C-I, Hsiao C-C, Kuo J-Y, Su C-H, Chen M-R, Hung C-L (2018): Clinical and Echocardiography Features of Diagnosed in Adulthood Isolated Left Ventricular Noncompaction: A Case Series Study. J Med Ultrasound 26, 37–41

Iascone M, Ciccone R, Galletti L, Marchetti D, Seddio F, Lincesso AR, Pezzoli L, Vetro A, Barachetti D, Boni L, et al. (2012): Identification of de novo mutations and rare variants in hypoplastic left heart syndrome. Clin Genet 81, 542–554

Ishii Y, Inamura N, Kayatani F, Iwai S, Kawata H, Arakawa H, Kishimoto H (2014): Evaluation of bilateral pulmonary artery banding for initial palliation in single-ventricle neonates and infants: risk factors for mortality before the bidirectional Glenn procedure. Interact Cardiovasc Thorac Surg 19, 807–811

Jacobs ML, Blackstone EH, Bailey LL (1998): Intermediate survival in neonates with aortic atresia: a multi-institutional study. The Congenital Heart Surgeons Society. J Thorac Cardiovasc Surg 116, 417–431

Jenni R, Oechslin EN, van der Loo B (2007): Isolated ventricular non-compaction of the myocardium in adults. Heart 93, 11–15

Johnson BA, Mussatto K, Uhing MR, Zimmerman H, Tweddell J, Ghanayem N (2008): Variability in the preoperative management of infants with hypoplastic left heart syndrome. Pediatr Cardiol 29, 515–520

Kanjuh V, Eliot RS, Edwards JE (1965): Coexistent mitral and aortic valvular atresia: a pathologic study of 14 cases. Am J Cardiol 15, 611–621

Kelly RG, Buckingham ME (2002): The anterior heart-forming field: voyage to the arterial pole of the heart. Trends Genet 18, 210–216

Kenchegowda D, Liu H, Thompson K, Luo L, Martin SS, Fisher SA (2014): Vulnerability of the developing heart to oxygen deprivation as a cause of congenital heart defects. J Am Heart Assoc 3, e000841

Kern JH, Hayes CJ, Michler RE, Gersony WM, Quaegebeur JM (1997): Survival and risk factor analysis for the Norwood procedure for hypoplastic left heart syndrome. Am J Cardiol 80, 170–174

Kim KH, Nakaoka Y, Augustin HG, Koh GY (2018): Myocardial Angiopoietin-1 Controls Atrial Chamber Morphogenesis by Spatiotemporal Degradation of Cardiac Jelly. Cell Rep 23, 2455–2466

Kinsella MG, Fitzharris TP (1980): Origin of cushion tissue in the developing chick heart: cinematographic recordings of in situ formation. Science 207, 1359–1360

Knott HW, Doty DB (1977): Experimental bypass of the left ventricle. J Thorac Cardiovasc Surg 74, 436–439

Kokoszka JE, Waymire KG, Flierl A, Sweeney KM, Angelin A, MacGregor GR, Wallace DC (2016): Deficiency in the mouse mitochondrial adenine nucleotide translocator isoform 2 gene is associated with cardiac noncompaction. Biochim Biophys Acta 1857, 1203–1212

Kreidberg JA, Sariola H, Loring JM, Maeda M, Pelletier J, Housman D, Jaenisch R (1993): WT-1 is required for early kidney development. Cell 74, 679–691

Krenning G, Zeisberg EM, Kalluri R (2010): The origin of fibroblasts and mechanism of cardiac fibrosis. J Cell Physiol 225, 631–637

Krishnan A, Samtani R, Dhanantwari P, Lee E, Yamada S, Shiota K, Donofrio MT, Leatherbury L, Lo CW (2014): A detailed comparison of mouse and human cardiac development. Pediatr Res 76, 500–507

Lamers WH, Moorman AFM (2002): Cardiac septation: a late contribution of the embryonic primary myocardium to heart morphogenesis. Circ Res 91, 93–103

Landi D, Gemignani F, Pardini B, Naccarati A, Garritano S, Vodicka P, Vodickova L, Canzian F, Novotny J, Barale R, Landi S (2012): Identification of candidate genes carrying polymorphisms associated with the risk of colorectal cancer by analyzing the colorectal mutome and microRNAome. Cancer 118, 4670–4680

Lee KF, Simon H, Chen H, Bates B, Hung MC, Hauser C (1995): Requirement for neuregulin receptor erbB2 in neural and cardiac development. Nature 378, 394–398

Lev M (1952): Pathologic anatomy and interrelationship of hypoplasia of the aortic tract complexes. Lab Invest 1, 61–70

Li J, Zhang G, McCrindle BW, Holtby H, Humpl T, Cai S, Caldarone CA, Redington AN, Van Arsdell GS (2007): Profiles of hemodynamics and oxygen transport derived by using continuous measured oxygen consumption after the Norwood procedure. J Thorac Cardiovasc Surg 133, 441–448

Li Y-Y, Zhang J-P (2006): Gene trapping techniques and current progress. Yi Chuan Xue Bao 33, 189–198

Liao W, Bisgrove BW, Sawyer H, Hug B, Bell B, Peters K, Grunwald DJ, Stainier DY (1997): The zebrafish gene cloche acts upstream of a flk-1 homologue to regulate endothelial cell differentiation. Development 124, 381–389

Lin F, Wang N, Zhang T-C (2012): The role of endothelial-mesenchymal transition in development and pathological process. IUBMB Life 64, 717–723

Lin Q, Schwarz J, Bucana C, Olson EN (1997): Control of mouse cardiac morphogenesis and myogenesis by transcription factor MEF2C. Science 276, 1404–1407

Lin Y, Wu Y, Li J, Dong C, Ye X, Chi Y-I, Evers BM, Zhou BP (2010): The SNAG domain of Snail1 functions as a molecular hook for recruiting lysine-specific demethylase 1. EMBO J 29, 1803–1816

Linask KK, Yu X, Chen Y, Han M-D (2002): Directionality of heart looping: effects of Pitx2c misexpression on flectin asymmetry and midline structures. Dev Biol 246, 407–417

Lloyd TR, Evans TC, Marvin WJ (1986): Morphologic determinants of coronary blood flow in the hypoplastic left heart syndrome. Am Heart J 112, 666–671

Loffredo CA, Chokkalingam A, Sill AM, Boughman JA, Clark EB, Scheel J, Brenner JI (2004): Prevalence of congenital cardiovascular malformations among relatives of infants with hypoplastic left heart, coarctation of the aorta, and d-transposition of the great arteries. Am J Med Genet A 124A, 225–230

Lurie PR (2010): Changing concepts of endocardial fibroelastosis. Cardiol Young 20, 115–123

Luxán G, D'Amato G, MacGrogan D, de la Pompa JL (2016): Endocardial Notch Signaling in Cardiac Development and Disease. Circ Res 118, e1–e18

Lyons I, Parsons LM, Hartley L, Li R, Andrews JE, Robb L, Harvey RP (1995): Myogenic and morphogenetic defects in the heart tubes of murine embryos lacking the homeo box gene Nkx2-5. Genes Dev 9, 1654–1666

Mahowald JM, Lucas RV, Edwards JE (1982): Aortic valvular atresia. Associated cardiovascular anomalies. Pediatr Cardiol 2, 99–105

Mäkikallio K, McElhinney DB, Levine JC, Marx GR, Colan SD, Marshall AC, Lock JE, Marcus EN, Tworetzky W (2006): Fetal aortic valve stenosis and the evolution of hypoplastic left heart syndrome: patient selection for fetal intervention. Circulation 113, 1401–1405

Maxwell D, Allan L, Tynan MJ (1991): Balloon dilatation of the aortic valve in the fetus: a report of two cases. Br Heart J 65, 256–258

McElhinney DB, Marshall AC, Wilkins-Haug LE, Brown DW, Benson CB, Silva V, Marx GR, Mizrahi-Arnaud A, Lock JE, Tworetzky W (2009): Predictors of technical success and postnatal biventricular outcome after in utero aortic valvuloplasty for aortic stenosis with evolving hypoplastic left heart syndrome. Circulation 120, 1482–1490

Meilhac SM, Esner M, Kelly RG, Nicolas J-F, Buckingham ME (2004): The clonal origin of myocardial cells in different regions of the embryonic mouse heart. Dev Cell 6, 685–698

Memczak S, Jens M, Elefsinioti A, Torti F, Krueger J, Rybak A, Maier L, Mackowiak SD, Gregersen LH, Munschauer M, et al. (2013): Circular RNAs are a large class of animal RNAs with regulatory potency. Nature 495, 333–338

Meyer D, Birchmeier C (1995): Multiple essential functions of neuregulin in development. Nature 378, 386–390

Miquerol L, Gertsenstein M, Harpal K, Rossant J, Nagy A (1999): Multiple developmental roles of VEGF suggested by a LacZ-tagged allele. Dev Biol 212, 307–322

Moens CB, Stanton BR, Parada LF, Rossant J (1993): Defects in heart and lung development in compound heterozygotes for two different targeted mutations at the N-myc locus. Development 119, 485–499

Moodie DS, Gallen WJ, Friedberg DZ (1972): Congenital aortic atresia. Report of long survival and some speculations about surgical approaches. J Thorac Cardiovasc Surg 63, 726–731

Moorman A, Webb S, Brown NA, Lamers W, Anderson RH (2003): Development of the heart: (1) formation of the cardiac chambers and arterial trunks. Heart 89, 806–814

Morris CD, Outcalt J, Menashe VD (1990): Hypoplastic left heart syndrome: natural history in a geographically defined population. Pediatrics 85, 977–983

Mu TS, McAdams RM, Bush DM (2005): A case of hypoplastic left heart syndrome and bicuspid aortic valve in monochorionic twins. Pediatr Cardiol 26, 884–885

Murphy MO, Bellsham-Revell H, Morgan GJ, Krasemann T, Rosenthal E, Qureshi SA, Salih C, Austin CB, Anderson DR (2015): Hybrid Procedure for Neonates With Hypoplastic Left Heart Syndrome at High-Risk for Norwood: Midterm Outcomes. Ann Thorac Surg 100, 2286–2290; discussion 2291-2292

Nagase T, Seki N, Ishikawa K, Tanaka A, Nomura N (1996): Prediction of the coding sequences of unidentified human genes. V. The coding sequences of 40 new genes (KIAA0161-KIAA0200) deduced by analysis of cDNA clones from human cell line KG-1. DNA Res 3, 17–24

Natowicz M, Kelley RI (1987): Association of Turner syndrome with hypoplastic left-heart syndrome. Am J Dis Child 141, 218–220

Natowicz M, Chatten J, Clancy R, Conard K, Glauser T, Huff D, Lin A, Norwood W, Rorke LB, Uri A (1988): Genetic disorders and major extracardiac anomalies associated with the hypoplastic left heart syndrome. Pediatrics 82, 698–706

Nebigil CG, Choi DS, Dierich A, Hickel P, Le Meur M, Messaddeq N, Launay JM, Maroteaux L (2000): Serotonin 2B receptor is required for heart development. Proc Natl Acad Sci USA 97, 9508–9513

Noonan JA, Nadas AS (1958): The hypoplastic left heart syndrome; an analysis of 101 cases. Pediatr Clin North Am 5, 1029–1056

Norwood WI, Lang P, Hansen DD (1983): Physiologic repair of aortic atresia-hypoplastic left heart syndrome. N Engl J Med 308, 23–26

Person AD, Klewer SE, Runyan RB (2005): Cell biology of cardiac cushion development. Int Rev Cytol 243, 287–335

Pignatelli RH, McMahon CJ, Dreyer WJ, Denfield SW, Price J, Belmont JW, Craigen WJ, Wu J, El Said H, Bezold LI, et al. (2003): Clinical characterization of left ventricular noncompaction in children: a relatively common form of cardiomyopathy. Circulation 108, 2672–2678

Poelmann RE, Gittenberger-de Groot AC (2018): Hemodynamics in Cardiac Development. J Cardiovasc Dev Dis 5, 54–73

Pradat P, Francannet C, Harris JA, Robert E (2003): The epidemiology of cardiovascular defects, part I: a study based on data from three large registries of congenital malformations. Pediatr Cardiol 24, 195–221

Pruetz JD, Carroll C, Trento LU, Chang R-K, Detterich J, Miller DA, Sklansky M (2014): Outcomes of critical congenital heart disease requiring emergent neonatal cardiac intervention. Prenat Diagn 34, 1127–1132

Pundi KN, Johnson JN, Dearani JA, Pundi KN, Li Z, Hinck CA, Dahl SH, Cannon BC, O'Leary PW, Driscoll DJ, Cetta F (2015): 40-Year Follow-Up After the Fontan Operation: Long-Term Outcomes of 1,052 Patients. J Am Coll Cardiol 66, 1700–1710

Puri MC, Partanen J, Rossant J, Bernstein A (1999): Interaction of the TEK and TIE receptor tyrosine kinases during cardiovascular development. Development 126, 4569–4580

Quéméner-Redon S, Bénech C, Audebert-Bellanger S, Friocourt G, Planes M, Parent P, Férec C (2013): A small de novo 16q24.1 duplication in a woman with severe clinical features. Eur J Med Genet 56, 211–215

Ramamoorthy C, Tabbutt S, Kurth CD, Steven JM, Montenegro LM, Durning S, Wernovsky G, Gaynor JW, Spray TL, Nicolson SC (2002): Effects of inspired hypoxic and hypercapnic gas mixtures on cerebral oxygen saturation in neonates with univentricular heart defects. Anesthesiology 96, 283–288

Risebro CA, Riley PR (2006): Formation of the ventricles. ScientificWorldJournal 6, 1862–1880

Roberts WC, Perry LW, Chandra RS, Myers GE, Shapiro SR, Scott LP (1976): Aortic valve atresia: a new classification based on necropsy study of 73 cases. Am J Cardiol 37, 753–756

Roger VL, Go AS, Lloyd-Jones DM, Adams RJ, Berry JD, Brown TM, Carnethon MR, Dai S, de Simone G, Ford ES, et al. (2011): Heart disease and stroke statistics--2011 update: a report from the American Heart Association. Circulation 123, e18–e209

Rychik J, Rome JJ, Collins MH, DeCampli WM, Spray TL (1999): The hypoplastic left heart syndrome with intact atrial septum: atrial morphology, pulmonary vascular histopathology and outcome. J Am Coll Cardiol 34, 554–560

Ryder E, Doe B, Gleeson D, Houghton R, Dalvi P, Grau E, Habib B, Miklejewska E, Newman S, Sethi D, et al. (2014): Rapid conversion of EUCOMM/KOMP-CSD alleles in mouse embryos using a cell-permeable Cre recombinase. Transgenic Res 23, 177–185

Samánek M, Benesová D, Goetzová J, Hrycejová I (1988): Distribution of age at death in children with congenital heart disease who died before the age of 15. Br Heart J 59, 581–585

Sanapo L, Pruetz JD, Slodki M, Goens MB, Moon-Grady AJ, Donofrio MT (2017): Fetal echocardiography for planning perinatal and delivery room care of neonates with congenital heart disease. Echocardiography 34, 1804–1821

Sato TN, Tozawa Y, Deutsch U, Wolburg-Buchholz K, Fujiwara Y, Gendron-Maguire M, Gridley T, Wolburg H, Risau W, Qin Y (1995): Distinct roles of the receptor tyrosine kinases Tie-1 and Tie-2 in blood vessel formation. Nature 376, 70–74

Sawai S, Shimono A, Wakamatsu Y, Palmes C, Hanaoka K, Kondoh H (1993): Defects of embryonic organogenesis resulting from targeted disruption of the N-myc gene in the mouse. Development 117, 1445–1455

Sedmera D, Thomas PS (1996): Trabeculation in the embryonic heart. Bioessays 18, 607–607

Sedmera D, Hu N, Weiss KM, Keller BB, Denslow S, Thompson RP (2002): Cellular changes in experimental left heart hypoplasia. Anat Rec 267, 137–145

Selamet Tierney ES, Wald RM, McElhinney DB, Marshall AC, Benson CB, Colan SD, Marcus EN, Marx GR, Levine JC, Wilkins-Haug L, et al. (2007): Changes in left heart hemodynamics after technically successful in-utero aortic valvuloplasty. Ultrasound Obstet Gynecol 30, 715–720

Shimada S, Robles C, Illigens BMW, Casar Berazaluce AM, del Nido PJ, Friehs I (2015): Distention of the Immature Left Ventricle Triggers Development of Endocardial Fibroelastosis: An Animal Model of Endocardial Fibroelastosis Introducing Morphopathological Features of Evolving Fetal Hypoplastic Left Heart Syndrome. Biomed Res Int 2015, 462-469

Shime N, Hashimoto S, Hiramatsu N, Oka T, Kageyama K, Tanaka Y (2000): Hypoxic gas therapy using nitrogen in the preoperative management of neonates with hypoplastic left heart syndrome. Pediatr Crit Care Med 1, 38–41

Silva JP da, Fonseca L da, Baumgratz JF, Castro RM, Franchi SM, Lianza AC, Vila JHA (2007): Hypoplastic left heart syndrome: the report of a surgical strategy and comparative results of Norwood x Norwood-Sano approach. Rev Bras Cir Cardiovasc 22, 160–168

Sinha SN, Rusnak SL, Sommers HM, Cole RB, Muster AJ, Paul MH (1968): Hypoplastic left ventricle syndrome. Analysis of thirty autopsy cases in infants with surgical considerations. Am J Cardiol 21, 166–173

Skarnes WC, Rosen B, West AP, Koutsourakis M, Bushell W, Iyer V, Mujica AO, Thomas M, Harrow J, Cox T, et al. (2011): A conditional knockout resource for the genome-wide study of mouse gene function. Nature 474, 337–342

Sokolowski L, Respondek-Liberska M, Pietryga M, Slodki M (2019): Prenatally diagnosed foramen ovale restriction in fetuses with hypoplastic left heart syndrome may be a predictor of longer hospitalization, but not of a need for an urgent rashkind procedure. Ginekol Pol 90, 31–38

Srivastava D, Thomas T, Lin Q, Kirby ML, Brown D, Olson EN (1997): Regulation of cardiac mesodermal and neural crest development by the bHLH transcription factor, dHAND. Nat Genet 16, 154–160

Stainier DY, Weinstein BM, Detrich HW, Zon LI, Fishman MC (1995): Cloche, an early acting zebrafish gene, is required by both the endothelial and hematopoietic lineages. Development 121, 3141–3150

Stallmeyer B, Fenge H, Nowak-Göttl U, Schulze-Bahr E (2010): Mutational spectrum in the cardiac transcription factor gene NKX2.5 (CSX) associated with congenital heart disease. Clin Genet 78, 533–540

Stalsberg H (1969): The origin of heart asymmetry: right and left contributions to the early chick embryo heart. Dev Biol 19, 109–127

Stanford WL, Cohn JB, Cordes SP (2001): Gene-trap mutagenesis: past, present and beyond. Nat Rev Genet 2, 756–768

Stieh J, Fischer G, Scheewe J, Uebing A, Dütschke P, Jung O, Grabitz R, Trampisch HJ, Kramer HH (2006): Impact of preoperative treatment strategies on the early perioperative outcome in neonates with hypoplastic left heart syndrome. J Thorac Cardiovasc Surg 131, 1122–1129

Stümpflen I, Stümpflen A, Wimmer M, Bernaschek G (1996): Effect of detailed fetal echocardiography as part of routine prenatal ultrasonographic screening on detection of congenital heart disease. Lancet 348, 854–857

Suri C, Jones PF, Patan S, Bartunkova S, Maisonpierre PC, Davis S, Sato TN, Yancopoulos GD (1996): Requisite role of angiopoietin-1, a ligand for the TIE2 receptor, during embryonic angiogenesis. Cell 87, 1171–1180

Tabbutt S, Ramamoorthy C, Montenegro LM, Durning SM, Kurth CD, Steven JM, Godinez RI, Spray TL, Wernovsky G, Nicolson SC (2001): Impact of inspired gas mixtures on preoperative infants with hypoplastic left heart syndrome during controlled ventilation. Circulation 104, I159–164

Tchervenkov CI, Jacobs JP, Weinberg PM, Aiello VD, Béland MJ, Colan SD, Elliott MJ, Franklin RCG, Gaynor JW, Krogmann ON, et al. (2006): The nomenclature, definition and classification of hypoplastic left heart syndrome. Cardiol Young 16, 339–368

Tennstedt C, Chaoui R, Körner H, Dietel M (1999): Spectrum of congenital heart defects and extracardiac malformations associated with chromosomal abnormalities: results of a seven-year necropsy study. Heart 82, 34–39

Thiene G, Gallucci V, Macartney FJ, Del Torso S, Pellegrino PA, Anderson RH (1979): Anatomy of aortic atresia. Cases presenting with a ventricular septal defect. Circulation 59, 173–178

Tola HT, Ergul Y, Saygi M, Ozyilmaz I, Guzeltas A, Odemis E (2015): Ductal stent implantation in tetralogy of fallot with aortic arch abnormality. Tex Heart Inst J 42, 281–284

Toyofuku T, Zhang H, Kumanogoh A, Takegahara N, Yabuki M, Harada K, Hori M, Kikutani H (2004): Guidance of myocardial patterning in cardiac development by Sema6D reverse signalling. Nat Cell Biol 6, 1204–1211

Tworetzky W, McElhinney DB, Reddy VM, Brook MM, Hanley FL, Silverman NH (2001): Improved surgical outcome after fetal diagnosis of hypoplastic left heart syndrome. Circulation 103, 1269–1273

Verzi MP, McCulley DJ, De Val S, Dodou E, Black BL (2005): The right ventricle, outflow tract, and ventricular septum comprise a restricted expression domain within the secondary/anterior heart field. Dev Biol 287, 134–145

Vlahos AP, Lock JE, McElhinney DB, van der Velde ME (2004): Hypoplastic left heart syndrome with intact or highly restrictive atrial septum: outcome after neonatal transcatheter atrial septostomy. Circulation 109, 2326–2330

Vogel M, Wilkins-Haug LE, McElhinney DB, Marshall AC, Benson CB, Silva V, Tworetzky W (2010): Reversible ductus arteriosus constriction due to maternal indomethacin after fetal intervention for hypoplastic left heart syndrome with intact/restrictive atrial septum. Fetal Diagn Ther 27, 40–45

von Both I, Silvestri C, Erdemir T, Lickert H, Walls JR, Henkelman RM, Rossant J, Harvey RP, Attisano L, Wrana JL (2004): Foxh1 is essential for development of the anterior heart field. Dev Cell 7, 331–345

von Rueden TJ, Knight L, Moller JH, Ewards JE (1975): Coarctation of the aorta associated with aortic valvular atresia. Circulation 52, 951–954

Waller BF, Smith ER, Blackbourne BD, Arce FP, Sarkar NN, Roberts WC (1980): Congenital hypoplasia of portions of both right and left ventricular myocardial walls. Clinical and

necropsy observations in two patients with parchment heart syndrome. Am J Cardiol 46, 885–891

Watson DG, Rowe RD (1962): Aortic-valve atresia. Report of 43 cases. JAMA 179, 14–18

Webb S, Brown NA, Anderson RH (1996): The structure of the mouse heart in late fetal stages. Anat Embryol 194, 37–47

Weinberg PM, Chin AJ, Murphy JD, Pigott JD, Norwood WI (1986): Postmortem echocardiography and tomographic anatomy of hypoplastic left heart syndrome after palliative surgery. Am J Cardiol 58, 1228–1232

Wessels A, Sedmera D (2003): Developmental anatomy of the heart: a tale of mice and man. Physiol Genomics 15, 165–176

Wilson WM, Valente AM, Hickey EJ, Clift P, Burchill L, Emmanuel Y, Gibson P, Greutmann M, Grewal J, Grigg LE, et al. (2018): Outcomes of Patients With Hypoplastic Left Heart Syndrome Reaching Adulthood After Fontan Palliation: Multicenter Study. Circulation 137, 978–981

Xu X, Friehs I, Zhong Hu T, Melnychenko I, Tampe B, Alnour F, Iascone M, Kalluri R, Zeisberg M, Del Nido PJ, Zeisberg EM (2015): Endocardial fibroelastosis is caused by aberrant endothelial to mesenchymal transition. Circ Res 116, 857–866

Yang P, Wang Y, Chen J, Li H, Kang L, Zhang Y, Chen S, Zhu B, Gao S (2011): RCOR2 is a subunit of the LSD1 complex that regulates ESC property and substitutes for SOX2 in reprogramming somatic cells to pluripotency. Stem Cells 29, 791–801

Yokoyama A, Takezawa S, Schüle R, Kitagawa H, Kato S (2008): Transrepressive function of TLX requires the histone demethylase LSD1. Mol Cell Biol 28, 3995–4003

Yun SW (2011): Congenital heart disease in the newborn requiring early intervention. Korean J Pediatr 54, 183–191

Zeisberg EM, Kalluri R (2010): Origins of cardiac fibroblasts. Circ Res 107, 1304–1312

Zhang J, Lin Y, Zhang Y, Lan Y, Lin C, Moon AM, Schwartz RJ, Martin JF, Wang F (2008): Frs2alpha-deficiency in cardiac progenitors disrupts a subset of FGF signals required for outflow tract morphogenesis. Development 135, 3611–3622

Zhang W, Chen H, Qu X, Chang C-P, Shou W (2013): Molecular mechanism of ventricular trabeculation/compaction and the pathogenesis of the left ventricular noncompaction cardiomyopathy (LVNC). Am J Med Genet C Semin Med Genet 163C, 144–156

Websites:

ensemble.org/Homo_sapiens

http://www.ensembl.org/Homo_sapiens/Gene/Phenotype?db=core;g=ENSG00000131149;r=16:85169525-85676204; accessed on April 19th, 2019

ensembl.org/Mus_musculus/Gene/Phenotype

http://www.ensembl.org/Mus_musculus/Gene/Phenotype?db=core;g=ENSMUSG00000031822;r=8:120228456-120581390; accessed on April 19th, 2019

ensembl.org/Mus_musculus/Gene/TranscriptComparison

http://www.ensembl.org/Mus_musculus/Gene/TranscriptComparison?db=core;g=ENSMUSG00000031822;r=8:120228456-120581390; accessed on April 19th, 2019

genecards.org

https://www.genecards.org/cgi-bin/carddisp.pl?gene=GSE1; accessed on April 19th, 2019

genome.gov

https://www.genome.gov/human-genome-project/What; accessed on April 19th, 2019

knockoutmouse.org

http://www.knockoutmouse.org/martsearch/project/71610; accessed on April 19th, 2019

mousephenotype.org

https://www.mousephenotype.org/about-impc/about-ikmc/eucomm/; accessed on April 19th, 2019

ncbi.nlm.nih.gov

https://www.ncbi.nlm.nih.gov/gene/23199; accessed on April 19th, 2019